TAMPERE UNIVERSITY OF TECHNOLOGY

ANTTI YLINEN

METHODS FOR MODELING COUPLED HYDRAULIC DRIVEN FLEXIBLE MULTIBODY SYSTEMS

Master's Thesis

Examiners: Professor Asko Ellman
Academy Research Fellow Jari Mäkinen
Examiners and subject were approved in the Automation, Mechanical and Materials Engineering Council meeting on 4th May 2011

ABSTRACT

TAMPERE UNIVERSITY OF TECHNOLOGY
Master's Degree Program in Mechanical Engineering
YLINEN, ANTTI: Methods for Modeling Coupled Hydraulic Driven Flexible Multibody Systems
Master's Thesis, 76 pages, 2 appendix pages
June 2011
Major: Applied Mechanics
Examiners: Professor Asko Ellman, Academy Research Fellow Jari Mäkinen
Keywords: Non-Linear Element Method, Geometrically Exact Beam, Coupled Problems

Hydraulic driven multibody systems are very common in industry and the behavior of these systems under transient load has been modeled in various ways. For instance, if one is interested in the response of the mechanical system, the hydraulic system has been excluded from the simulation model and the actuator, like the hydraulic cylinder, has been replaced with a length controlled rod element. In this case, the mechanical system can be modeled as a non-linear system. However, if the hydraulic system is the one to study, the mechanical system is modeled as a rigid body or with linear element method.

In this master's thesis a new modeling technique is presented, where the hydraulic system is modeled using the finite element method. In this way, the hydraulic system can be included to the simulation model and the mechanical system can be modeled using non-linear elements. In addition, the coupling tangential matrices between the mechanical system and the hydraulic system can be calculated analytically.

This new modeling technique is applied to a numerical example, which is based on the maintenance robot of the ITER fusion reactor. The system is simulated using this new modeling technique as well as the length controlled rod element. The responses of the mechanical structure in this simulation show that the length controlled rod element cannot represent the behavior of the multibody system whereas the new modeling technique gives realistic results.

The purpose of this thesis is to present a new technique for modeling coupled hydraulic driven multibody systems, not to provide accurate simulation results of the maintenance robot. This new method provides good results and thereby research on this field should be continued. Modeling of the hydraulic cylinder requires special attention, because it couples the mechanical system to the hydraulic system. With these sophisticated hydraulic cylinder models it is also possible to develop the old modeling techniques.

TIIVISTELMÄ

TAMPEREEN TEKNILLINEN YLIOPISTO
Konstruktiotekniikan koulutusohjelma
YLINEN, ANTTI: Hydraulisesti käytettyjen joustavien monikappalejärjestelmien mallintaminen
Diplomityö, 76 sivua, 2 liitesivua
Kesäkuu 2011
Pääaine: Teknillinen mekaniikka
Tarkastajat: Professori Asko Ellman, Akatemiatutkija Jari Mäkinen
Avainsanat: Epälineaarinen elementtimenetelmä, geometrisesti tarkka palkki, kytketyt ongelmat

Hydraulikäyttöiset monikappalejärjestelmät ovat hyvin yleisiä teollisuudessa ja niiden toimintaa on mallinnettu useilla tavoilla tarpeen mukaan. Jos on haluttu mallintaa mekaanisen järjestelmän dynaamista käyttäytymistä, hydrauliikka on yleensä jätetty simulaatiosta pois ja toimilaite, esimerkiksi sylinteri, korvattu pituuttaan muuttavalla sauvaelementillä. Tällöin mekaaninen järjestelmä on mallinnettu epälineaarisena systeeminä. Jos puolestaan on haluttu mallintaa hydraulijärjestelmän toimintaa tarkasti, mekaaninen järjestelmä on mallinnettu jäykkänä kappaleena tai lineaarisella elementtimenetelmällä.

Tässä työssä esitellään mallinnustapa, jossa hydraulijärjestelmä mallinnetaan elementtimenetelmän keinoin, jolloin saadaan mallinnettua hydraulijärjestelmä mekaanisen järjestelmän ohella ja tällöin voidaan käyttää myös epälineaarisia elementtejä mekaanisen järjestelmän kuvaamiseen. Lisäksi mekaanisen järjestelmän ja hydraulijärjestelmän väliset kytkentämatriisit saadaan laskettua analyyttisessä muodossa.

Uutta mallinnustapaa sovelletaan laskentaesimerkkiin, joka pohjautuu ITER fuusioreaktorin huoltorobottiin. Tätä järjestelmää simuloidaan käyttämällä niin pituuttaan muuttavaa sauvaelementtiä kuin uutta kytkettyä mallinnustapaa, jossa myös hydraulijärjestelmä on mukana. Tulokset osoittavat, että kyseisessä simulaatioesimerkissä pituuttaan muuttava sauvaelementti ei kuvaa järjestelmän todellista käyttäytymistä, kun taas hydraulijärjestelmällä toteutetun simulaatiomallin tulokset ovat realistisia.

Tässä diplomityössä esitellään uutta mallinnustapaa hydraulisesti käytettyjen laitteiden simulointiin ja etsitään parannuskeinoja vanhoihin menetelmiin, ei niinkään mallinneta huoltorobottia tarkasti. Uusi menetelmä antaa hyviä tuloksia, joten tutkimusta tällä saralla on syytä jatkaa. Erityistä huomiota tulee kiinnittää hydraulisylinterin mallinnukseen, sillä se kytkee mekaanisen järjestelmän hydrauliseen järjestelmään. Hydraulisylinterin mallin kehittämisellä voidaan myös parantaa vanhojen mallinnusmenetelmien, kuten muuttuvapituuksisen sauvan, toimintaa.

PREFACE

This master's thesis has been made at Tampere University of Technology at the department of Mechanics and Design.

I would like to thank Academy Research Fellow Jari Mäkinen for offering me this wonderful opportunity to take part in this groundbreaking research and giving me the support and guidance during my work. His knowledge of applied mathematics has saved the day often. I would like to show special gratitude to Heikki Marjamäki for our conversations and for his great advice during problems. Finally I would like to thank Professor Asko Ellman for his interest in my thesis and for the comments he gave.

19th May 2011 at Tampere

Antti Ylinen

CONTENTS

NOMENCLATURE

$!$	factorial
$\bullet$	vector inner product
$\otimes$	vector outer product
$\underset{s}{\otimes}$	symmetric vector outer product
$\frac{\delta}{\delta \mathbf{x}}$	partial derivative to **x**
$\int_L ds$	integral over the domain of s
$Lin(\mathbf{f}_{\text{int}};\mathbf{u})$	linearization of $\mathbf{f}_{\text{int}}$ in the direction of **u**
$\dot{\mathbf{a}}, \ddot{\mathbf{a}}$	first and second time derivatives of vector **a**
$\tilde{\mathbf{a}}$	skew symmetric matrix of vector **a**
α	Newmark damping parameter
β	Newmark parameter
δ	variation
ε	friction coefficient
ε_G	Green strain
ε_i	i:th modal damping coefficient
γ	Newmark parameter
Γ^2	propagation operator for the transmission line friction
$\boldsymbol{\Gamma}$	material strain vector
$\mathbf{K}$	material curvature vector
ω_i	i:th natural modal frequency
ψ	rotation angle
ψ_j	j:th linearly independent function
$\boldsymbol{\Psi}$	rotation vector
ρ, ρ_0	density
$\boldsymbol{\Theta}_{\text{R}}$	material incremental rotation vector
σ_G	Piola-Kirchhoff second stress
ν_0	kinematic viscosity
A_{or}	orifice area
B_0	bulk modulus
$\mathbf{B}$	kinematic matrix
c_0	speed of sound
$\mathbf{C}$	tangential damping matrix
exp	exponential function

D_{or}	orifice diameter
$\mathbf{E}$	total material strain vector
$\mathbf{f}_{\text{int}}$	internal force vector
$\mathbf{f}_{\text{cyl}}$	cylinder excitation vector
$\mathbf{f}_{\text{hyd}}$	hydraulic excitation vector
F_{Cou}	Coulomb friction
F_{st}	static friction
F_{v}	viscose friction
$\mathbf{I}$	identity matrix
J_0, J_1	Bessel functions of zeroth and first degree
$\mathbf{J}$	material inertia matrix
k_0	stiffness coefficient of the friction model
k_1	damping coefficient of the friction model
$\mathbf{K}$	tangential stiffness matrix
L_0	initial length
L_c	current length
$L(t)$	length change as function of time
$\mathbf{M}$	mass matrix
$\mathbf{n}$	normal vector, rotation axis
$N_i(s)$	shape function i as function of s
s	current position parameter on beam neutral axis
P	pressure
$\tilde{P}$	trial function for pressure
p_j	Ritz coefficient
$\mathbf{P}$	shape function matrix for the beam element
Q	flow rate
$\mathbf{Q}$	shape function matrix for the beam element
r_0	inner diameter
$\mathbf{r}^*$	mechanical residue
$\mathbf{R}$	rotation matrix
$\mathbf{s}^*$	cylinder residue
$\mathbf{S}$	material stress resultant vector
$\mathbf{t}^*$	hydraulics residue
$\mathbf{T}$	material tangential transformation matrix
$\mathbf{u}$	nodal displacement vector
V	volume
$SO(3)$	three dimensional orthogonal group

$\mathbf{x}_0(s)$	current absolute position of the beam neutral axis as function of s
$\mathbf{X}$	initial position vector
$\mathbf{Y}$	local cross section vector
z	bristle deflection
Z_0	series impedance

CAD	Computer Aided Design
CMM	Cassette Multifunctional Mover
FEM	Finite Element Method
SCEE	Second Cassette End Efector

1 INTRODUCTION

Hydraulically driven mechanisms are commonplace systems in various applications today. Hydraulics is used not only in robust application, for instance in excavators and mining, but also in precision instruments as in fusion reactor maintenance robot and in all applications in between. In all these applications hydraulic systems are in connection with mechanical systems and the coupling of these systems occurs in the hydraulic actuators. Therefore study of these actuators and the coupling is important if accurate and reliable results are wanted from the simulation models.

Traditionally hydraulic driven mechanical systems have been computed as separate systems, mechanical system and hydraulics apart and the coupling has been made in the actuator. However, this formulation is inconsistent. When these systems are solved separately the coupling tangential matrices are inadequate and in addition the time step for each system is independent. These inconsistent systems have been solved with iterative approaches by balancing these two separate systems separately. However, the mechanical system and the hydraulic system are not in equilibrium at the same time due to the different time steps of each system. This inconsistent formulation is ineffective and it degrades convergence.

In this thesis mechanic and hydraulic systems are modeled together as one system which can then be partitioned into small pieces, elements. For instance we can create elements representing pipes, valves and actuators and they are in straight interaction with the elements of the mechanical system and the system equation can be assembled together as it is done in finite element method.

Special interest is focused on modeling the hydraulic cylinder. Traditionally hydraulic cylinder has been modeled as rod elements and no hydraulics is taken into simulation but in this thesis also the coupled system with hydraulics is introduced. Both of these methods are applied on a structure that is based on one of the maintenance robots of the ITER fusion reactor. This thesis is not however, concentrated on simulating the maintenance robot itself but more likely an opening to a new way of simulating coupled hydraulically driven mechanism and comparing this new method with the old methods.

2 THEORETICAL BACKGROUND

This chapter deals with the theory behind this master's thesis. This thesis concentrates on applying finite element method not only to traditional mechanical structures but also on hydraulic systems. In the Finite Element Method (FEM), the basic idea is to solve governing differential equations using approximation functions instead of solving the differential equation analytically. This same procedure can then be used to solve the differential equations for pressure and flow rate thus giving formulation for hydraulic elements. Hydraulic cylinder is then the actuator dealing with the coupling of the hydraulic system and mechanical system.

First in this chapter we deal with the mechanical elements used in this thesis. Second chapter introduces the new way of modeling hydraulic systems and then the hydraulic cylinder is presented. Finally the solution methods for statics and dynamic simulations are considered.

2.1 Finite rotations

In order to develop elements for large displacements and large rotations we need to discuss the matter of finite rotations. In two-dimensional cases the rotation axis is perpendicular to the calculation plane and therefore all rotations are additive no matter how large they are. This originates from the condition that the direction of the rotation axis is constant. In three dimensional cases there is possibility, that the rotation axis itself undergoes rotations changing the direction of the axis. If these rotations are infinitesimal rotations are additive but in case of finite rotations other approaches are needed in order to calculate rotations.

2.1.1 Rotation vector

First thing in defining finite rotations is to study spherical motion where vector $\mathbf{p}_0$ rotates about axis $\mathbf{n}$ to a new vector $\mathbf{p}_1$. Idea is to find and operator which defines this rotational motion. Therefore we take a look at Figure 1 where this rotation is presented.

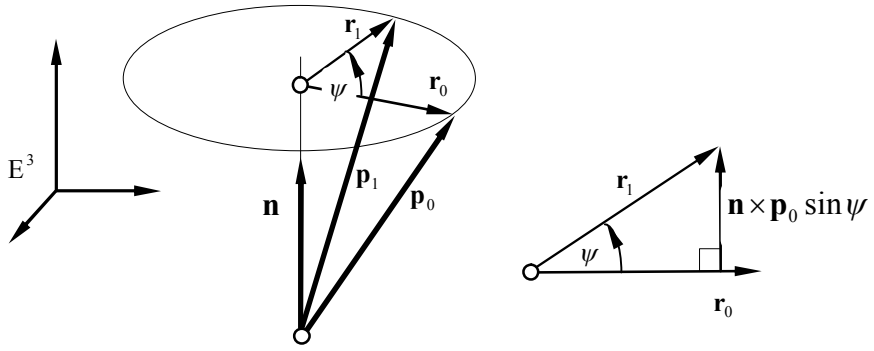

Figure 1 *A rotational motion about* $\mathbf{n}$*-axis where* $\mathbf{p}_0$ *is the original vector and* $\mathbf{p}_1$ *is the rotated vector in Euclidean space (Marjamäki, et al., 2006)*

From Figure 1 we can write the new vector $\mathbf{p}_1$ using the original vector and the radius vectors $\mathbf{r}_0$ and $\mathbf{r}_1$

$$\begin{aligned}\mathbf{p}_1 &= \mathbf{p}_0 - \mathbf{r}_0 + \mathbf{r}_1 \\ &= \mathbf{p}_0 + (1-\cos\psi)\,\mathbf{n}\times(\mathbf{n}\times\mathbf{p}_0) + \mathbf{n}\times\mathbf{p}_0\sin\psi \\ &= \mathbf{R}\mathbf{p}_0\end{aligned} \tag{1}$$

where $\mathbf{R}$ is the rotation operator, the rotation matrix. This operator can be calculated by using new vector $\boldsymbol{\Psi}$ called the rotation vector. Rotation vector is defined as

$$\boldsymbol{\Psi} = \psi\,\mathbf{n} \tag{2}$$

where ψ is the non-negative rotation angle about the unit vector of the rotation axis $\mathbf{n}$. Using equation (2) the rotation matrix $\mathbf{R}$ goes into form (Géradin, et al., 2001).

$$\mathbf{R} = \mathbf{I} + \frac{\sin\psi}{\psi}\tilde{\boldsymbol{\Psi}} + \frac{1-\cos\psi}{\psi^2}\tilde{\boldsymbol{\Psi}}^2 = \exp(\tilde{\boldsymbol{\Psi}}), \quad \psi = \left\|\tilde{\boldsymbol{\Psi}}\right\| \tag{3}$$

The rotation matrix is an orthogonal operator and it is defined so that it preserves the right handedness. Rotation matrix has 9 components but due to the orthogonality it contains six independent constraints and only three components are independent. Thus the rotation matrix can always be presented using rotation vector $\boldsymbol{\Psi}$ .The tilde sign over a symbol defines a skew symmetric matrix which satisfies condition

$$\tilde{\boldsymbol{\Psi}} = \boldsymbol{\Psi}\times \tag{4}$$

Thus equation (4) defines cross product between two vectors as a matrix product (Géradin, et al., 2001).

2.1.2 Non-additive nature of the rotation vector

In this chapter we discuss the rotation vector $\boldsymbol{\Psi}$ and its properties. In two dimensional cases the direction of the axis of the rotation vector is perpendicular to the plane and the direction is always constant. Therefore the rotations in two dimensional problems are additive. When three dimensional problems are considered the direction of the rotation vector is not constant and in addition the rotation vector does not follow vector summation rules. Therefore the rotation vector is not additive in three dimensions.

To show the non-additive nature of the rotation vector more precisely we define a combined rotation. There are two alternatives in defining this rotation, material form and spatial form. Material formulation is defined in the initial state of the vector and spatial form is associated to the present state of the vector. In this thesis only the material form is used.

The material form for compound rotation is (Cardona, et al., 1988)

$$\mathbf{R}_{\text{new}} = \mathbf{R}\mathbf{R}_{\text{inc}}^{\text{mat}} = \mathbf{R}\exp(\tilde{\boldsymbol{\Theta}}_{\text{R}}) \tag{5}$$

This formula defines a new rotation matrix consisting two consecutive rotations. The incremental rotation is written as function of incremental material rotation $\boldsymbol{\Theta}_{\text{R}}$. This material rotation is defined at the point $\mathbf{R}$ of the rotation space, see Figure 2. Rotation matrix has 9 components but due to the orthogonality only three independent components remain. Thus the rotation matrix defines a 3-dimensional surface to 9-dimensional space. This 3-dimensional group is called Special Orthogonal Group and it abbreviates to $SO(3)$. According to this the rotation matrix $\mathbf{R} \in SO(3)$.

The non-additive nature can be seen when equation (5) is modified by adding parameter t and differentiating to this parameter at $t = 0$ we get a tangent space at arbitrary material space point $\mathbf{R} \in SO(3)$ (Mäkinen, 2001).

$${}_{\text{mat}}T_{\mathbf{R}}SO(3) = \left\{ \tilde{\boldsymbol{\Theta}}_{\mathbf{R}} = (\mathbf{R}, \tilde{\boldsymbol{\Theta}}) \,\middle|\, \mathbf{R}\tilde{\boldsymbol{\Theta}}, \mathbf{R} \in SO(3), \tilde{\boldsymbol{\Theta}} \in so(3) \right\} \tag{6}$$

Figure 2 offers a graphic presentation of equation (6).

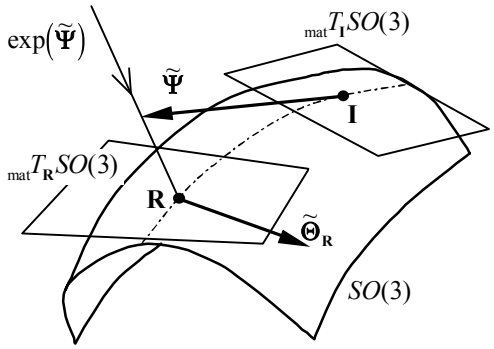

Figure 2 *Presentation of material rotations and their increments on the rotation space* $SO(3)$ *(Mäkinen, 2007)*

Together with equation (6) and Figure 2 we can see, that at the initial point **I** which belongs to tangent space ${}_{\text{mat}}T_{\mathbf{I}}SO(3)$ and at the point **R** where $\mathbf{R} \in {}_{\text{mat}}T_{\mathbf{R}}SO(3)$ the tangent spaces differ from each other. Therefore the rotations at three-dimensional cases are not additive. For further development of theory of finite rotations we need to find connection between the rotation vector $\boldsymbol{\Psi}$ and the material rotation increment vector $\boldsymbol{\Theta}_{\text{R}}$.

2.1.3 Connection between rotation vector and incremental rotation

In order to find connection between two vectors in different spaces we write yet again the equation (5) in a slightly different form. The rotation matrix can be presented using the exponential mapping of the skew symmetric matrix of the rotation vector $\boldsymbol{\Psi}$, see equation (3). By writing the left hand side of equation (5) with sum of the original rotation vector and a variation of the rotation vector $\delta\boldsymbol{\Psi}$ and introducing parameter t we get

$$\exp\left(\tilde{\boldsymbol{\Psi}} + t\,\delta\tilde{\boldsymbol{\Psi}}\right) = \exp\left(\tilde{\boldsymbol{\Psi}}\right)\exp\left(t\,\delta\tilde{\boldsymbol{\Theta}}_{\mathbf{R}}\right) \tag{7}$$

Objective is to find variation vector $\delta\boldsymbol{\Psi}$ that belongs to the same vector space as the original rotation vector $\boldsymbol{\Psi}$. By differentiating equation (7) to the parameter t following formulas emerge (Cardona, et al., 1988)

$$\begin{aligned}
&\delta\boldsymbol{\Theta}_{\mathbf{R}} = \mathbf{T}\cdot\delta\boldsymbol{\Psi} \\
&\mathbf{T} = \frac{\sin\psi}{\psi}\mathbf{I} - \frac{1-\cos\psi}{\psi^2}\tilde{\boldsymbol{\Psi}} + \frac{\psi-\sin\psi}{\psi^3}\boldsymbol{\Psi}\otimes\boldsymbol{\Psi} \\
&\psi = \left\|\boldsymbol{\Psi}\right\|, \quad \mathbf{R} = \exp(\tilde{\boldsymbol{\Psi}}), \quad \lim_{\boldsymbol{\Psi}\to\mathbf{0}}\mathbf{T}(\boldsymbol{\Psi}) = \mathbf{I}
\end{aligned} \tag{8}$$

Vector $\delta\boldsymbol{\Psi}$ is the variation of the total rotation vector $\boldsymbol{\Psi}$ and $\delta\boldsymbol{\Theta}_{\mathbf{R}}$ is the variation of the incremental material rotation vector. The most interesting matrix is the material tangential transformation matrix **T** because it is the linear mapping matrix dealing with the transformation between two vector spaces as ${}_{\text{mat}}T_{\mathbf{I}}SO(3) \rightarrow {}_{\text{mat}}T_{\mathbf{R}}SO(3)$.

Because $\delta\boldsymbol{\Psi}$ is defined in material space we can define new rotation vector as

$$\boldsymbol{\Psi}_{\text{new}} = \boldsymbol{\Psi} + \delta\boldsymbol{\Psi} \tag{9}$$

Equation (9) states that material rotation vectors are additive and therefore it is suitable to transform all incremental rotation vectors $\delta\boldsymbol{\Theta}_{\mathbf{R}}$ to rotation vector increments $\delta\boldsymbol{\Psi}$ because these vectors are additive when increments are considered small. The rotation vector itself can be large.

2.1.4 Time derivatives of the rotation vector

It has been stated that the rotation vector is additive in the material space and therefore it is suitable to use material angular velocities and accelerations. These vectors can also be presented by using the rotation vector and its time derivatives. Material angular velocity as skew symmetric matrix is defined by following formula (Cardona, et al., 1988)

$$\tilde{\boldsymbol{\Omega}}_{\mathbf{R}} = \mathbf{R}^{\mathrm{T}}\dot{\mathbf{R}} \in {}_{\text{mat}}T_{\mathbf{R}}SO(3) \tag{10}$$

Equation (10) states, that the angular velocity belongs to the rotation space, but the tangent space differs from the initial tangent space where the rotation vector is defined, see also Figure 2. For this reason it is practical to write the material angular velocity by using the rotation vector which belongs to the initial tangent space ${}_{\text{mat}}T_{\mathbf{I}}$. It also should be noted, that the rotation vectors does not belong to the special orthogonal group $SO(3)$ although it belongs to the tangent space at $\mathbf{I}$. The material angular velocity as function of the rotation matrix is (Cardona, et al., 1988)

$$\boldsymbol{\Omega}_{\mathbf{R}} = \mathbf{T}(\boldsymbol{\Psi})\cdot\dot{\boldsymbol{\Psi}}, \quad \boldsymbol{\Omega}_{\mathbf{R}} \in {}_{\text{mat}}T_{\mathbf{R}};\ \boldsymbol{\Psi}, \tilde{\boldsymbol{\Psi}} \in {}_{\text{mat}}T_{\mathbf{I}}, \tag{11}$$

where the material tangential vector space can be defined (Mäkinen, 2008)

$${}_{\text{mat}}T_{\mathbf{R}} = \left\{ \boldsymbol{\Theta}_{\mathbf{R}} \in \mathbf{E}^3 \,\middle|\, \tilde{\boldsymbol{\Theta}}_{\mathbf{R}} \in {}_{\text{mat}}T_{\mathbf{R}}SO(3) \right\} \tag{12}$$

For the equations of motion the angular acceleration vector is also needed and it is calculated by differentiating equation (11) as follows

$$\dot{\tilde{\boldsymbol{\Omega}}}_{\mathbf{R}} = \mathbf{T}\cdot\ddot{\boldsymbol{\Psi}} + \dot{\mathbf{T}}\cdot\dot{\boldsymbol{\Psi}}, \quad \dot{\boldsymbol{\Omega}}_{\mathbf{R}} \in {}_{\text{mat}}T_{\mathbf{R}};\ \ \boldsymbol{\Psi}, \dot{\boldsymbol{\Psi}}, \ddot{\boldsymbol{\Psi}} \in {}_{\text{mat}}T_{\mathbf{I}}, \tag{13}$$

Angular velocity and acceleration vectors can be presented using the rotation vector and it's time derivatives and the transformation matrix $\mathbf{T}$. From equation (8) we see that also

the transformation matrix is function of the rotation vector and therefore all rotational motion can be written using the rotation vector $\boldsymbol{\Psi}$.

2.2 Change of variables

In order to create elements with kinematic couplings, change of measurement system needs to be discussed. In this thesis so called master-slave technique is exploited. Basic idea in this technique is to express the slave displacements as function of the master displacements. This kinematic connection can be flexible or rigid and this technique can be used in various calculation cases.

The kinematic connection couples two measurement systems $\mathbf{u}$ and $\mathbf{v}$ (Marjamäki, et al., 2006)

$$\mathbf{u} = \mathbf{f}(\mathbf{v}) \tag{14}$$

where $\mathbf{f}$ is differentiable mapping between these two displacement vectors. At this point these vectors can be arbitrary. Important fact is that $\mathbf{u}$ is the slave displacement vector and thus $\mathbf{v}$ is the master displacement. Coupling between these quantities can be achieved by variating equation (14) (Marjamäki, et al., 2006)

$$\delta\mathbf{u} = D_{\mathbf{v}}\mathbf{f}(\mathbf{v})\cdot\delta\mathbf{v} = \mathbf{B}_{\mathrm{o}}(\mathbf{v})\cdot\delta\mathbf{v} \tag{15}$$

where subscript in $D_{\mathbf{v}}$ denotes that the mapping function $\mathbf{f}$ is differentiated to variable $\mathbf{v}$. This derivative is then definition for kinematic matrix $\mathbf{B}_{\mathrm{o}}$ for the chance of measurement. This kinematic matrix then relates virtual displacement vectors $\delta\mathbf{u}$ and $\delta\mathbf{v}$ together. Virtual work is invariant when the measurement system is changed and thereby stands (Marjamäki, et al., 2006)

$$\delta W = \delta\mathbf{u}\cdot\mathbf{F}_{\mathbf{u}} = \delta\mathbf{v}\cdot\mathbf{F}_{\mathbf{v}} \tag{16}$$

Substituting from equation (15) to (16) emerges connection between force vectors in different measurement systems

$$\mathbf{F}_{\mathbf{v}} = \mathbf{B}_{\mathrm{o}}^{\mathrm{T}}\mathbf{F}_{\mathbf{u}} \tag{17}$$

Tangent matrices are then calculated by linearizing above equation to direction $\Delta\mathbf{v}$.

$$\begin{aligned} Lin(\mathbf{F}_{\mathbf{v}};\Delta\mathbf{v}) &= \mathbf{B}_{\mathrm{o}}^{\mathrm{T}}\mathbf{F}_{\mathrm{u}_0} + \left(\mathbf{B}_{\mathrm{o}}^{\mathrm{T}}D_{\mathbf{v}}(\mathbf{F}_{\mathrm{u}}) + D_{\mathbf{v}}(\mathbf{B}_{\mathrm{o}}^{\mathrm{T}}\overline{\mathbf{F}_{\mathrm{u}}})\right)\cdot\Delta\mathbf{v} \\ &= \mathbf{F}_{\mathrm{v}_0} + \left(\mathbf{B}_{\mathrm{o}}^{\mathrm{T}}\mathbf{K}_{\mathrm{u}}\mathbf{B}_{\mathrm{o}} + \mathbf{K}_{g}\right)\cdot\Delta\mathbf{v} \end{aligned} \tag{18}$$

From (18) it can be seen, that stiffness matrix of the slave element is transformed to the master element stiffness matrix using the kinematic matrix $\mathbf{B}_o$. This kinematic connection also creates geometric stiffness matrix $\mathbf{K}_g$ to the system. (Marjamäki, et al., 2006).

Kinematic connection also introduces changes to mass matrix and therefore the virtual acceleration work is needed as

$$\delta W_{\text{acc}} = \delta \mathbf{u} \cdot (\mathbf{M}_u \ddot{\mathbf{u}}) \tag{19}$$

Time derivatives of the mapping (14) are as follows (Marjamäki, et al., 2006)

$$\begin{aligned} \dot{\mathbf{u}} &= \mathbf{B}_o \dot{\mathbf{v}} \\ \ddot{\mathbf{u}} &= \mathbf{B}_o \ddot{\mathbf{v}} + \dot{\mathbf{B}}_o \dot{\mathbf{v}} \end{aligned} \tag{20}$$

Substituting these time derivatives to virtual acceleration work and taking connection (15) into account equation (19) goes into form

$$\begin{aligned} \delta W_{\text{acc}} &= \delta \mathbf{v} \cdot \mathbf{B}_o^T \mathbf{M}_u \left(\mathbf{B}_o \ddot{\mathbf{v}} + \dot{\mathbf{B}}_o \dot{\mathbf{v}} \right) \\ &= \delta \mathbf{v} \cdot \left(\mathbf{B}_o^T \mathbf{M}_u \mathbf{B}_o \ddot{\mathbf{v}} + \mathbf{B}_o^T \mathbf{M}_u \dot{\mathbf{B}}_o \dot{\mathbf{v}} \right) \end{aligned} \tag{21}$$

From this equation the mass matrix and centrifugal force vector can be identified (Marjamäki, et al., 2006)

$$\begin{aligned} \mathbf{M}_v &= \mathbf{B}_o^T \mathbf{M}_u \mathbf{B}_o \\ \mathbf{F}_{\text{cent}} &= \mathbf{B}_o^T \mathbf{M}_u \dot{\mathbf{B}}_o \end{aligned} \tag{22}$$

From (22) it can be seen that whenever kinematic matrix $\mathbf{B}_o$ is function of the master displacements $\mathbf{v}$ mass matrix is depended on the configuration of the system. (Marjamäki, et al., 2006)

2.3 Mechanical elements

Finite element method is a fast and efficient way to perform structural analyses for different kinds of structures. Nowadays the element library is vast and there is suitable element for almost any kind of situation. In this work, the emphasis is on line bodies with bending stiffness and thereby beam element is suitable for this kind of analysis.

2.3.1 Geometrically exact beam element

In this master's thesis, Reissner's kinematically exact beam theory is applied for the mechanical structure and thereby this element is introduced in this chapter. Reissner's beam element can be applied for large displacements, large rotations and large deforma-

tions. This element also takes shear deformation into account. This shear deformation can be significant in case of high-profile beams (Mäkinen, 2007).

3D-beam has two nodes each having 6 degrees of freedom and total degrees of freedom is 12. In one node the freedoms are three translational freedoms and three rotational freedoms. In Reissner's beam theory translation and rotation interpolations are also independent.

For this thesis simple linear shape functions are used

$$N_1(s) = 1 - \frac{s}{L_0} \quad , \qquad N_2(s) = \frac{s}{L_0}, \quad s \in [0, L_0] \tag{23}$$

In equation (23) s is the coordinate along the neutral axis of the beam element in spatial configuration. Using these interpolation functions point at beam's neutral axis in spatial configuration can be written

$$\mathbf{x}_0(s) = N_1\mathbf{x}_1 + N_2\mathbf{x}_2 \tag{24}$$

where $\mathbf{x}_1$ and $\mathbf{x}_2$ are the spatial position vectors of the beam nodes as can be seen in Figure 3.

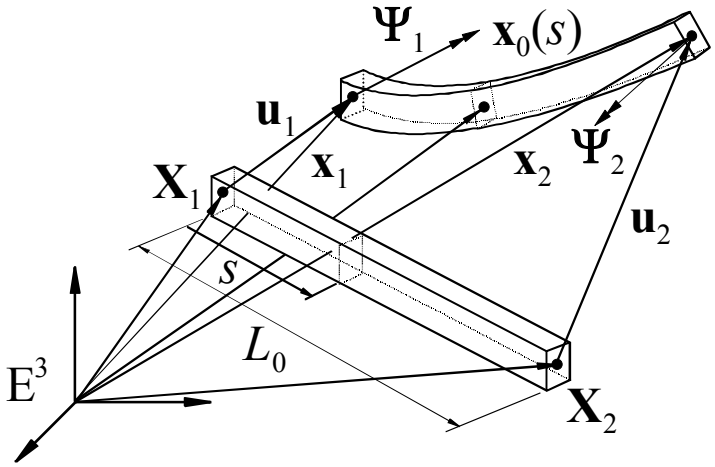

Figure 3 *Reissner's beam element in initial configuration and in deformed state (Marjamäki, et al., 2009)*

The material strain vector can then be written (Géradin, et al., 2001)

$$\mathbf{E} = \begin{pmatrix} \boldsymbol{\Gamma} \\ \mathbf{K} \end{pmatrix} = \begin{pmatrix} \Gamma_1 \\ \Gamma_2 \\ \Gamma_3 \\ K_1 \\ K_2 \\ K_3 \end{pmatrix} = \begin{pmatrix} \mathbf{R}^{\mathrm{T}}\mathbf{x}_0' - \mathbf{E}_1 \\ \mathbf{T}(\boldsymbol{\Psi})\boldsymbol{\Psi}' \end{pmatrix} \qquad (\bullet)' = d(\bullet)/ds \tag{25}$$

where Γ_i is material strain for the beam and K_i is the material curvature. For further derivation of the beam element strain vector (25) is variated yielding

$$\delta\mathbf{E} = \begin{pmatrix} \delta\boldsymbol{\Gamma} \\ \delta\mathbf{K} \end{pmatrix} = \begin{pmatrix} \mathbf{R}^{\mathrm{T}} & \mathbf{0} & \widetilde{\mathbf{R}^{\mathrm{T}}\mathbf{x}_0'}\mathbf{T} \\ \mathbf{0} & \mathbf{T} & \mathbf{C}_1(\boldsymbol{\Psi}', \boldsymbol{\Psi}) \end{pmatrix} \begin{pmatrix} \delta\mathbf{x}_0' \\ \delta\boldsymbol{\Psi}' \\ \delta\boldsymbol{\Psi} \end{pmatrix} \tag{26}$$

For the finite element formulation it is necessary to write this variation using nodal displacements $\mathbf{u} = (u_1, u_2, u_3, u_4, u_5, u_6, u_7, u_8, u_9, u_{10}, u_{11}, u_{12})$ we get (Marjamäki, et al., 2009)

$$\delta\mathbf{E} = \begin{pmatrix} \mathbf{R}^{\mathrm{T}} & \mathbf{0} & \widetilde{\mathbf{R}^{\mathrm{T}}\mathbf{x}_0'}\mathbf{T} \\ \mathbf{0} & \mathbf{T} & \mathbf{C}_1(\boldsymbol{\Psi}', \boldsymbol{\Psi}) \end{pmatrix} \mathbf{Q}\delta\mathbf{u} = \mathbf{B}\delta\mathbf{u}$$

$$\mathbf{Q} = \begin{pmatrix} N_1'\mathbf{I} & \mathbf{0} & N_2'\mathbf{I} & \mathbf{0} \\ \mathbf{0} & N_1'\mathbf{I} & \mathbf{0} & N_2'\mathbf{I} \\ \mathbf{0} & N_1\mathbf{I} & \mathbf{0} & N_2\mathbf{I} \end{pmatrix} \tag{27}$$

Using the kinematic matrix **B** it is now possible to write the internal force vector of the beam element. Matrix $\mathbf{C}_1$ is presented in Appendix A.

$$\mathbf{f}_{\mathrm{int}} = \int_{L_0} \mathbf{B}^{\mathrm{T}}\mathbf{S}\,ds \tag{28}$$

The domain of the integration is only the length parameter *s* in case of beam element because the area of the cross section can be determined without integration. The material stress resultant vector **S** is composed of force components N_i and moment components M_i (Géradin, et al., 2001)

$$\mathbf{S}=\begin{pmatrix}\mathbf{N}\\ \mathbf{M}_{\mathrm{R}}\end{pmatrix}=\begin{pmatrix}N\\ Q_2\\ Q_3\\ M_1\\ M_2\\ M_3\end{pmatrix}=\begin{pmatrix}EA & 0 & 0 & 0 & 0 & 0\\ 0 & GA_{\mathrm{zy}} & 0 & 0 & 0 & 0\\ 0 & 0 & GA_{\mathrm{sz}} & 0 & 0 & 0\\ 0 & 0 & 0 & GI_{\mathrm{x}} & 0 & 0\\ 0 & 0 & 0 & 0 & EI_{\mathrm{y}} & 0\\ 0 & 0 & 0 & 0 & 0 & EI_{\mathrm{z}}\end{pmatrix}\begin{pmatrix}\Gamma_1\\ \Gamma_2\\ \Gamma_3\\ K_1\\ K_2\\ K_3\end{pmatrix}=\mathbf{D}_2\boldsymbol{\varepsilon} \tag{29}$$

Matrix $\mathbf{D}_2$ is the constitutive matrix which appends corresponding force magnitude to deformation. Diagonal terms in matrix $\mathbf{D}_2$ are axial stiffness EA, the shear stiffness GA_{sy} and GA_{sz}, bending stiffness EI_{sy} and EI_{sz} and finally torsion stiffness GI_{v}. Tangential stiffness matrix is then formulated by directional derivative of the internal force in the direction of $\Delta\mathbf{u}$. In derivation product rule is used.

$$\mathbf{K}_{\mathrm{t}}=\int_{L_0}\mathbf{B}^{\mathrm{T}}\mathbf{D}_2\mathbf{B}\,ds+\int_{L_0}D_{\mathbf{u}}\mathbf{B}^{\mathrm{T}}\bar{\mathbf{S}}\,ds \tag{30}$$

The bar symbol over the stress resultant vector defines, that in derivation **S** is considered as constant vector. The first part in the integral (30) is the material stiffness matrix and the latter part is called the geometric stiffness matrix. The material stiffness matrix is fairly easy to calculate but the geometric part is more complicated (Mäkinen, 2007) and it is defined as directional derivative

$$D_{\mathbf{u}}\mathbf{B}^{\mathrm{T}}\bar{\mathbf{S}}=\mathbf{Q}^{\mathrm{T}}\begin{pmatrix}\mathbf{0} & \mathbf{0} & -\mathbf{R}\tilde{\mathbf{N}}\mathbf{T}\\ \mathbf{0} & \mathbf{0} & \mathbf{C}_2(\mathbf{M}_{\mathbf{R}},\boldsymbol{\Psi})\\ \mathbf{T}^{\mathrm{T}}\tilde{\mathbf{N}}\mathbf{R}^{\mathrm{T}} & \mathbf{C}_2^{\mathrm{T}}(\mathbf{M}_{\mathrm{R}},\boldsymbol{\Psi}) & \mathbf{C}_3(\mathbf{M}_{\mathrm{R}},\boldsymbol{\Psi},\boldsymbol{\Psi}')+\mathbf{C}_2(\tilde{\mathbf{N}}\mathbf{R}^{\mathrm{T}}\mathbf{x}_0',\boldsymbol{\Psi})+\mathbf{T}^{\mathrm{T}}\tilde{\mathbf{N}}\widetilde{\mathbf{R}^{\mathrm{T}}\mathbf{x}_{\mathrm{c}}'}\mathbf{T}\end{pmatrix}\mathbf{Q} \tag{31}$$

Matrices $\mathbf{C}_2$ and $\mathbf{C}_3$ are defined in Appendix A.

Mass matrix can be written in form of (Marjamäki, et al., 2009)

$$\mathbf{M}=\int_{L_0}\mathbf{P}^{\mathrm{T}}\begin{pmatrix}m\mathbf{I} & \mathbf{0}\\ \mathbf{0} & \mathbf{T}^{\mathbf{T}}\mathbf{J}\mathbf{T}\end{pmatrix}\mathbf{P}\,ds \tag{32}$$

where m is the beam mass density **P** is shape function matrix and **J** is the material inertia matrix

$$\mathbf{P}(s)=\begin{pmatrix}N_1\mathbf{I} & \mathbf{0} & N_1\mathbf{I} & \mathbf{0}\\ \mathbf{0} & N_2\mathbf{I} & \mathbf{0} & N_2\mathbf{I}\end{pmatrix} \tag{33}$$

$$\mathbf{J} = \int_{A_0} \rho \widetilde{\mathbf{Y}} \widetilde{\mathbf{Y}}^{\mathrm{T}} dA_0 \tag{34}$$

In equation (34) $\mathbf{Y} = X_2\mathbf{E}_2 + X_3\mathbf{E}_3$ and it defines location on the cross section of the beam.

For now we have derived tangential stiffness matrices from the internal force and the mass matrix of the beam element. Due to the inertia of mass also inertial forces occur in dynamical analysis of the beam element. The inertial force can be written in two parts; one that is depended only on mass and accelerations of the beam and second that derives from gyroscopic effects of the beam (Marjamäki, et al., 2009)

$$\begin{aligned} \mathbf{f}_{\mathrm{acc}} &= \mathbf{f}_{\mathrm{accA}} + \mathbf{f}_{\mathrm{accB}} \\ &= \mathbf{M}\ddot{\mathbf{u}} + \int_{L_0} \mathbf{P}(s)^{\mathrm{T}} \begin{pmatrix} \mathbf{0} \\ \mathbf{T}^{\mathrm{T}}(\mathbf{J}\dot{\mathbf{T}} + \widetilde{\boldsymbol{\Omega}}\mathbf{J}\mathbf{T})\dot{\boldsymbol{\Psi}} \end{pmatrix} ds \end{aligned} \tag{35}$$

When these terms are linearized in direction of $\Delta\ddot{\mathbf{u}}$ mass matrix (32) is obtained. There is also possibility to linearize these terms in direction of $\Delta\dot{\mathbf{u}}$ and $\Delta\mathbf{u}$. When these linearizations are completed gyroscopic damping matrix and centrifugal stiffness matrix can be written respectively (Mäkinen, 2007)

$$\mathbf{C}_{\mathrm{gyro}} = \mathbf{T}^{\mathrm{T}} \left[\left(\widetilde{\boldsymbol{\Omega}}\mathbf{J} - \widetilde{\mathbf{J}\boldsymbol{\Omega}} \right) \mathbf{T} + \mathbf{J}\mathbf{C}_4(\dot{\boldsymbol{\Psi}}, \boldsymbol{\Psi}) \right] \tag{36}$$

$$\begin{aligned} \mathbf{K}_{\mathrm{cent}} = \mathbf{C}_2(\boldsymbol{\Omega}\mathbf{J}\boldsymbol{\Omega} + \mathbf{J}\dot{\boldsymbol{\Omega}}, \boldsymbol{\Psi}) + \mathbf{T}^{\mathrm{T}} \cdot \left(\tilde{\boldsymbol{\Omega}}\mathbf{J} - \widetilde{\mathbf{J}\boldsymbol{\Omega}} \right) \mathbf{C}_1(\dot{\boldsymbol{\Psi}}, \boldsymbol{\Psi}) + \\ + \mathbf{T}^{\mathrm{T}}\mathbf{J} \cdot \left(\mathbf{C}_5(\dot{\boldsymbol{\Psi}}, \boldsymbol{\Psi}) + \mathbf{C}_1(\ddot{\boldsymbol{\Psi}}, \boldsymbol{\Psi}) \right) \end{aligned} \tag{37}$$

Matrices $\mathbf{C}_4$ and $\mathbf{C}_5$ are defined in Appendix A.

All of these matrices and vectors that are introduced in this chapter are computed for each element individually and then using normal procedures the global stiffness, damping and mass matrices are calculated. For the solution process also internal force vectors and inertial vectors are computed.

2.3.2 Offset beam element

In beam element the nodes are located at the ends of the element and on the center axis of the element. This modeling is effective for instance in boom modeling where several beams are connected together and the centerline of the boom is straight. However, in several situations it is useful to change the location of the nodes for example in cases when hydraulic cylinder is connected to the beam. Usually cylinder is connected to the boom via plate lug and the connection point is not on the central axis of the element.

Therefore it is useful to create offset beam element where the nodes of the beam can be transferred to wanted locations. This connection is considered to be rigid in this context.

In Figure 4 there is a presentation of the offset beam element. In this Figure 4 displacement **u** is the slave displacement vector and **v** is the actual master displacement vector.

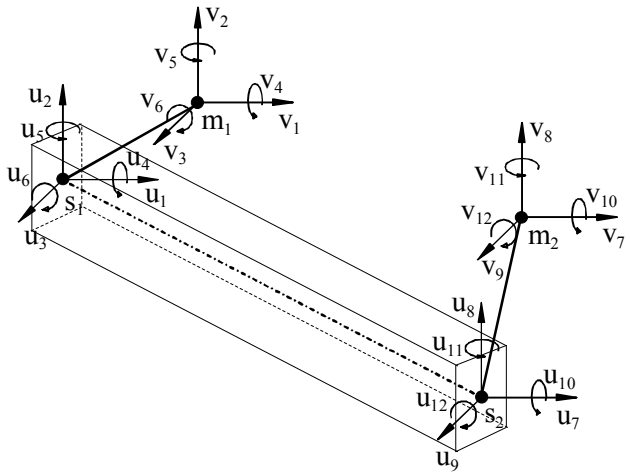

Figure 4 *Reissner's offset beam element (Marjamäki, et al., 2006)*

To shorten the following expressions only the first node is inspected. The slave and master displacement vectors are

$$\begin{aligned}\mathbf{u}_1 &= \left(u_1, u_2, u_3, u_4, u_5, u_6\right) = \begin{pmatrix}\mathbf{d}_{s1}\\ \boldsymbol{\Psi}_{s1}\end{pmatrix}\\ \mathbf{v}_1 &= \left(v_1, v_2, v_3, v_4, v_5, v_6\right) = \begin{pmatrix}\mathbf{d}_{m1}\\ \boldsymbol{\Psi}_{m1}\end{pmatrix}\end{aligned} \tag{38}$$

where subscript *s* denotes slave and *m* denotes master. Equation (38) merely shows that the displacement vector in one node can be divided to displacement vector **d** and to rotation vector $\boldsymbol{\Psi}$. Because rigid connection was assumed between the master and slave nodes connection between master and slave rotations is (Marjamäki, et al., 2006)

$$\boldsymbol{\Psi}_{m1} = \boldsymbol{\Psi}_{s1} = \boldsymbol{\Psi}_1 \tag{39}$$

For the displacement relation offset vector in initial configuration is defined as

$$\mathbf{X}_{s1/m1} = \mathbf{X}_{s1} - \mathbf{X}_{m1} \tag{40}$$

Using this vector and the assumption of rigid connection the slave nodes current location can be expressed using the master node

$$\mathbf{x}_{s1} = \mathbf{x}_{m1} + \mathbf{R}_1 \mathbf{X}_{s1/m1} \tag{41}$$

where $\mathbf{R}_1 = \exp(\tilde{\boldsymbol{\Psi}}_1)$. By variating expression (41) connection between virtual placements is achieved (Marjamäki, et al., 2006)

$$\delta\mathbf{x}_{s1} = \delta\mathbf{x}_{m1} + \delta\mathbf{R}_1 \mathbf{X}_{s1/m1} \tag{42}$$

Material variation for the rotation matrix is

$$\delta\mathbf{R}_1\mathbf{X}_{s1/m1} = \mathbf{R}_1\delta\tilde{\boldsymbol{\Theta}}_1\mathbf{X}_{s1/m1} = -\mathbf{R}_1\tilde{\mathbf{X}}_{s1/m1}\delta\boldsymbol{\Theta}_1 = -\mathbf{R}_1\tilde{\mathbf{X}}_{s1/m1}\mathbf{T}_1\delta\boldsymbol{\Psi}_1 \tag{43}$$

where equation (8). Using (43) the kinematic matrix for offset can be formulated. In this matrix both nodes are taken into account (Marjamäki, et al., 2006)

$$\mathbf{B}_o = \begin{pmatrix} \mathbf{I}_{3x3} & -\mathbf{R}_1\tilde{\mathbf{X}}_{s1/m1}\mathbf{T}_1 & \mathbf{0} & \mathbf{0} \\ \mathbf{0} & \mathbf{I}_{3x3} & \mathbf{0} & \mathbf{0} \\ \mathbf{0} & \mathbf{0} & \mathbf{I}_{3x3} & -\mathbf{R}_2\tilde{\mathbf{X}}_{s2/m2}\mathbf{T}_2 \\ \mathbf{0} & \mathbf{0} & \mathbf{0} & \mathbf{I}_{3x3} \end{pmatrix} \tag{44}$$

For the geometric stiffness matrix in (18) following derivative is needed

$$D_{\mathbf{v}}(\mathbf{B}_o^{\mathrm{T}}\overline{\mathbf{F}_u}) = D_{\mathbf{v}}\begin{pmatrix} \overline{\mathbf{F}}_{u,1\text{-}3} \\ \mathbf{T}_1^{\mathrm{T}}\tilde{\mathbf{X}}_{s1/m1}\mathbf{R}_1^{\mathrm{T}}\cdot\overline{\mathbf{F}}_{u,1\text{-}3} + \overline{\mathbf{F}}_{u,4\text{-}6} \\ \overline{\mathbf{F}}_{u,7\text{-}9} \\ \mathbf{T}_2^{\mathrm{T}}\tilde{\mathbf{X}}_{s2/m2}\mathbf{R}_2^{\mathrm{T}}\cdot\overline{\mathbf{F}}_{u,7\text{-}9} + \overline{\mathbf{F}}_{u,10\text{-}12} \end{pmatrix} = \begin{pmatrix} \mathbf{0} & \mathbf{0} & \mathbf{0} & \mathbf{0} \\ \mathbf{0} & \mathbf{A}_1 & \mathbf{0} & \mathbf{0} \\ \mathbf{0} & \mathbf{0} & \mathbf{0} & \mathbf{0} \\ \mathbf{0} & \mathbf{0} & \mathbf{0} & \mathbf{A}_2 \end{pmatrix} \tag{45}$$

In this equation $\overline{\mathbf{F}}_{u,i}$ denote components of the slave element internal force vector. Submatrices in (45) can be written in form (Marjamäki, et al., 2006)

$$\begin{aligned} \mathbf{A}_1 &= \mathbf{C}_2\left(\tilde{\mathbf{X}}_{s1/m1}\mathbf{R}_1^{\mathrm{T}}\cdot\overline{\mathbf{F}}_{u,1\text{-}3}, \boldsymbol{\Psi}_1\right) + \mathbf{T}_1^{\mathrm{T}}\tilde{\mathbf{X}}_{s1/m1}\mathbf{R}_1^{\mathrm{T}}\cdot\overline{\mathbf{F}}_{u,1\text{-}3}\mathbf{T}_1 \\ \mathbf{A}_2 &= \mathbf{C}_2\left(\tilde{\mathbf{X}}_{s2/m2}\mathbf{R}_2^{\mathrm{T}}\cdot\overline{\mathbf{F}}_{u,7\text{-}9}, \boldsymbol{\Psi}_2\right) + \mathbf{T}_2^{\mathrm{T}}\tilde{\mathbf{X}}_{s2/m2}\mathbf{R}_2^{\mathrm{T}}\cdot\overline{\mathbf{F}}_{u,7\text{-}9}\mathbf{T}_2 \end{aligned} \tag{46}$$

where matrix $\mathbf{C}_2$ is defined in Appendix A.

Using equations presented in this chapter and in chapter 2.2 it is now possible to formulate tangential matrices for the offset beam element.

2.3.3 Length controlled rod element

The simplest way to model hydraulic cylinder in mechanical system is to use variable length rod element. In this element, it is possible to change the unstressed length L_c of the rod element as function of time as $L_c = L_0 + L(t)$ where L_0 is the initial length of the bar. Initial length of the rod element can be expressed using the nodal coordinates $\mathbf{X} = (X_1, Y_1, X_2, Y_2, X_3, Y_3)^T$ and symmetric matrix $\mathbf{A_r}$ as follows in equation (47)

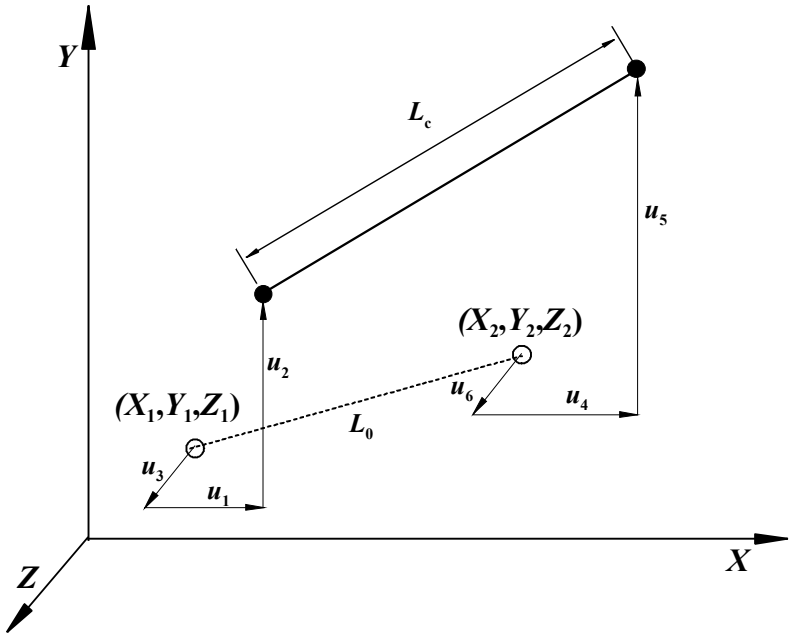

Figure 5 *Rod element at initial state with dotted line and element in current configuration solid line (Marjamäki, et al., 2006)*

$$L_0 = \sqrt{\mathbf{X}^T \mathbf{A}_r \mathbf{X}} \tag{47}$$

$$\mathbf{A}_r = \begin{pmatrix} 1 & 0 & 0 & -1 & 0 & 0 \\ 0 & 1 & 0 & 0 & -1 & 0 \\ 0 & 0 & 1 & 0 & 0 & -1 \\ -1 & 0 & 0 & 1 & 0 & 0 \\ 0 & -1 & 0 & 0 & 1 & 0 \\ 0 & 0 & -1 & 0 & 0 & 1 \end{pmatrix}$$

Due to loads the rod undergoes deformations and the square of the stressed length of the rod element at time *t* can be written as

$$L_c^2 = (\mathbf{X} + \mathbf{u})^T \mathbf{A}_r (\mathbf{X} + \mathbf{u}) = \mathbf{x}^T \mathbf{A}_r \mathbf{x} \tag{48}$$

where vector $\mathbf{u} = (u_1, u_2, u_3, u_4, u_5, u_6)$ is the nodal displacement vector. For non-linear finite element analysis we choose to use Green's strain instead of engineering strain. Green's strain can then be expressed

$$\varepsilon_{\mathrm{G}} = \frac{L_{\mathrm{c}}^2 - L_0^2}{2L_0^2} \tag{49}$$

For the internal force vector the variation of the Green strain is needed and it can be calculated as

$$\delta\varepsilon_{\mathrm{G}} = \frac{L_{\mathrm{c}}}{L_0^2}\delta L_c = \frac{1}{L_0^2}\mathbf{x}^{\mathrm{T}}\mathbf{A}_{\mathbf{r}}\delta\mathbf{u} = \mathbf{B}_{\mathbf{r}}\delta\mathbf{u} \tag{50}$$

In equation (50) matrix $\mathbf{B_r}$ is kinematic matrix for bar element and it connects virtual strain to virtual nodal displacements. Using these formulas the internal force of a rod element can then be written

$$\mathbf{f}_{\mathrm{int}} = \int_{V_0} \mathbf{B}_{\mathbf{r}}^{\mathrm{T}}\sigma_{\mathrm{G}}\,dV_0 = \frac{A_0 E\varepsilon_{\mathrm{G}}}{L_0}\mathbf{A}_{\mathbf{r}}\mathbf{x} \tag{51}$$

where A_0 is the initial area of the cross-section and E is the elastic modulus. The stress magnitude σ_{G} is stress component related to the initial area A_0. In other words it is component of the second Piola-Kirchhoff stress tensor. Property of this stress is that it has no physical interpretation because second Piola-Kirchhoff is related to the initial cross section in initial rod configuration. The real stress related to the current cross section in current configuration is the Cauchy stress and it can be calculated from the second Piola-Kirchhoff stress by using scale factor $\sigma_{\mathrm{C}} = L_{\mathrm{n}}/L_{\mathrm{c}}\sigma_{\mathrm{G}}$.

The stiffness matrix is achieved by linearization of the internal force vector to direction $\Delta\mathbf{u}$. Linearization can also be interpreted as directional derivative to direction $\Delta\mathbf{u}$.

$$\begin{aligned} Lin(\mathbf{f}_{\mathrm{int}};\Delta\mathbf{u}) &= \mathbf{f}_{\mathrm{int0}} + \left(\frac{A_0\sigma_G}{L_n}\mathbf{A}_{\mathbf{r}} + \left(\frac{EA_0}{L_n^2 L_c} - \frac{A_0\sigma_G}{L_n^3}\right)\mathbf{A}_{\mathbf{r}}\mathbf{x}\mathbf{x}^{\mathrm{T}}\mathbf{A}_{\mathbf{r}}\right)\bullet\Delta\mathbf{u} \\ &= \mathbf{f}_{\mathrm{int0}} + \left(\mathbf{K}_{\mathbf{E}} + \mathbf{K}_{\sigma}\right)\bullet\Delta\mathbf{u} \end{aligned} \tag{52}$$

This linearization produces two different stiffness matrixes, $\mathbf{K_E}$ and $\mathbf{K}_\sigma$ and they are called material and geometric stiffness matrices respectively.

Because the current unstressed length of the bar L_{c} is function of time the linearization procedure could be done also in direction of time increment Δt but usually these terms are small in comparison and this derivative is neglected.

Mass matrix is also needed for the equation of motion of the bar element. To obtain this matrix we write the virtual work of the acceleration forces and take normal linear interpolation in account

$$\delta W_{acc} = \int_{V_0} \delta\left(\mathbf{N}_\mathrm{r}\mathbf{u}\right) \bullet \rho\left(\mathbf{N}_\mathrm{r}\ddot{\mathbf{u}}\right) dV_0 = \delta\mathbf{u} \bullet \int_{V_0} \rho \mathbf{N}_\mathrm{r}^\mathrm{T} \mathbf{N}_\mathrm{r} dV_0 \, \ddot{\mathbf{u}} = \delta\mathbf{u} \bullet \mathbf{M}\ddot{\mathbf{u}} \tag{53}$$

where ρ is the density of the rod and matrix $\mathbf{N}_\mathrm{r}$ contains element shape functions as follows

$$\mathbf{N}_\mathbf{r} = \begin{pmatrix} 1-\xi & 0 & \xi & 0 \\ 0 & 1-\xi & 0 & \xi \end{pmatrix} \qquad \xi \in \left[0, L_0\right] \tag{54}$$

Rod element is interpolated using linear shape functions as is the Reissner's beam element.

2.3.4 Spring element

Spring elements are used in the CMM model to represent the flexibility of the bearings. Spring elements are also connecting the end defector to the manipulator lift arm. In this chapter simple linear translation spring element is presented. This spring element is zero length element in initial configuration. Therefore the length of the element can be calculated using only the nodal displacement vector $\mathbf{u} = (u_1, u_2, u_3, u_4, u_5, u_6)$ using formula very close to equation (47). The strain energy of the spring is

$$W_{\mathrm{int}} = \frac{1}{2} k_\mathrm{s} \mathbf{u}^\mathbf{T} \mathbf{A}_\mathbf{s} \mathbf{u} \tag{55}$$

where matrix $\mathbf{A_s}$ is introduced in equation (47) as $\mathbf{A_r}$ and k_s is the spring constant of the spring. Internal force vector is then calculated by differentiating the strain energy to the displacement vector yielding

$$\mathbf{f_{int}} = k_\mathrm{s} \mathbf{A}_\mathbf{s} \mathbf{u} \tag{56}$$

Finally the stiffness matrix of the spring element is calculated by linearizing the internal force vector

$$\begin{aligned} Lin(\mathbf{f}_{\mathrm{int}}; \Delta\mathbf{u}) &= \mathbf{f}_{\mathrm{int0}} + k_\mathrm{s} \mathbf{A}_\mathrm{s} \bullet \Delta\mathbf{u} \\ &= \mathbf{f}_{\mathrm{int0}} + \left(\mathbf{K_E}\right) \bullet \Delta\mathbf{u} \end{aligned} \tag{57}$$

2.4 Transmission line elements

Transmission lines are the basic elements used in hydraulic systems because hydraulic components are joined together by hydraulic pipes. Therefore modeling of these transmission lines is essential part when the hydraulic system is simulated. For the mathematical model of these pipes some assumptions are made. First of all the flow has to be laminar and motion in the radial direction is negligible. In laminar flow all particles are traveling parallel whereas in turbulent flow there are vortices which make modeling much harder. Therefore we are confined to laminar flows only. Fluid is also restricted to be Newtonian. In Newtonian fluid the stress-strain connection is linear. When the pipes themselves are considered the walls of the pipes are considered rigid and material properties are constant. (Mäkinen, et al., 2000)

2.4.1 Starting points for the transmission line elements

This chapter introduces the mathematical background of the transmission line elements. The derivation starts with differential equations of continuity and momentum and then the solution is presented. This chapter is based on paper by Mäkinen et al in 2000.

Basic formulas for the volume flow in pipe can be derived from the momentum and continuity conditions by taking differential control volumes and studying the conservation of mass and conservation of momentum. Study of these differential control volumes leads to governing differential equations and they can be expressed in Laplace transformed forms as follows in equations (58) and (59) (Mäkinen, et al., 2000). In Laplace transformation magnitudes have been transformed from time domain to frequency domain to help the solution of the problem.

$$\frac{dP(x,\overline{s})}{dx} = -\frac{Z_0\Gamma^2(\overline{s})}{L\overline{s}}Q(x,\overline{s}) \tag{58}$$

$$\frac{dQ(x,\overline{s})}{dx} = -\frac{\overline{s}}{LZ_0}P(x,\overline{s}), \qquad x \in (0,L), \qquad \overline{s} \in \mathbb{C} \tag{59}$$

In these equations (58) and (59) P and Q are Laplace transformed mean pressure and mean flow rate and x is the coordinate on the pipe. The series impedance is defined as $Z_0 = (\rho_0 c_0) / (\pi r_0^2)$, where ρ_0 is the density of fluid, c_0 is the speed of sound, and r_0 is the inner radius of the pipe. The wave time is defined as $T = L / c_0$, where L is the length of transmission line. Symbol ν_0 is the mean kinematic viscosity. Using definitions from above normalized Laplace variable is $\overline{s} = Ts$. Γ^2 is a propagation operator defining the friction model that is used.

We can see that equations (58) and (59) are both functions of Q and P. We can eliminate volume flow by solving Q from the equation (58) and substituting it into equation

(59) giving equation (60). This equation is then ordinary second degree differential equation.

$$-L^2 \frac{d^2 P(x)}{dx^2} + \Gamma^2 P(x) = 0 \qquad x \in (0, L) \tag{60}$$

For differential equations we have three types of boundary conditions, essential, natural and mixed boundary conditions. In essential boundary conditions we have values of the function at the end of the domain as given values whereas in natural boundary conditions we have values of the function derivatives as given values. In mixed boundary conditions we have both essential and natural boundary values given at the end of the domain (Reddy, 1986 pp. 155-158). Natural boundary conditions for equation (60) can be achieved from equation (58) and they are when inflow is assumed positive

$$P'(0) = -\frac{Z_0 \Gamma^2}{L\bar{s}} Q_0, \qquad P'(L) = \frac{Z_0 \Gamma^2}{L\bar{s}} Q_1 \tag{61}$$

Apostrophe symbol denotes derivative with respect to coordinate x. Essential boundary conditions are in (62) and mixed boundary conditions are in equation (63).

$$P(0) = P_0, \qquad P(L) = P_1 \tag{62}$$

$$P(0) = P_0, \qquad P'(L) = \frac{Z_0 \Gamma^2}{L\bar{s}} Q_1 \tag{63}$$

Naturally we can derive similar equations if we eliminate pressure P from equations (58) and (59) which leads to governing differential equation (64) and we get natural boundary conditions (65) and essential boundary conditions (66) and mixed boundary conditions

$$-L^2 \frac{d^2 Q(x)}{dx^2} + \Gamma^2 Q(x) = 0 \qquad x \in (0, L) \tag{64}$$

$$Q'(0) = -\frac{\bar{s}}{LZ_0} P_0, \qquad Q'(L) = -\frac{\bar{s}}{LZ_0} P_1 \tag{65}$$

$$Q(0) = Q_0, \qquad Q(L) = Q_1 \tag{66}$$

$$Q(0) = Q_0, \qquad Q'(L) = -\frac{\bar{s}}{LZ_0} P_1 \tag{67}$$

There are two differential equations and three boundary conditions for each differential equation. It means, that six different transmission line models can be defined by solving the differential equations.

Solution for these equations is searched by applying variation method. The variation form of the equation (60) can be achieved by multiplying the equation with admissible variation δP and integrating the expression over the domain.

$$\int_0^L \delta P(-L^2 P'' + \Gamma^2 P)dx = 0 \tag{68}$$

Integrating by parts and noticing the natural boundary conditions (61) in the substitution term we get equation (69). The objective is to find *P(x)* that it applies for all admissible variations δP.

$$\int_0^L (L^2 P'\delta P' + \Gamma^2 P\delta P)dx = LZ_0 \frac{\Gamma^2}{\bar{s}}(Q_1\delta P_1 + Q_0\delta P_0) \tag{69}$$

If we use essential boundary conditions we get equation (70) and with mixed boundary conditions equation (71).

$$\int_0^L (L^2 P'\delta P' + \Gamma^2 P\delta P)dx = 0 \tag{70}$$

$$\int_0^L (L^2 P'\delta P' + \Gamma^2 P\delta P)dx = LZ_0 \frac{\Gamma^2}{\bar{s}}(Q_1\delta P) \tag{71}$$

Variation forms for the flow rate differential equation (64) can be derived in the same manner as equation (68) presents. However, in this case the goal is to find *Q(x)* that applies for all admissible variations δQ. As we can now see, there are six different transmission line models than can be used.

Solution for these variation problems is sought using Ritz method. Ritz method is approximation technique where approximation is sought by using sum of arbitrary base functions (Reddy, 1986 p. 259). Approximation for the pressure can be given as

$$\tilde{P}(x) = \sum_{j=1}^{n} p_j \psi_j(x) \tag{72}$$

where $\psi_j(x)$ is linearly independent set of functions and p_j are known as the Ritz coefficients and *j* is the number of approximation functions (Reddy, 1986 p. 259). It has to be noticed that the trial function $\tilde{P}(x)$ has to fulfill the requirements set by the boundary conditions.

For the variation form (69) the approximation function can be written in form (73).

$$\tilde{P}(x) = \sum_{j=0}^{n} p_j \cos\left(\frac{j\pi x}{L}\right) \tag{73}$$

In this case the approximation is sought as a cosine series and it reveals that these series represents the eigenmodes of the problem. When these eigenmodes are used as interpolation functions, the solution method is called spectral element method. In spectral methods solution is sought using series of smooth functions and it is very useful in fluid dynamics as is the case now (Gottlieb, et al., 1977). Similar approximations can be written for all the other models as well and they are presented in Mäkinen et al. (2000).

Finally the propagation operator Γ^2 needs to be treated. The operator represents the friction model to the transmission lines. It can be written as follows in equation (74) (Mäkinen, et al., 2000)

$$\Gamma^2(\bar{s}) = \begin{cases} \bar{s}^2 & \text{lossless flow} \\ \bar{s}^2 + \varepsilon\bar{s} & \text{linear friction flow} \\ \dfrac{\bar{s}^2}{1 - \dfrac{2J_1(\kappa)}{\kappa J_0(\kappa)}} & \text{dissipative flow} \end{cases} \tag{74}$$

where $\kappa^2 = -8\bar{s}/\varepsilon$ and the friction coefficient $\varepsilon = 8\nu_0 L/r_0^2 c_0$. In dissipative flow J_0 and J_1 are Bessel functions. From these alternatives the dissipative flow model is the only including frequency dependent friction effect and thereby it is the best alternative for the transmission line models. Viscous friction increases with frequency because the velocity profile of the flow changes as function of the frequency. The higher the specific frequency is the flatter the velocity profile is compared to the parabolic profile of the steady flow. This happens because shear stresses of the fluid become higher near the walls of the pipe. Bessel functions arise when solving the Bessel's differential equation in the dissipative model. Next thing is to approximate the propagation operator and many suggestions are available. In this context the propagation operator is treated as in Mäkinen et al. (2000) suggests. The denominator of the operator is approximated in quadratic form as is presented in equation (75)

$$\Gamma^2(\bar{s}) + \alpha^2 \approx \bar{s}^2 + \bar{s}\varepsilon_i + \omega_i^2 \tag{75}$$

Thus we get the natural modal frequency ω_i and the modal damping coefficient ε_i and they can be expressed as follows

$$\omega_i = \alpha_i - \frac{1}{4}\sqrt{\alpha_i\varepsilon} + \frac{1}{16}\varepsilon, \quad \varepsilon_i = \frac{1}{2}\sqrt{\alpha_i\varepsilon} + \frac{1}{8}\varepsilon, \quad \varepsilon = \frac{8\nu_0 L}{r_0^2 c_0}, \quad i = 1,2,...,n \tag{76}$$

The attenuation factors with Riemann windowing are $w_i = \sin \beta_i / \beta_i$ .For the Q-model, the model parameters can be written.

$$\alpha_i = i\pi, \quad \beta_i = \frac{i\pi}{n+1}, \quad b_n = \left(8 \sum_{i=1,3,\ldots}^{n-1} w_i / \omega_i^2 \right)^{-1} \tag{77}$$

Windowing is needed because modeling technique is based on approximating smooth solutions and small amount of modes. When solutions are not smooth numerical approximation introduces spurious oscillation known as Gibbs phenomenon. Using windowing we can smoothen the solution and therefore we get better results.

2.4.2 Space state realization of transmission line elements

From these starting points we can focus on the space state realization of the transmission line elements. Pipe elements have two nodes and there are three different pipe models: Q-model, P-model and PQ model. These models are presented in Figure 6.

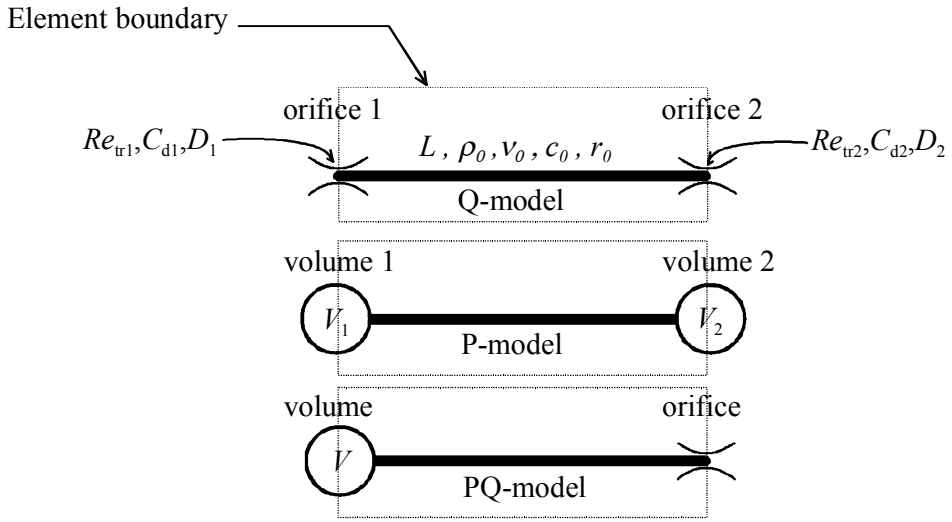

Figure 6 *Three pipe models. From top to bottom Q-model, P-model and PQ-model*

In Q-model flow rates at the ends of the pipes are given as inputs and then pressures are calculated within the domain of the element. This pipe element model can be used in situations where pipe connects components with negligible volumes such as directional valves. The P-model is opposite to the Q-model because it has pressures as given input and then volume flows are calculated from the pressure differences. The P-model is used to connect components with large volume but negligible resistance. The PQ-model is a hybrid of these two elements and it is exploited when the other end of the pipe is connected to volume and other end can be connected directly to an orifice.

These three models are introduced in paper by Mäkinen et al. (2000) where models are introduced mainly in transformation function form. In this thesis only state space realization is considered. State space realization is easier to implement into program-

ming environments because it produces ordinary differential equations. For the time integration we also need Jacobian matrixes and they can be derived by differentiating the state equation. First we deal with the pipes themselves without taking any consideration of the orifices or volumes at the ends of the pipes. Thereby following equations apply only in the domain of the pipe.

For the Q-model the state space realization can be written as follows in equation (78). The Q-model can be derived from equations (60) and (61).

$$\begin{aligned} \dot{\mathbf{x}} &= \mathbf{A}\mathbf{x} + \mathbf{B}\mathbf{Q} \\ \mathbf{P} &= \mathbf{C}\mathbf{x} \end{aligned} \tag{78}$$

where the **x** is the state variable vector, in this case it contains pressures, **Q** is the input vector and **P** is the output vector. These vectors can be written as follows (79). In these formulas *n* modes can be calculated for the pressure.

$$\mathbf{Q} = \begin{pmatrix} Q_1 & Q_2 \end{pmatrix}^{\mathrm{T}}, \quad \mathbf{P} = \begin{pmatrix} P_1 & P_2 \end{pmatrix}^{\mathrm{T}}, \quad \mathbf{x} = \begin{pmatrix} p_0 & r_1 & p_1 & \cdots & r_n & p_n \end{pmatrix}^{\mathrm{T}} \tag{79}$$

The state space matrices can now be written as

$$\mathbf{A} = \operatorname{diag}\left(0, \mathbf{A}_1, \mathbf{A}_2, \ldots, \mathbf{A}_n\right), \quad \mathbf{A}_i = \begin{pmatrix} 0 & -\dfrac{\omega_i^2}{T^2} \\ 1 & -\dfrac{\varepsilon_i}{T} \end{pmatrix}$$

$$\mathbf{B} = \begin{pmatrix} \mathbf{B}_0 \\ \mathbf{B}_1 \\ \vdots \\ \mathbf{B}_n \end{pmatrix}_{2n+1\times 2} \qquad \begin{aligned} \mathbf{B}_0 &= \frac{Z_0}{T}\begin{pmatrix} 1 & -1 \end{pmatrix} \\ \mathbf{B}_{2i-1} &= \frac{2Z_0 w_{2i-1}}{T^2}\begin{pmatrix} \varepsilon b_n & \varepsilon b_n \\ T & T \end{pmatrix} \\ \mathbf{B}_{2i} &= \frac{2Z_0 w_{2i}}{T^2}\begin{pmatrix} \varepsilon & -\varepsilon \\ T & -T \end{pmatrix} \end{aligned} \tag{80}$$

$$\mathbf{C} = \begin{pmatrix} 1 & 0 & 1 & 0 & 1 & 0 & 1 & \cdots \\ 1 & 0 & -1 & 0 & 1 & 0 & -1 & \cdots \end{pmatrix}_{2\times 2n+1}$$

The modal damping coefficient and modal frequencies can be calculated using equations (76) and windowing parameters are presented in equation (77).

For the P-model we can write same kind of connections as we wrote for the Q-model and it is derived from equations (64) and (65). The space state realization can be written as

$$\begin{aligned} \dot{\mathbf{x}} &= \mathbf{A}\mathbf{x} + \mathbf{B}\mathbf{P} \\ \mathbf{Q} &= \mathbf{C}\mathbf{x} \end{aligned} \tag{81}$$

where the **x** is the state variable vector, in this case it contains volume flows, P is the input vector and **Q** is the output vector and they are expressed as

$$\mathbf{P} = \begin{pmatrix} P_1 & P_2 \end{pmatrix}^{\mathrm{T}}, \quad \mathbf{Q} = \begin{pmatrix} Q_1 & Q_2 \end{pmatrix}^{\mathrm{T}}, \quad \mathbf{x} = \begin{pmatrix} q_0 & r_1 & q_1 & \cdots & r_n & q_n \end{pmatrix}^{\mathrm{T}} \tag{82}$$

And finally the state space matrices are

$$\begin{aligned} \mathbf{A} &= \operatorname{diag}\left(-\frac{\varepsilon}{T}, \mathbf{A}_1, \mathbf{A}_2, \ldots, \mathbf{A}_n \right), \qquad \mathbf{A}_i = \begin{pmatrix} 0 & -\dfrac{\omega_i^2}{T^2} \\ 1 & -\dfrac{\varepsilon_i}{T} \end{pmatrix} \\ \mathbf{B} &= \begin{pmatrix} \mathbf{B}_0 \\ \mathbf{B}_1 \\ \vdots \\ \mathbf{B}_n \end{pmatrix}_{2n+1\times 2} \quad \begin{aligned} \mathbf{B}_0 &= \frac{1}{T}\begin{pmatrix} 1 & -1 \end{pmatrix} \\ \mathbf{B}_{2i-1} &= \frac{2w_{2i-1}}{TZ_0}\begin{pmatrix} 0 & 0 \\ 1 & 1 \end{pmatrix}, \\ \mathbf{B}_{2i} &= \frac{2w_{2i}}{TZ_0}\begin{pmatrix} 0 & 0 \\ 1 & -1 \end{pmatrix} \end{aligned} \\ \mathbf{C} &= \begin{pmatrix} 1 & 0 & 1 & 0 & 1 & 0 & 1 & \cdots \\ 1 & 0 & -1 & 0 & 1 & 0 & -1 & \cdots \end{pmatrix}_{2\times 2n+1} \end{aligned} \tag{83}$$

For the P-model we can use the same modal frequencies and modal damping coefficients as we did for the Q-model and they are written in equation (76). Also same windowing parameters can be used as in formulas (77).

For the PQ-model the space state realization is more complicated because this element combines properties from Q-element and P-element presented above. PQ-element is derived from mixed boundary conditions (63) of differential equation (60). First we write the space state form for the PQ-model

$$\begin{aligned} \dot{\mathbf{x}} &= \mathbf{A}\mathbf{x} + \mathbf{B}\begin{pmatrix} P_1 \\ Q_2 \end{pmatrix}, \\ \mathbf{p} &= \mathbf{C}\mathbf{x} + \mathbf{D}\begin{pmatrix} P_1 \\ Q_2 \end{pmatrix}, \\ \dot{Q}_1 &= \mathbf{E}\begin{pmatrix} Q_1 \\ \mathbf{p} \end{pmatrix}, \\ P_2 &= \mathbf{F}\begin{pmatrix} P_1 \\ \mathbf{p} \end{pmatrix} \end{aligned} \tag{84}$$

In equation (84) **x** is the state variable vector and state space matrices can be expressed as follows.

$$\mathbf{x} = \begin{pmatrix} x_0 & x_1 & \cdots & x_{2n} \end{pmatrix}^{\mathrm{T}}, \quad \mathbf{p} = \begin{pmatrix} p_1 & p_2 & \cdots & p_n \end{pmatrix}^{\mathrm{T}}$$

$$\mathbf{A} = \begin{pmatrix} & \mathbf{A}_1 & & & \\ \mathbf{a} & & \mathbf{A}_2 & & \\ & & & \ddots & \\ & & & & \mathbf{A}_n \end{pmatrix}, \qquad \mathbf{B} = \begin{pmatrix} \mathbf{B}_0 \\ \mathbf{B}_1 \\ \vdots \\ \mathbf{B}_n \end{pmatrix},$$

$$\mathbf{C} = \begin{pmatrix} \mathbf{c} & \mathbf{C}^* \end{pmatrix}, \qquad \mathbf{D} = \begin{pmatrix} \mathbf{d} & \mathbf{0} \end{pmatrix}, \tag{85}$$

$$\mathbf{E} = \begin{pmatrix} e_0 & \mathbf{e}^{\mathrm{T}} \end{pmatrix}, \qquad \mathbf{F} = \begin{pmatrix} 1 & \mathbf{f}^{\mathrm{T}} \end{pmatrix}$$

Elements of the matrices presented above can then be calculated using following formulas (86)

$$a_{2i} = (-1)^{i+1} \frac{Z_0}{T}, \qquad \mathbf{A}_i = \begin{pmatrix} -\frac{\varepsilon_i}{T} & -\frac{\omega_i^2}{T^2} \\ 1 & 0 \end{pmatrix},$$

$$\mathbf{B}_0 = \begin{pmatrix} 0 & 1 \end{pmatrix}, \qquad \mathbf{B}_i = -\frac{2}{(2i-1)\pi} \begin{pmatrix} 1 & 0 \\ 0 & 0 \end{pmatrix}$$

$$c_i = (-1)^{i+1} \frac{2w_i Z_0}{T}, \qquad C^*_{i,2i} = \frac{2w_i (b_1 \varepsilon - \varepsilon_i)}{T}, \qquad C^*_{i,2i+1} = -\frac{2w_i \omega_i^2}{T^2} \tag{86}$$

$$d_i = -\frac{4w_i}{(2i-1)\pi},$$

$$e_0 = -\frac{b_2 \varepsilon}{T}, \qquad e_i = -\frac{(2i-1)\pi}{2TZ_0},$$

$$f_i = (-1)^{i+1}$$

Modal frequencies, damping coefficients are calculated using formulas (76) but for the windowing parameters different formulas are used

$$\alpha_i = \frac{(2i-1)\pi}{2}, \qquad \beta_i = \frac{(2i-1)\pi}{2n+1},$$

$$b_1 = \left(2\sum_{i=1}^{n} w_i / \omega_i^2 \right)^{-1}, \qquad b_2 = \pi b_1 \sum_{i=1}^{n} (-1)^{i+1} (2i-1) w_i / \omega_i^2 \tag{87}$$

Using the previous state space realizations we can create the transmission line elements. However, these models represent only the transmission line without the orifices and volumes shown in Figure 6. Therefore we need models for orifices and volumes because these components take care of the boundary conditions of the transmission line elements.

2.5 Hydraulic components

Advantage in finite element method is that we can divide the structure into elements and these elements are joined together via nodes of the elements. This same concept is then applied on hydraulics. For this we need to create hydraulic elements which can then be joined to create hydraulic system. In mechanical elements typical nodal freedoms are displacements and rotations of the nodes but in hydraulic corresponding magnitudes are pressure and volume flow. So depending on the element type we can have pressures as inputs and volume flows as variables or vice versa. The hydraulic elements are then assembled together to give the system equation which is ordinary differential equation.

In this chapter we present some hydraulic elements used in finite element modeling of a hydraulic system. First we take a look at transmission line elements then 4/3 directional valve is presented and finally pressure relief element is derived.

2.5.1 Orifice model

For the pipe models presented above and for general use we need to derive calculation models for orifice and hydraulic volume. These models are needed in the transmission line models because at the ends of the lines are either orifice or volume.

In orifice the flow area of the transmission line suddenly diminishes and then enlarges again causing a pressure drop in the system. We can also calculate the flow rate going through the orifice when the pressures are known at the both sides and thus we know the pressure difference over the orifice as presented in Figure 7.

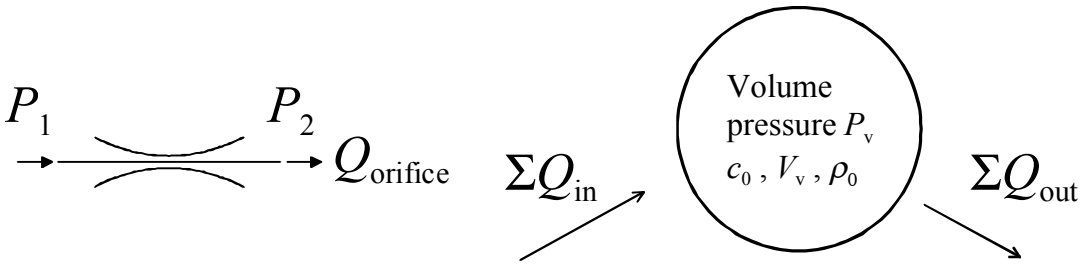

***Figure** 7 On the left the orifice model where pressures are given inputs and flow rate is state variable, on the right hydraulic volume where flow rates are given inputs and pressure is a state variable*

For modeling the orifice there are multiple choices and zeroth order and first order orifice models are presented in this thesis. The zeroth order orifice model can be derived from the Bernoulli's principle which is a energy equation for fluids. The zeroth order model gets its name from the fact that it is a zeroth order differential equation, thus it is a algebraic equation. In the transmission line models we assumed that the flow is laminar but in orifice the flow can be laminar or turbulent and both of these flow types have to be taken into account. As explained earlier we want to calculate the flow rate through the orifice when the pressure difference over the orifice is known. This means that there

is a limit pressure where the flow transforms from laminar to turbulent, the transition pressure, and it can be calculated using following formula (Ellman, et al., 1996).

$$P_{\mathrm{tr}} = \frac{9\,\mathrm{Re}_{\mathrm{tr}}^2\,\rho_0 \nu_0^2}{8 C_{\mathrm{d}}^2 D_{\mathrm{or}}^2} \tag{88}$$

where $\mathrm{Re}_{\mathrm{tr}}$ is the transition Reynolds number, ρ_0 is the density of the fluid, ν_0 is the kinematic viscosity, D_{or} is the diameter of the orifice and C_{d} is the discharge coefficient and it has a value 0.611 (Viersma, 1980 p. 15).

At the transition pressure the flow transforms from turbulent to laminar or other way around. It is also desired that the derivative of the flow rate is continuous in this transformation and it can be achieved using orifice flow model presented in equation (89). If the pressure difference is higher than the transition pressure flow is turbulent and if pressure difference is lower than the transition pressure the flow is laminar. (Ellman, et al., 1996)

$$Q_{\mathrm{or}} = \begin{cases} C_{\mathrm{d}} A_{\mathrm{or}} \sqrt{\dfrac{2\left|\Delta P_{\mathrm{or}}\right|}{\rho}}\,\mathrm{sgn}(\Delta P_{\mathrm{or}}) & \text{when } \left|\Delta P_{\mathrm{or}}\right| > P_{\mathrm{tr}} \\ \dfrac{3 A_{\mathrm{or}} \nu\,\mathrm{Re}_{\mathrm{tr}}}{4 D_{\mathrm{or}}} \left(\dfrac{\Delta P_{\mathrm{or}}}{P_{\mathrm{tr}}}\right)\left(3 - \dfrac{\left|\Delta P_{\mathrm{or}}\right|}{P_{\mathrm{tr}}}\right) & \text{when } \left|\Delta P_{\mathrm{or}}\right| \le P_{\mathrm{tr}} \end{cases} \tag{89}$$

The other formulation for the orifice model is the first order model where the orifice is modeled as first order differential equation. This equation can be derived from the momentum equation of a fluid particle and the expression for the derivative of the flow rate is in equation (90).

$$\dot{Q}_{\mathrm{or}} = \frac{1}{V_{\mathrm{or}}}\left(\frac{\Delta P_{\mathrm{or}} A_{\mathrm{or}}^2}{\rho_0} - \frac{Q_{\mathrm{or}}\left|Q_{\mathrm{or}}\right|}{2 C_{\mathrm{d}}^2}\right) \tag{90}$$

If the volume V_{or} which represents the volume of the fluid particle, in this case the volume of the orifice, is small the differential equation becomes stiff. In stiff problems there are variables that can lead to fast variation of the solution although the solution is stable and smooth. This implies from the fact that when the denominator, in this case the volume, becomes small the time derivative of flow rate becomes very large and usually volume of the orifice is small compared to other volumes in the system. Stiff problems mean that the time integration has to be made with small time step although the analytical solution would be smooth. Stiffness can also be detected by studying the eigenvalues of the Jacobian matrix. If the dominant eigenvalue of the Jacobian matrix is at the border of the stability domain the problem is stiff (Hairer, et al., 1991). Although

equation (90) is usually stiff it is used in transmission line models because it is easy to implement to programming environments and it is effective to calculate.

2.5.2 Volume model

The other important model in hydraulics is the hydraulic volume model. In orifice model flow rate is calculated from the pressure difference whereas in hydraulic volume model the pressure is calculated from the flow rates. In this context only the first order volume model is considered.

Pressure of the hydraulic systems rises in cases where the volume flow is restricted. In case where there is a volume to which volume is flowing to and flowing out, see Figure 7, the differential equation can be written as follows in formula

$$\dot{P}_{\mathrm{v}} = \frac{B}{V_{\mathrm{v}}}\left(\sum Q_{\mathrm{in}} - \sum Q_{\mathrm{out}}\right) \tag{91}$$

where B is the bulk modulus and V_{v} is the volume.

2.5.3 Combined transmission line, orifice and volume models

For complete transmission line modeling orifice and volume models needs to be combined with the transmission line models. This is needed because in the derivation of the transmission line elements boundary conditions are set in the solution process and using either volume or orifice model these boundary conditions can be satisfied. For example in Figure 6 it can be seen, that in Q-model there is transmission line model combined with two orifice models. Same applies for the rest transmission line models except we need also the volume model. These can brought together when the state equation of the component is written. This equation is first order differential equation. For the Q-model transmission line we take equations (78) and combine it with equation (90) and we get the state equation for the Q-model transmission line as follows in formula (92)

$$\begin{pmatrix} \dot{Q}_1 \\ \dot{\mathbf{x}} \\ \dot{Q}_2 \end{pmatrix}_{\text{Q-model}} = \begin{pmatrix} \frac{1}{V_1}\left(\frac{\Delta P_1 A_1}{\rho_0} - \frac{Q_1|Q_1|}{2C_{d,1}^2}\right) \\ \mathbf{A}\mathbf{x} + \mathbf{B}\mathbf{Q} \\ \frac{1}{V_2}\left(\frac{\Delta P_2 A_2}{\rho_0} - \frac{Q_2|Q_2|}{2C_{d,2}^2}\right) \end{pmatrix} \tag{92}$$

For the time integration the Jacobian matrix of the state equation needs to be calculated. Numerical difference method is one way to execute this but it is more efficient to calculate analytic Jacobian matrix for the system. This is achieved by differentiating the state

equation (92) to all state variables. By doing so we get the Jacobian matrix for the Q-model and the expression is in formula (93)

$$\mathbf{J}_{\text{Q-model}} = \begin{pmatrix} -\dfrac{|Q_1|}{V_1 C_{d,1}^2} & \dfrac{\mathbf{c}_1^{\mathrm{T}} A_1^2}{V_1 C_{d,1}^2} & 0 \\ \mathbf{b}_1 & \mathbf{A} & \mathbf{b}_2 \\ 0 & \dfrac{\mathbf{c}_2^{\mathrm{T}} A_2^2}{V_2 C_{d,2}^2} & -\dfrac{|Q_2|}{V_2 C_{d,2}^2} \end{pmatrix} \tag{93}$$

where $\mathbf{c}_1$ is the first column of $\mathbf{C}$ from equation (80). Same notation applies for all space state matrices.

Corresponding presentation for P-model can be written when we use the P-model transmission line and the differential equation (91) for the hydraulic volume. The state equation for complete P-model can be written as follows in equation

$$\begin{pmatrix} \dot{P}_1 \\ \dot{\mathbf{x}} \\ \dot{P}_2 \end{pmatrix}_{\text{P-model}} = \begin{pmatrix} \dfrac{-B\mathbf{c}_1^{\mathrm{T}}\mathbf{x}}{V_1} \\ \mathbf{A}\mathbf{x} + \mathbf{B}\mathbf{P} \\ \dfrac{-B\mathbf{c}_2^{\mathrm{T}}\mathbf{x}}{V_2} \end{pmatrix} \tag{94}$$

The Jacobian matrix can be calculated in the same manner that the Jacobian matrix is calculated for the Q-model except that space matrixes are taken from equation (81), (82) and (83)

$$\mathbf{J}_{\text{P-model}} = \begin{pmatrix} 0 & \dfrac{-B\mathbf{c}_2^{\mathrm{T}}}{V_1} & 0 \\ \mathbf{b}_1 & \mathbf{A} & \mathbf{b}_2 \\ 0 & \dfrac{-B\mathbf{c}_2^{\mathrm{T}}}{V_2} & 0 \end{pmatrix} \tag{95}$$

Finally for the combined PQ-element we get the differential equation

$$\begin{pmatrix} \dot{P}_1 \\ \dot{Q}_1 \\ \dot{\mathbf{x}} \\ \dot{Q}_2 \end{pmatrix}_{\text{PQ-model}} = \begin{pmatrix} -BQ_1/V_1 \\ e_0 Q_1 + \mathbf{e}^{\mathrm{T}}\left(\mathbf{C}\mathbf{x} + P_1\mathbf{d}\right) \\ \mathbf{A}\mathbf{x} + \begin{pmatrix} \mathbf{b}_1 & \mathbf{b}_2 \end{pmatrix}\begin{pmatrix} P_1 \\ -Q_2 \end{pmatrix} \\ \dfrac{1}{V_2}\left(\dfrac{\Delta P_2 A_2^2}{\rho_0} - \dfrac{Q_2|Q_2|}{2C_{d,2}^2}\right) \end{pmatrix}, \tag{96}$$

And the Jacobian matrix can be calculated by differentiation to all state variables

$$\mathbf{J}_{\text{PQ-model}} = \begin{pmatrix} 0 & \frac{-B}{V_1} & \mathbf{0}^{\mathrm{T}} & 0 \\ \mathbf{e}^{\mathrm{T}}\mathbf{d} & e_0 & \mathbf{e}^{\mathrm{T}}\mathbf{C} & 0 \\ \mathbf{b}_1 & 0 & \mathbf{A} & 0 \\ \frac{A_2^2}{V_2\rho_0}\left(1+\mathbf{f}^{\mathrm{T}}\mathbf{d}\right) & 0 & \frac{A_2^2}{V_2\rho_0}\mathbf{f}^{\mathrm{T}}\mathbf{C} & \frac{-|Q_2|}{V_2 C_{d,2}^2} \end{pmatrix} \tag{97}$$

Hydraulic systems can be constructed using elements described above but with these elements only straight lines can be modeled. Usually hydraulic systems contain branches where several transmission lines are connected together. This is the case in directional valve, for instance. Therefore, branching of the transmission lines needs to be discussed in derivation of the directional valve element.

2.5.4 Directional valve element

Directional valve is placed between the pump and the actuator in a hydraulic system. Function of the directional valve is to control the movements of the actuators by throttling the flow rate going to the actuator. Directional valves are presented as fractions like 4/3-valve. This means that in this valve there are 4 flow paths and three different possibilities how these flow paths are connected together. 4/3-directional valve is presented in Figure 8 although this figure does not take notice how the valve is operated. Possibilities are for example solenoids which pushes the outermost blocks to the center and then springs returns the valve to normal position.

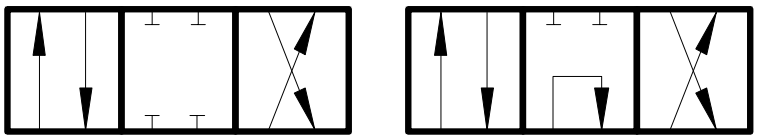

Figure 8 *Two different settings of 4/3-directional valve. On the left closed center position and on the right center position with unloading circuit*

When directional valve is modeled using finite element formulation, we can exploit the transmission line models presented above using the Wheatstone bridge connection. In this master's thesis, directional valve has closed center position and therefore a pressure relief valve is needed in the system. For this we can create branched transmission line elements where the other end can have volume and the other end is branched. If the end to be branched has orifice then all the branches also have orifices. Directional valve and its elements are shown in Figure 9.

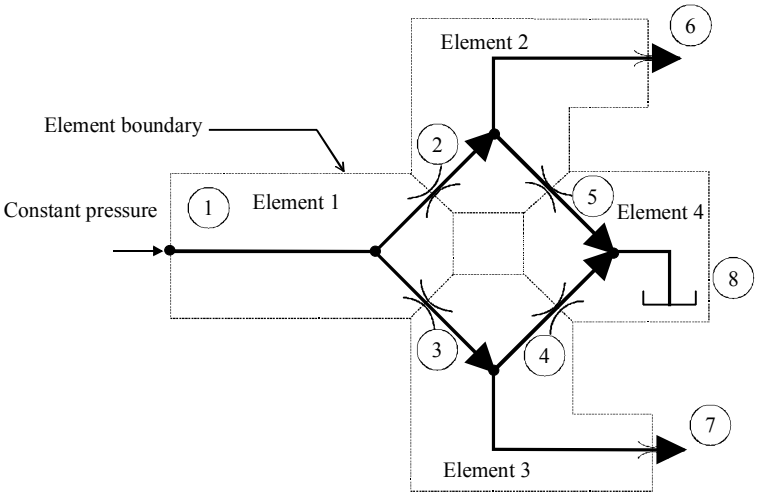

Figure 9 *4/3-directional valve using element method*

As Figure 9 shows directional valve can be assembled using two elements with one volume and two orifices and two elements with three orifices. It should be noted that the element boundary goes through the orifice. For instance element 1 and element 2 share same orifice 2 thus both have half of the orifice. The element 1 (see Figure 9) is a branched PQ-element with three nodes. The first node has a volume and nodes 2 and 3 have orifices. The state equation for the transmission line can be written according to equation (96). In this equation the time derivative of the pressure can be ignored because the pressure can be given as input, it is a boundary condition. This constant pressure assumption is made for simplicity. On the other end of the element there are two orifices and the first order orifice model (90) is exploited. When these equations are combined we get the state equation for first element in the directional valve. State variables for this element are Q_1 in node 1 and correspondingly Q_2 and Q_3 in nodes 2 and 3 respectively.

$$\begin{pmatrix} \dot{Q}_1 \\ \dot{\mathbf{x}} \\ \dot{Q}_2 \\ \dot{Q}_3 \end{pmatrix}^{(1)} = \begin{pmatrix} \mathbf{E}^{(1)} \begin{pmatrix} Q_1 \\ \mathbf{p} \end{pmatrix} \\ \mathbf{A}\mathbf{x} + \begin{pmatrix} \mathbf{b}_1 \mathbf{b}_2 \end{pmatrix} \begin{pmatrix} P_1 \\ -Q_2 - Q_3 \end{pmatrix} \\ \frac{1}{V_2} \left(\frac{(\Delta P_2) A_2^2}{\rho_0} - \frac{Q_2 |Q_2|}{2C_{d,2}^2} \right) \\ \frac{1}{V_3} \left(\frac{(\Delta P_3) A_3^2}{\rho_0} - \frac{Q_3 |Q_3|}{2C_{d,3}^2} \right) \end{pmatrix}^{(1)} \tag{98}$$

The minus signs can be explained with sign convention made when transmission line models were derived. Convention is that inward flows are assumed positive. For the time integration Jacobian matrix needs to be calculated. Because the input pressure is a given input, rows and columns corresponding the pressure can be neglected.

$$\mathbf{J}^{(1)}=\begin{pmatrix} e_0\left(\mathbf{e}\right)^{\mathrm{T}}\mathbf{C} & 0 & 0 \\ 0 & \mathbf{A}^{(1)} & -\mathbf{b}_2 & -\mathbf{b}_2 \\ 0 & \dfrac{A_2^2}{\rho_0 V_2}\mathbf{FC} & -\left|Q_2\right|/\left(V_2 C_{d,2}^2\right) & 0 \\ 0 & \dfrac{A_3^2}{\rho_0 V_3}\mathbf{FC} & 0 & -\left|Q_3\right|/\left(V_3 C_{d,3}^2\right) \end{pmatrix}^{(1)} \tag{99}$$

In element 2, Q-model transmission line and first order orifice models are exploited. Combining these equations (78) and (90) we get state equation and the Jacobian matrix. The nodal variables are flow rates Q_2, Q_4 and Q_6 in nodes 2, 4 and 6. The state vector **x** describes the pressure in the domain of the transmission line.

$$\begin{pmatrix} \dot{Q}_2 \\ \dot{Q}_4 \\ \dot{\mathbf{x}} \\ \dot{Q}_6 \end{pmatrix}^{(2)}=\begin{pmatrix} \dfrac{1}{V_2}\left(\dfrac{\left(\Delta P_2\right)A_2^2}{\rho_0}-\dfrac{Q_2\left|Q_2\right|}{2C_{d,2}^2}\right) \\ \dfrac{1}{V_4}\left(\dfrac{\left(\Delta P_4\right)A_4^2}{\rho_0}-\dfrac{Q_4\left|Q_4\right|}{2C_{d,4}^2}\right) \\ \mathbf{A}\mathbf{x}+\left(\mathbf{b}_1\mathbf{b}_2\right)\begin{pmatrix} Q_2-Q_4 \\ -Q_6 \end{pmatrix} \\ \dfrac{1}{V_6}\left(\dfrac{\left(\Delta P_6\right)A_6^2}{\rho_0}-\dfrac{Q_6\left|Q_6\right|}{2C_{d,6}^2}\right) \end{pmatrix}^{(2)} \tag{100}$$

$$\mathbf{J}^{(2)}=\begin{pmatrix} -\left|Q_2\right|/\left(V_2 C_{d,2}^2\right) & 0 & -\left(\mathbf{c}_1\right)^{\mathrm{T}}A_2^2/\left(V_2\rho_0\right) & 0 \\ 0 & -\left|Q_4\right|/\left(V_4 C_{d,4}^2\right) & \left(\mathbf{c}_1\right)^{\mathrm{T}}A_4^2/\left(V_4\rho_0\right) & 0 \\ \mathbf{b}_1 & -\mathbf{b}_1 & \mathbf{A} & -\mathbf{b}_2 \\ 0 & 0 & \left(\mathbf{c}_2\right)^{\mathrm{T}}A_6^2/\left(V_6\rho_0\right) & -\left|Q_6\right|/\left(V_6 C_{d,6}^2\right) \end{pmatrix}^{(2)} \tag{101}$$

What makes the finite element method so efficient is the way that the system equation can be assembled. In this case these two elements are connected together in node 2 where the state variable is flow rate Q_2. Therefore the system equation and the Jacobian matrix for these two elements can be written as

$$\begin{pmatrix} \dot{Q}_1 \\ \dot{\mathbf{x}}^{(1)} \\ \dot{Q}_2 \\ \dot{Q}_3 \\ \dot{Q}_4 \\ \dot{\mathbf{x}}^{(2)} \\ \dot{Q}_6 \end{pmatrix}^{(1)+(2)} = \begin{pmatrix} \mathbf{E}^{(1)} \begin{pmatrix} Q_1 \\ \mathbf{p} \end{pmatrix} \\ \mathbf{A}^{(1)}\mathbf{x}^{(1)} + \mathbf{B}^{(1)} \begin{pmatrix} P_1 \\ -Q_2 - Q_3 \end{pmatrix} \\ \frac{1}{V_2}\left(\frac{(\Delta P_2) A_2^2}{\rho_0} - \frac{Q_2 |Q_2|}{2C_{\mathrm{d},2}^2} \right) \\ \frac{1}{V_3}\left(\frac{(\Delta P_3) A_3^2}{\rho_0} - \frac{Q_3 |Q_3|}{2C_{\mathrm{d},3}^2} \right) \\ \frac{1}{V_4}\left(\frac{(\Delta P_4) A_4^2}{\rho_0} - \frac{Q_4 |Q_4|}{2C_{\mathrm{d},4}^2} \right) \\ \mathbf{A}^{(2)}\mathbf{x}^{(2)} + \left(\mathbf{b}_1^{(2)} \;\; \mathbf{b}_2^{(2)} \right) \begin{pmatrix} Q_2 - Q_4 \\ Q_6 \end{pmatrix} \\ \frac{1}{V_6}\left(\frac{(\Delta P_6) A_6^2}{\rho_0} - \frac{Q_6 |Q_6|}{2C_{\mathrm{d},6}^2} \right) \end{pmatrix}^{(1)+(2)} \tag{102}$$

$$\mathbf{J}^{(1)+(2)} = \begin{pmatrix} e_0^{(1)} & \left(\mathbf{e}^{(1)}\right)^{\mathrm{T}} \mathbf{C}^{(1)} & 0 & 0 & 0 & \mathbf{0}^{\mathrm{T}} & 0 \\ \mathbf{0} & \mathbf{A}^{(1)} & -\mathbf{b}_2^{(1)} & -\mathbf{b}_2^{(1)} & \mathbf{0} & \mathbf{0}^{\mathrm{T}} & \mathbf{0} \\ 0 & \frac{A_2^2}{\rho_0 V_2}\mathbf{F}^{(1)}\mathbf{C}^{(1)} & -|Q_2|/\left(V_2 C_{\mathrm{d},2}^2\right) & 0 & 0 & -\left(\mathbf{c}_1^{(2)}\right)^{\mathrm{T}} A_2^2/\left(V_2\rho_0\right) & 0 \\ 0 & \frac{A_3^2}{\rho_0 V_3}\mathbf{F}^{(1)}\mathbf{C}^{(1)} & 0 & -|Q_3|/\left(V_3 C_{\mathrm{d}3}^2\right) & 0 & \mathbf{0}^{\mathrm{T}} & 0 \\ 0 & 0 & 0 & 0 & -|Q_4|/\left(V_4 C_{\mathrm{d}4}^2\right) & \mathbf{0}^{\mathrm{T}} & 0 \\ \mathbf{0} & \mathbf{0} & \mathbf{b}_1^{(2)} & \mathbf{0} & -\mathbf{b}_1^{(2)} & \mathbf{A}^{(2)} & -\mathbf{b}_2^{(2)} \\ 0 & 0 & 0 & 0 & 0 & \left(\mathbf{c}_2^{(2)}\right)^{\mathrm{T}} A_6^2/V_6 & -|Q_6|/\left(V_6 C_{\mathrm{d},6}^2\right) \end{pmatrix}^{(1)+(2)} \tag{103}$$

As it can be seen, no summing is needed because these two elements share the same state variable in node 2. This explains why the elemental boundary goes through the orifice. When both elements have the same state variable the assembly of the hydraulic model is fairly simple. Likewise the rest of the 4/3-directional valve can be assembled by adding the branched Q-model element where there are three orifices at the ends of the transmission line and one QP-element representing the tank line.

2.5.5 Pressure relief element

Pressure relief valve is a valve that controls maximum pressure of the system. Without the pressure relief valve system pressure could rise over the maximum operating pressure causing damage to the components and danger to operators of the machine. Pressure relief valves can be poppet or spool valves but in this context we are dealing only the spool valve.

Pressure relief valves are normally closed and when the system pressure reaches the opening pressure of the valve flow path starts to open. Pressure increase occurs when flow of the fluid is restricted and volume of the fluid increases in the system. When the flow path of the valve opens the fluid can flow through the orifice and therefore the sys-

tem pressure descends. Usually pressure relief valve is installed near to the pump outlet and thereby in this pressure relief element the pump or the source of the volume flow is modeled in the same element. Pressure relief element is presented in Figure 10.

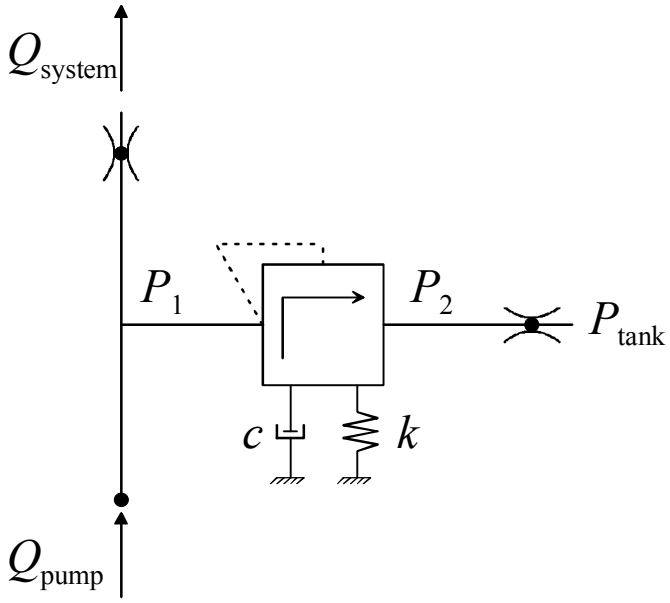

Figure 10 *Presentation of the pressure relief element. Dots are the boundaries of the element*

Modeling of the pressure relief element can be started on the question how to calculate the orifice flow area as function of the spool displacement. In fact, the flow area is just a segment Figure 11 (right) of a circle and therefore it is easy to derive using basic geometry. Area of the segment can be calculated using following formula (Wolfram).

$$A_{\text{orifice}}(x) = R^2 \cos^{-1}\left(\frac{R-x}{R}\right) - (R-x)\sqrt{2Rx - x^2} \tag{104}$$

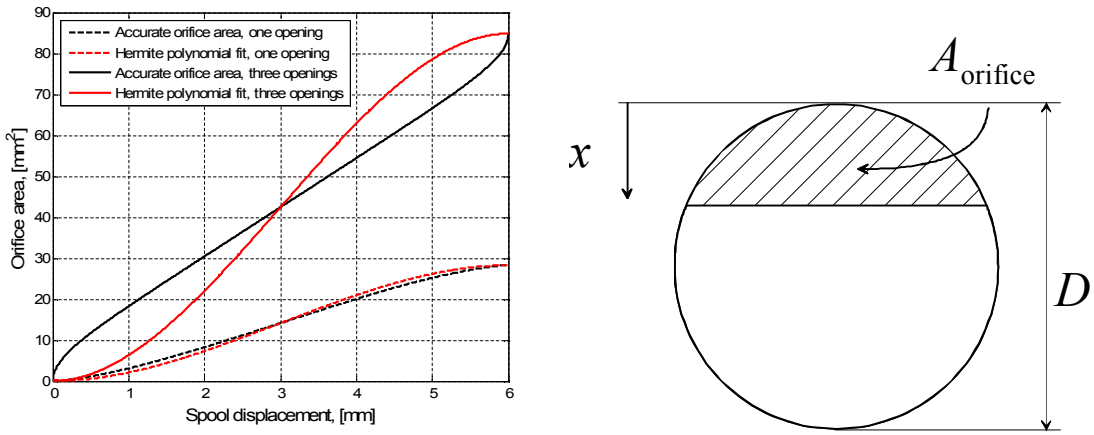

Figure 11 *On the left orifice areas as function of displacement and on the right area of circle segment*

where x is the displacement of the spool. Although this formula (104) is accurate, it is quite complicated because it requires calculation of arcus cosine and square root. Also differentiation in respect of x and the derivative would have same problems. Therefore it would be good idea to fit a polynomial curve that would represent same behavior. Hermite polynomials are good way to approximate the area and these polynomials have also properties which makes numerical calculations more powerful. Hermite polynomials are polynomials of third order as presented in formula (105).

$$H(x) = ax^3 + bx^2 + cx + d \tag{105}$$

What makes an third degree polynomial a Hermite polynomial is the way that the coefficients *a, b, c* and *d* are solved. These boundary conditions are presented in equations (106)

$$H(0) = 0, \qquad H(R) = 1, \qquad H'(0) = 0, \qquad H'(R) = 0 \tag{106}$$

The orifice area can then be calculated using equation (107). This equation takes also care of that the area has limited maximum value.

$$A_{\text{orificeH}}(x) = \begin{cases} 0 & \text{when} \quad x \le x_{\text{st}} \\ \pi R^2 \cdot H(x) & \text{when} \quad x > x_{\text{st}} \\ \pi R^2 & \text{when} \quad x \ge 2R \end{cases} \tag{107}$$

In this equation (107) term x_{st} is the static displacement and it can be calculated using formula. In this equation P_{open} is the opening pressure of the pressure relief valve.

$$x_{\text{st}} = \frac{P_{\text{open}} A_{\text{sl}}}{k} \tag{108}$$

Equations (106) show why Hermite polynomials are used in modeling of the flow area. It is preferable to have constant derivatives at the ends of the domain and in this case derivatives are zero. In Figure 11 there is comparison between the accurate formula (104) and the approximated equation (107). From this figure we can see, that when we approximate area of one segment Hermite polynomial gives very good approximation. However, in real valve constructions there are usually several openings. Figure 11 also presents curves for three openings and we can see that in this case the Hermite polynomial is not that good approximation. Nevertheless it is justified to use the polynomial in question because of the derivative. When modeling three openings the accurate formula (104) produces high derivative values at the ends of the domain and this can cause oscillation to the system. Hermite polynomial offers zero derivatives and thereby some

damping preventing oscillation when flow area is small or near the maximum values. From the figure we can also see that both curves are one-to-one correspondence and therefore both area formulas produce same area but spool displacement is different. This also justifies the usage of Hermite polynomial because change in flow area just produces different spool displacements. In further context when calculating orifice area we use the Hermite polynomial fit and therefore the flow area is denoted as $A_{or.}$ and it is function of x.

In real valve constructions the orifice area is desired to be linear with respect to the spool displacement. Therefore the valve body or the spool has grooves to smoothen the behavior of the valve. In this thesis this construction is neglected and the orifice area is calculated using the Hermite polynomial.

Modeling of the orifice area is just one thing in the pressure relief element and next thing would be to define the state variables of the element. Quite obvious ones are the displacement and velocity of the spool because they come from the equation of the motion. This equation can be derived from the free body diagram of the spool presented in Figure 12. Equation of motion is written into equation (109)

$$m\ddot{x} + c\dot{x} + kx = P_1 A_{s1} - P_2 A_{s2} + F_{flow} \tag{109}$$

Flow force can then be calculated using following formula (110).

$$F_{flow} = 2C_d A_{or} \left(P_1 - P_2\right)\cos(\alpha) \tag{110}$$

In equation (110) the last term presents the change in the flow direction and if the orifice openings have sharp edges and the radial clearance is small compared to the opening the angle gets value α = 69° (Fonselius, et al., 2006 p. 19).

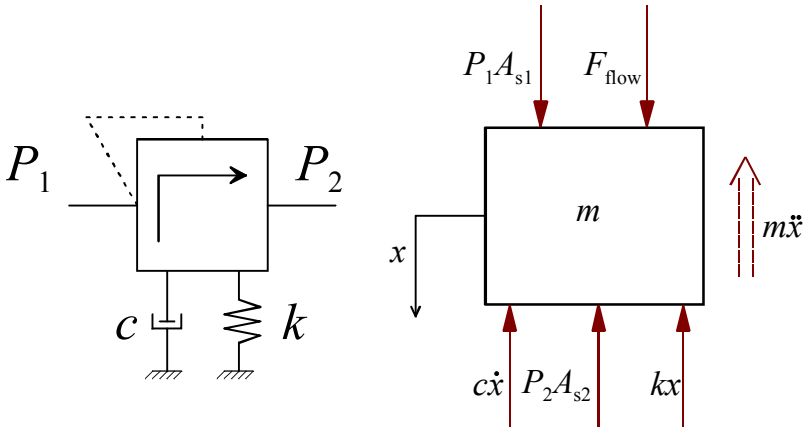

Figure 12 *Free body diagram of the valve spool*

Because pump produces volume flow that is in this case constant flow we should calculate pressures p_1 and $p_{2.}$ These pressures define how much volume flow goes to the system and how much of the flow goes through the pressure relief valve. These flows

are connected together by continuity equation (111) where PRV denotes pressure relief valve and Q_{PRV} means the volume flow going through the pressure relief valve.

$$Q_{\text{pump}} = Q_{\text{system}} + Q_{\text{PRV}} \tag{111}$$

Using all the equations in this chapter we can now assemble the state space realization of the pressure relief element. Equation is first order differential but equation of motion (109) is second degree differential equation and therefore it should be transformed into two first order differential equations and we get the state space realization of the pressure relief element (112). Subscripts 1 and 2 refer to the magnitudes before the pressure relief valve and after the pressure relief valve as presented in Figure 10. Flow rates Q_{PRV}, Q_{system} and Q_{tank} are calculated using the zeroth order orifice model of the equation (89).

$$\begin{pmatrix} \dot{P}_1 \\ \dot{P}_2 \\ \dot{x} \\ \dot{v} \end{pmatrix}_{\text{PRV}} = \begin{pmatrix} \frac{B}{V_1}\left(Q_{\text{pump}} - Q_{\text{PRV}} - Q_{\text{system}}\right) \\ \frac{B}{V_2}\left(Q_{\text{PRV}} - Q_{\text{tank}}\right) \\ v \\ \frac{1}{m}\left(P_1 A_1 - P_2 A_2 + F_{\text{flow}} - cv - kx\right) \end{pmatrix} \tag{112}$$

Although pressure relief element itself is a hydro mechanical element because it has both mechanical equations and hydraulic equations it can still be considered as pure hydraulic element and mechanical magnitudes as displacement and velocity of the spool are taken as internal variables.

For the time integration it is necessary to compute the Jacobian matrix of the space state realization. Of course the Jacobian matrix can be calculated using numerical methods like difference method but it is more efficient to calculate analytic Jacobian matrix for the system. For the this we need to differentiate equation (112) in respect to all state variables. For the differentiation we notice that volume flows are functions of pressures and orifice areas whereas motion of equation is function of pressures, spool displacement and spool velocity. Now we can write the Jacobian matrix as follows, see equation (113). Zero derivatives have been taken into account when deriving this equation.

$$\mathbf{J}_{\mathrm{PRV}} = \begin{pmatrix} -\frac{B}{V_1}\frac{\partial(Q_{\mathrm{PRV}}+Q_{\mathrm{system}})}{\partial P_1} & -\frac{B}{V_1}\frac{\partial Q_{\mathrm{PRV}}}{\partial P_2} & -\frac{B}{V_1}\frac{\partial Q_{\mathrm{PRV}}}{\partial x} & 0 \\ \frac{B}{V_2}\frac{\partial Q_{\mathrm{PRV}}}{\partial P_1} & \frac{B}{V_2}\frac{\partial(Q_{\mathrm{PRV}}-Q_{\mathrm{tank}})}{\partial P_2} & \frac{B}{V_2}\frac{\partial Q_{\mathrm{PRV}}}{\partial x} & 0 \\ 0 & 0 & 0 & 1 \\ \frac{1}{m}\left(A_1+\frac{\partial F_{\mathrm{flow}}}{\partial P_1}\right) & \frac{1}{m}\left(-A_2+\frac{\partial F_{\mathrm{flow}}}{\partial P_2}\right) & \frac{1}{m}\left(-k+\frac{\partial F_{\mathrm{flow}}}{\partial x}\right) & -\frac{c}{m} \end{pmatrix} \tag{113}$$

The state equation of pressure relief valve and Jacobian matrix can be added to the system matrices in a way shown in 2.5.3. Also no summing is needed because the pressure relief element connects to the system via volume and thereby it shares the pressure variable of the volume with the first transmission line element.

2.6 Hydraulic cylinder element

Hydraulic cylinder can be interpreted as a hydro mechanical element for it has both mechanical state variables and hydraulic variables. Hydro mechanical elements are used in calculation models to couple the mechanical system with the hydraulic system and therefore hydraulic motor and hydraulic pump can also be treated as hydro mechanical elements. In this chapter a model for hydraulic cylinder with friction is presented. First we treat the hydraulic state variables and afterwards the mechanical tangent matrices. Also the interactions between different systems are discussed. Hydro mechanical system can be treated as three field problem because there are hydraulic system and mechanical system and also the interaction between these two systems.

2.6.1 Interaction between hydraulic system and hydraulic cylinder

Using the procedures and equations presented we can model the hydraulic part of the hydraulic cylinder as volume pair using equation (91). Taking notation from Figure 13 the coupling between the chamber pressures of the cylinder and the flow rates going in and out of the cylinder can be written as

$$\begin{pmatrix} \dot{P}_{\mathrm{A}} \\ \dot{P}_{\mathrm{B}} \end{pmatrix} = \begin{pmatrix} \frac{Q_{\mathrm{A}} - A_{\mathrm{A}}\dot{x}_{\mathrm{c}}}{V_{\mathrm{A}} + A_{\mathrm{A}}x_{\mathrm{c}}} B_0 \\ \frac{-Q_{\mathrm{B}} + A_{\mathrm{B}}\dot{x}_{\mathrm{c}}}{V_{\mathrm{B}} - A_{\mathrm{B}}x_{\mathrm{c}}} B_0 \end{pmatrix} \tag{114}$$

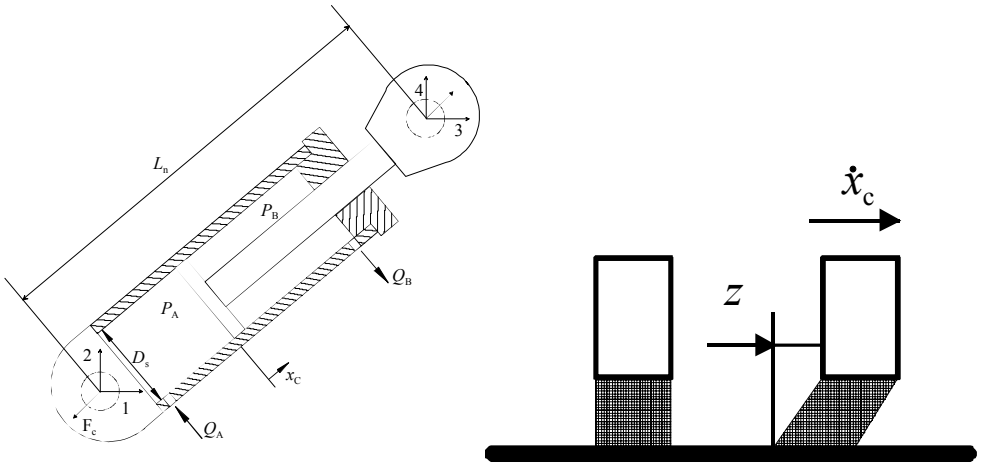

Figure 13 *Hydraulic cylinder element and state variables on the left and on the right a bristle representing a piston sealing and the bristle deflection z*

Equation (114) takes only the chamber pressures into account. We still need to add friction model to the system because friction drops the maximum force that the cylinder can produce. Forming the equilibrium equation for the cylinder rod we get

$$f_{\text{cyl}} = A_{\text{A}} P_{\text{A}} - A_{\text{B}} P_{\text{B}} - F_{\text{friction}} \tag{115}$$

where P_{A} and P_{B} are chamber pressures and A_{A} and A_{B} are corresponding cylinder areas. The last term F_{friction} is then the friction force.

There are many alternatives in modeling the friction between the cylinder piston sealing and cylinder pipe but in thesis Olsson's friction model is used (Olsson, 1996). First we divide the friction force into two functions as presented in equation (116), one is independent of the pressure but is depended of the velocity of the cylinder piston. Thus, the other is depended on the pressure but independent on the cylinder velocity. The pressure independent function however, takes the deformation of the sealing into account.

$$F_{\text{friction}} = f_{\text{pr}}(P_{\text{A}}, P_{\text{B}}) f_{\mu}(z, \dot{x}_{\text{c}}) \tag{116}$$

The pressure depended friction is assumed as linear relation as follows

$$f_{\text{pr}}(P_{\text{A}}, P_{\text{B}}) = 1 + k_{\text{pr}}(P_{\text{A}} + P_{\text{B}}) \tag{117}$$

For the pressure independent part the friction model is more complicated. First the time derivative of the bristle deflection can be written according to Olsson as

$$\frac{dz}{dt} = \dot{x}_{\text{c}} - \frac{|\dot{x}_{\text{c}}|}{g(\dot{x}_{\text{c}})} z \tag{118}$$

In case of the hydraulic cylinder the bristle can be interpreted as cylinder piston sealing ring. This deviation is calculated as average value over the sliding surfaces, in this case a piston sealing. The first term tells that the bristle deviation is proportional to the relative velocities of the sliding surfaces. The second term then defines that the bristle deviation cannot become infinite. In equation (118) there is a unknown function $g(\dot{x}_c)$ and it can be written as (Olsson, 1996 p. 50)

$$g(\dot{x}_c) = \frac{1}{k_0}\left(F_{Cou} + (F_{st} - F_{Cou})e^{-(\dot{x}_c/v_{Str})^2}\right) \tag{119}$$

In this equation (119) term k_0 is stiffness coefficient and it is always positive. F_{Cou} represents the Coulomb friction. Coulomb friction is independent of the velocity but it is depended on the direction of the velocity. This implies that the Coulomb friction opposes the movement (Olsson, 1996 p. 25). F_{st} is the maximum value of the static friction. Static friction occurs only when relative velocity is zero and when velocity is non-zero friction changes to the Coulomb friction. Symbol v_{Str} is called the Stribeck velocity. Stribeck velocity is attributed to Stribeck effect where the friction force changes as function of the sliding velocity. This Stribeck effect is defined by the exponential function in equation (119). When the friction force at is over the constant Coulomb friction it is called the Stribeck friction and the limit velocity is the Stribeck velocity.

Finally the pressure independent friction can be written as

$$f_\mu = k_0 z + k_1 \frac{dz}{dt} + F_v \dot{x}_c \tag{120}$$

The first and second terms in equation (120) represent the solid contact in the sliding. The friction is depended on the deflection of the bristle but also on the rate of deformation of the bristle. The term k_1 is a damping coefficient and it is always positive. The last term in equation (120) represents the viscous friction in the sliding and F_v is the viscous friction coefficient.

For the final state equation of the hydraulic cylinder the rate of bristle deflection is appended to the state equation finally yielding

$$\begin{pmatrix} \dot{P}_A \\ \dot{P}_B \\ \dot{z} \end{pmatrix} = \begin{pmatrix} \dfrac{Q_A - A_A \dot{x}_c}{V_A + A_A x_c} B_0 \\ \dfrac{-Q_B + A_B \dot{x}_c}{V_B - A_B x_c} B_0 \\ \dot{x}_c - \dfrac{|\dot{x}_c|}{g(\dot{x}_c)} z \end{pmatrix} \tag{121}$$

In the time integration Jacobian matrices are also needed and for the hydraulic cylinder it can be derived into form of

$$\mathbf{J}_c = \begin{pmatrix} 0 & 0 & 0 \\ 0 & 0 & 0 \\ 0 & 0 & -\dfrac{|\dot{x}_c|}{g(\dot{x}_c)} \end{pmatrix} \tag{122}$$

For the hydraulic cylinder it is also possible to calculate different Jacobian matrices. As explained earlier hydraulic cylinder deals with the interaction between hydraulic and mechanical systems. Therefore we must also differentiate the state equation (121) of the cylinder to the hydraulic variables, in this case they are the flow rates Q_A and Q_B. On the other hand the hydraulic system state equation has to be differentiated to the cylinder variables, the pressures in chambers A and B and the bristle deflection. This derivative is presented in (122). It is also noticeable that cylinder displacement and its time derivative are state variables in the mechanical system. Therefore the state equation (121) needs also to be differentiated to these mechanical variables. These derivatives are then used in the system matrix of the whole system. The interaction Jacobian matrix can then be written as where the differentials of variables are also presented so that it is possible to follow the derivations.

$$\mathbf{J}_{\text{cyl}} \begin{pmatrix} \delta Q_A \\ \delta Q_B \\ \delta z \\ \delta x_c \\ \delta \dot{x}_c \end{pmatrix} = \begin{pmatrix} \dfrac{B_0}{V_A + A_A x_c} & 0 & 0 & -\dfrac{Q_A - A_A \dot{x}_c}{(V_A + A_A x_c)^2} A_A B_0 & \dfrac{-A_A}{V_A + A_A x_c} B_0 \\ 0 & \dfrac{-B_0}{V_B - A_B x_c} & 0 & \dfrac{-Q_B + A_B \dot{x}_c}{(V_B + A_B x_c)^2} A_B B_0 & \dfrac{A_B}{V_B + A_B x_c} B_0 \\ 0 & 0 & -\dfrac{|\dot{x}_c|}{g(\dot{x}_c)} & 0 & H(z, \dot{x}_c) \end{pmatrix} \begin{pmatrix} \delta Q_A \\ \delta Q_B \\ \delta z \\ \delta x_c \\ \delta \dot{x}_c \end{pmatrix} \tag{123}$$

In this equation the function $H(z, \dot{x}_c)$ can be calculated as

$$H\left(z,\dot{x}_{\mathrm{c}}\right)=1-\frac{z}{g\left(\dot{x}_{\mathrm{c}}\right)}\operatorname{sgn}\left(\dot{x}_{\mathrm{c}}\right)+\frac{g'\left(\dot{x}_{\mathrm{c}}\right)}{g^{2}\left(\dot{x}_{\mathrm{c}}\right)}\left|\dot{x}_{\mathrm{c}}\right|z$$
$$g'\left(\dot{x}_{\mathrm{c}}\right)=-\frac{2\dot{x}_{\mathrm{c}}}{v_{\mathrm{Str}}^{2}k_{0}}\left(F_{\mathrm{st}}-F_{\mathrm{Cou}}\right)\mathrm{e}^{-\left(\dot{x}_{\mathrm{c}}/v_{\mathrm{Str}}\right)^{2}} \tag{124}$$

This augmented Jacobian matrix is essential in the coupling of the mechanical system and hydraulic system. The plain Jacobian matrix of the cylinder is simple to form but because the state equation of the cylinder contains variables of both hydraulic system and mechanical system we can differentiate to these variables to achieve accurate coupling.

2.6.2 Interaction between hydraulic cylinder and mechanical system

In previous chapter the formulation of the hydraulic part of the hydraulic cylinder is presented and now in this chapter the mechanical part is introduced. As said, for the hydraulic cylinder Jacobian matrices are more complicated due to the coupling nature of the cylinder. In this chapter we derive the mechanical Jacobian matrix also known as stiffness matrix for the hydraulic cylinder. When equations are derived we also obtain the interaction matrix and damping matrix for the cylinder

Basic procedure for deriving the tangential matrices is to variate the force created by the hydraulic cylinder. In this case we variate equation (115) yielding

$$\delta f_{\mathrm{c}}=A_{\mathrm{A}}\delta P_{\mathrm{A}}-A_{\mathrm{B}}\delta P_{\mathrm{B}}-\left(k_{0}\delta z+k_{1}\delta\dot{z}+F_{\mathrm{v}}\delta\dot{x}_{\mathrm{c}}\right)f_{\mathrm{pr}}\left(P_{\mathrm{A}},P_{\mathrm{B}}\right)-f_{\mu}k_{\mathrm{pr}}\left(\delta P_{\mathrm{A}}+\delta P_{\mathrm{B}}\right) \tag{125}$$

where product rule for the variations has been applied. When the variations are made we can collect all variations into a vector. Thus we get equation

$$\delta f_{\mathrm{c}}=\left(-\left(k_{0}-\frac{\left|\dot{x}_{\mathrm{c}}\right|}{g\left(\dot{x}_{\mathrm{c}}\right)}k_{1}\right)f_{\mathrm{pr}},\quad A_{\mathrm{A}}-k_{\mathrm{pr}}f_{\mu},\quad -A_{\mathrm{B}}-k_{\mathrm{pr}}f_{\mu},\quad -\left(F_{\mathrm{v}}+k_{1}H\left(z,\dot{x}_{\mathrm{c}}\right)\right)f_{\mathrm{pr}}\right)\begin{pmatrix}\delta z\\ \delta P_{\mathrm{A}}\\ \delta P_{\mathrm{B}}\\ \delta\dot{x}_{\mathrm{c}}\end{pmatrix} \tag{126}$$

Finally we can vectorize this equation and we get the final form for the variation of the cylinder force.

$$\delta f_{\mathrm{c}}=\begin{pmatrix}\mathbf{w}_{\mathrm{cyl}}\\ w_{\dot{x}_{\mathrm{c}}}\end{pmatrix}^{\mathrm{T}}\begin{pmatrix}\delta z\\ \delta P_{\mathrm{A}}\\ \delta P_{\mathrm{B}}\\ \delta\dot{x}_{\mathrm{c}}\end{pmatrix}=\mathbf{W}_{\mathrm{cyl}}^{\mathrm{T}}\delta\mathbf{X}_{\mathrm{cyl}} \tag{127}$$

In this equation the multiplier vector contains the variations of the force produced by the hydraulic cylinder. The last scalar term is related only to the velocity of the cylinder piston.

For the derivation of tangent matrices we can write the force vectors seen in Figure 13 using the normal vector of the cylinder. First we define the normal vector as

$$\mathbf{n}_\mathrm{c} = \frac{\mathbf{x}_\mathrm{B} - \mathbf{x}_\mathrm{A}}{\left\| \mathbf{x}_\mathrm{B} - \mathbf{x}_\mathrm{A} \right\|} \tag{128}$$

where the subscript refers to the cylinder ends and vector **x** contains the nodal coordinates, see Figure 13. Using the normal vector the cylinder force can also be written in vector form. We get forces acting on both ends of the cylinder and they must be to opposite directions that the equilibrium is satisfied.

$$\begin{aligned} \mathbf{F}_{\mathrm{c},A} &= -f_\mathrm{c}\mathbf{n}_\mathrm{c} \\ \mathbf{F}_{\mathrm{c},B} &= f_\mathrm{c}\mathbf{n}_\mathrm{c} \end{aligned} \tag{129}$$

For the calculation of the tangent matrices we need to variate the force presented in equation (129). For the variation it should be discussed on which variables the forces depend. First of all forces are functions of cylinder chamber pressures P_A and P_B. The force f_c also contains dependency on the bristle deformation *z* and position and velocity of the cylinder, x_c and $\dot{x}_\mathrm{c}$. There is also connection to the nodal coordinates of the cylinder ends in position vectors $\mathbf{x}_\mathrm{A}$ and $\mathbf{x}_\mathrm{B}$. Now the variation can be performed for the force vector $\mathbf{F}_{\mathrm{c,B}}$.

$$\delta\mathbf{F}_{\mathrm{c,B}} = \mathbf{n}_\mathrm{c}\delta f_\mathrm{c} + f_\mathrm{c}\delta\mathbf{n}_\mathrm{c} \tag{130}$$

The variation for the cylinder force δf_c is presented in equation (127) and the variation for the normal vector can then be written as

$$\delta\mathbf{F}_{\mathrm{c},B} = (\mathbf{n}_\mathrm{c} \otimes \mathbf{W}_\mathrm{cyl})\delta\mathbf{X}_\mathrm{cyl} + \frac{f_\mathrm{c}}{\left\| \mathbf{x}_\mathrm{B} - \mathbf{x}_\mathrm{A} \right\|}\begin{pmatrix} -\mathbf{I} + \mathbf{n}_\mathrm{c} \otimes \mathbf{n}_\mathrm{c} & \mathbf{I} - \mathbf{n}_\mathrm{c} \otimes \mathbf{n}_\mathrm{c} \end{pmatrix}\begin{pmatrix} \delta\mathbf{x}_\mathrm{A} \\ \delta\mathbf{x}_\mathrm{B} \end{pmatrix} \tag{131}$$

The last term is conditional on the cylinder force and therefore the last term can be called as the geometric stiffness matrix of the hydraulic cylinder thus giving equation (131) form

$$\delta\mathbf{F}_{\mathrm{c,B}} = \mathbf{W}_\mathrm{cyl}^\mathrm{T}\delta\mathbf{X}_\mathrm{cyl} + \mathbf{K}_{\sigma\mathrm{cyl},B}\delta\mathbf{x}_\mathrm{AB} \tag{132}$$

Next step is to variate the first term in equation (132). Therefore we need first calculate few results that can be exploited in the derivation. First thing is to calculate the position of the hydraulic cylinder piston

$$x_c = \left\| \mathbf{x}_B - \mathbf{x}_A \right\| - l_{init} \tag{133}$$

And variation of this scalar produces a vector.

$$\delta x_c = \begin{pmatrix} -\mathbf{n}_c^T & \mathbf{n}_c^T \end{pmatrix} \begin{pmatrix} \delta \mathbf{x}_A \\ \delta \mathbf{x}_B \end{pmatrix} = \mathbf{b}_{c1}^T \delta \mathbf{x}_{AB} \tag{134}$$

In equation (134) the term $\mathbf{b}_{c1}^T$ is a kinematic vector. In the same manner we can write the velocity of the cylinder

$$\dot{x}_c = \mathbf{n}_c \bullet \left(\dot{\mathbf{x}}_B - \dot{\mathbf{x}}_A \right) \tag{135}$$

And variation produces

$$\begin{aligned} \delta \dot{x}_c &= \begin{pmatrix} -\mathbf{n}_c^T & \mathbf{n}_c^T \end{pmatrix} \begin{pmatrix} \delta \dot{\mathbf{x}}_A \\ \delta \dot{\mathbf{x}}_B \end{pmatrix} + \frac{\left(\dot{\mathbf{x}}_B - \dot{\mathbf{x}}_A \right)^T}{\left\| \mathbf{x}_B - \mathbf{x}_A \right\|} \begin{pmatrix} -\mathbf{I} + \mathbf{n}_c \otimes \mathbf{n}_c & \mathbf{I} - \mathbf{n}_c \otimes \mathbf{n}_c \end{pmatrix} \begin{pmatrix} \delta \mathbf{x}_A \\ \delta \mathbf{x}_B \end{pmatrix} \\ &= \mathbf{b}_{c1}^T \delta \dot{\mathbf{x}}_{AB} + \mathbf{b}_{c2}^T \delta \mathbf{x}_{AB} \end{aligned} \tag{136}$$

In this equation $\mathbf{b}_{c1}^T$ and $\mathbf{b}_{c2}^T$ are kinematic vectors. It is useful to notice that variation of the cylinder velocity is also dependable on the cylinder coordinates through the normal vector of the cylinder. Now we can substitute equation (136) to equation (131)'s first term on the right hand side and using equation (127)

$$\begin{aligned} (\mathbf{n}_c \otimes \mathbf{W}_{cyl}^T) \delta \mathbf{X}_{cyl} &= \begin{pmatrix} \mathbf{n}_c \otimes \begin{pmatrix} \mathbf{w}_{cyl} \\ w_{\dot{x}_c} \end{pmatrix} \end{pmatrix} \begin{pmatrix} \delta z \\ \delta P_A \\ \delta P_B \\ \delta \dot{x}_c \end{pmatrix} \\ &= \left(\mathbf{n}_c \otimes \mathbf{w}_{cyl} \right) \begin{pmatrix} \delta z \\ \delta P_A \\ \delta P_B \end{pmatrix} + \left(w_{\dot{x}_c} \mathbf{n}_c \otimes \mathbf{b}_{c1} \right) \delta \dot{\mathbf{x}}_{AB} + \left(w_{\dot{x}_c} \mathbf{n}_c \otimes \mathbf{b}_{c2} \right) \delta \mathbf{x}_{AB} \end{aligned} \tag{137}$$

Finally by adding corresponding derivative to $\mathbf{F}_{c,A}$ and identifying terms we get

$$\begin{pmatrix}\delta\mathbf{F}_{\mathrm{c,A}}\\ \delta\mathbf{F}_{\mathrm{c,B}}\end{pmatrix}=\begin{pmatrix}-\mathbf{n}_{\mathrm{c}}\otimes\mathbf{w}_{\mathrm{cyl}}\\ \mathbf{n}_{\mathrm{c}}\otimes\mathbf{w}_{\mathrm{cyl}}\end{pmatrix}\begin{pmatrix}\delta z\\ \delta P_{\mathrm{A}}\\ \delta P_{\mathrm{B}}\end{pmatrix}+\begin{pmatrix}-w_{\dot{x}_{\mathrm{c}}}\mathbf{n}_{\mathrm{c}}\otimes\mathbf{b}_{\mathrm{c1}}\\ w_{\dot{x}_{\mathrm{c}}}\mathbf{n}_{\mathrm{c}}\otimes\mathbf{b}_{\mathrm{c1}}\end{pmatrix}\delta\dot{\mathbf{x}}_{\mathrm{AB}}+\left(\begin{pmatrix}-w_{\dot{x}_{\mathrm{c}}}\mathbf{n}_{\mathrm{c}}\otimes\mathbf{b}_{\mathrm{c2}}\\ w_{\dot{x}_{\mathrm{c}}}\mathbf{n}_{\mathrm{c}}\otimes\mathbf{b}_{\mathrm{c2}}\end{pmatrix}+\begin{pmatrix}-\mathbf{K}_{\sigma\mathrm{cyl,B}}\\ \mathbf{K}_{\sigma\mathrm{cyl,B}}\end{pmatrix}\right)\delta\mathbf{x}_{\mathrm{AB}}$$

$$=\mathbf{K}_{\mathrm{inter}}\begin{pmatrix}\delta z\\ \delta P_{\mathrm{A}}\\ \delta P_{\mathrm{B}}\end{pmatrix}+\mathbf{C}_{\mathrm{cyl}}\delta\dot{\mathbf{x}}_{\mathrm{AB}}+\left(\mathbf{K}_{E\mathrm{cyl}}+\mathbf{K}_{\sigma\mathrm{cyl}}\right)\delta\mathbf{x}_{\mathrm{AB}} \tag{138}$$

Tangential matrices for the hydraulic cylinder can be calculated using equation (138). From this equation we notice that terms that are related to coordinates of the nodes of the hydraulic cylinder produce stiffness matrices. Correspondingly terms that are related to velocities produce damping matrix. Finally terms that are related to the hydraulic cylinder state variables create the interaction matrix between hydraulic and mechanical systems.

In this cylinder model no material values for the steel structures of the cylinder are needed. This implies that the mechanical part of the hydraulic system is completely rigid. The flexibility is taken into account only by the compressibility of the hydraulic fluid. If the material properties of the cylinder were taken into account, the forces induced by the deformations of the cylinder had to be added to the force equilibrium equation (115).

2.7 Assembly of the calculation model

Now we have presented various Jacobian matrices, stiffness matrices, damping matrices and mass matrices for different elements. The final step in forming the calculation model is to assemble these matrices together. For mechanical elements such as beam element we can use the standard summing procedure where cells of the element mass, damping and stiffness matrices can be summed together when elements share same nodal freedom. For the hydraulic system there is no need for summing as stated in previous chapter because elements share the same state variable. The dynamic system equation can then be written in form

$$\begin{cases}\mathbf{M}\ddot{\mathbf{q}} &= \mathbf{g}(\mathbf{q},\dot{\mathbf{q}},\mathbf{x}_{\mathrm{cyl}},t)\\ \dot{\mathbf{x}}_{\mathrm{cyl}} &= \mathbf{f}_{\mathrm{cyl}}(\mathbf{x}_{\mathrm{cyl}},\mathbf{x}_{\mathrm{hyd}},\mathbf{q},\dot{\mathbf{q}})\\ \dot{\mathbf{x}}_{\mathrm{hyd}} &= \mathbf{f}_{\mathrm{hyd}}(\mathbf{x}_{\mathrm{hyd}},\mathbf{x}_{\mathrm{cyl}})\end{cases} \tag{139}$$

where the first row presents the mechanical system, second row contains the cylinder variables and the last row describes the state of the hydraulic system. The exiciting term for the mechanical system, function $\mathbf{g}(\mathbf{q},\dot{\mathbf{q}},\mathbf{x}_{\mathrm{cyl}},t)$, is sum of external, internal and iner-

tial loads. In case of the cylinder and hydraulics the functions are presented in equations (121) and (102) respectively. For the hydraulic system the function is always depended on the hydraulic system and it has to be assembled according to the system. For instance in equation (102) we have combined two transmission line elements using the orifice model. By differentiating equation (139) the linearized equations of equilibrium can be written

$$\begin{pmatrix} \mathbf{M} & \mathbf{0} & \mathbf{0} \\ \mathbf{0} & \mathbf{0} & \mathbf{0} \\ \mathbf{0} & \mathbf{0} & \mathbf{0} \end{pmatrix} \begin{pmatrix} \Delta\ddot{\mathbf{q}} \\ \Delta\ddot{\mathbf{x}}_{\text{cyl}} \\ \Delta\ddot{\mathbf{x}}_{\text{hyd}} \end{pmatrix} + \begin{pmatrix} \mathbf{C} & \mathbf{0} & \mathbf{0} \\ -\dfrac{\partial \mathbf{f}_{\text{cyl}}}{\partial \dot{\mathbf{q}}} & \mathbf{I} & \mathbf{0} \\ \mathbf{0} & \mathbf{0} & \mathbf{I} \end{pmatrix} \begin{pmatrix} \Delta\dot{\mathbf{q}} \\ \Delta\dot{\mathbf{x}}_{\text{cyl}} \\ \Delta\dot{\mathbf{x}}_{\text{hyd}} \end{pmatrix} + \begin{pmatrix} \mathbf{K} & -\dfrac{\partial \mathbf{g}}{\partial \mathbf{x}_{\text{cyl}}} & \mathbf{0} \\ -\dfrac{\partial \mathbf{f}_{\text{cyl}}}{\partial \mathbf{q}} & -\dfrac{\partial \mathbf{f}_{\text{cyl}}}{\partial \mathbf{x}_{\text{cyl}}} & -\dfrac{\partial \mathbf{f}_{\text{cyl}}}{\partial \mathbf{x}_{\text{hyd}}} \\ \mathbf{0} & -\dfrac{\partial \mathbf{f}_{\text{hyd}}}{\partial \mathbf{x}_{\text{cyl}}} & -\dfrac{\partial \mathbf{f}_{\text{hyd}}}{\partial \mathbf{x}_{\text{hyd}}} \end{pmatrix} \begin{pmatrix} \Delta\mathbf{q} \\ \Delta\mathbf{x}_{\text{cyl}} \\ \Delta\mathbf{x}_{\text{hyd}} \end{pmatrix} = \begin{pmatrix} \mathbf{r}^* \\ \mathbf{s}^* \\ \mathbf{t}^* \end{pmatrix} \tag{140}$$

This equation (140) is the equation of motion for the coupled system. For clarity we study this equation. First of all it is noticeable, that only the mechanical system produces mass matrix **M**. The second term in equation (140) represents the damping terms duo to time derivatives. As expected, the mechanical system produces damping matrix **C** but also the hydraulic cylinder introduces damping to the system. The damping matrix of the cylinder is presented in equation (138). It is also noticeable that frictionless cylinder element does not introduce damping. Elements of the matrix **C** does not however, include any real damping model as viscous damping or Rayleigh damping. Instead these damping models are to be added separately to matrix **C**.

The last multiplier matrix represents the derivatives to the system variables. From the mechanical system we get the stiffness matrix **K** which is assembled by basic elemental addition. Stiffness matrices for different elements are shown in previous chapters. Next term on the diagonal is the hydraulic cylinder Jacobian matrix presented in equation (122) and the last diagonal term is the hydraulic Jacobian matrix. This term is assembled from the Jacobian matrices of different transmission line elements presented in equations (93), (95) and (97) in a procedure explained in construction of equation (103).

Off-diagonal terms then represent the connection between these three different systems. This hydro-mechanical system can be treated as three-field problem where we have mechanical system, cylinder system and hydraulic system. For instance cell (2,1) is the connection between mechanical system and hydraulic cylinder and this matrix is introduced in equation (138) as $\mathbf{K}_{\text{inter}}$.

On the right hand side we have the residual vectors from the linearization. The superscript denotes, that the residuals are calculated in the linearization point. The residual vectors are calculated using following formulas

$$\begin{cases} \mathbf{r}^* = \mathbf{g}(\mathbf{q},\dot{\mathbf{q}},t) - \mathbf{M}\ddot{\mathbf{q}} \\ \mathbf{s}^* = -\dot{\mathbf{x}}_{\text{cyl}} + \mathbf{f}_{\text{cyl}}(\mathbf{x}_{\text{cyl}},\mathbf{x}_{\text{hyd}},\mathbf{q},\dot{\mathbf{q}}) \\ \mathbf{t}^* = -\dot{\mathbf{x}}_{\text{hyd}} + \mathbf{f}_{\text{hyd}}\left(\mathbf{x}_{\text{cyl}},\mathbf{x}_{\text{hyd}}\right) \end{cases} \tag{141}$$

This equation system (141) is the equation of motion for the whole coupled hydraulically driven flexible multibody system. Different solution methods are applied to these equations depending on the simulation case.

The assembly of the mechanical system is dealt with traditional technique where the local matrices are scattered to the global matrices. For this scattering node table is needed where local node numbers are transferred to global numbers. Using this node table the gathering of the global matrices is achieved. Same kind of procedure is used for the hydraulic system and for the cylinder element. Hydraulic transmission line elements have local numbering for the flow rates and pressures and then these local numbers are transferred to global system and the Jacobian matrix can then be assembled. Example of this assembly is presented in Chapter 2.5.4.

2.8 Newton-Raphson algorithm

For the statics computation Newton-Raphson algorithm is applied to the first equation of the set (141) with one main difference. In statics calculations the load is assumed to be independent of time and therefore inertial loads can be ignored and no mass matrix is needed for the system. This implies that only the stiffness matrix of the system appears in the equations.

The Newton-Raphson algorithm can be derived from Taylor series of the residual vector defined in (141) (Bonet, et al., 2009)

$$\mathbf{r}^* \approx \mathbf{r}_0^* + \frac{\partial \mathbf{g}}{\partial \mathbf{q}}\Delta\mathbf{q} + \frac{1}{2!}\frac{\partial \mathbf{g}}{\partial \mathbf{q}\partial \mathbf{q}}\Delta\mathbf{q}^2 + \ldots = \mathbf{0} \tag{142}$$

When the system is in equilibrium the residual vector vanishes which explains why the linearization of the residual vector is equal to zero. Taking only the first derivative into account and assuming the higher order derivatives to be insignificant and defining the derivative term as stiffness matrix the Newton-Raphson algorithm can be written

$$\begin{aligned} \mathbf{K}_{\text{T}} &= -\frac{\partial \mathbf{g}}{\partial \mathbf{q}} \\ \mathbf{K}_{\text{T}}\Delta\mathbf{q} &= \mathbf{r}_0^* \end{aligned} \tag{143}$$

The stiffness matrices for different elements are given in sections where elements are introduced. The iteration formula for Newton-Raphson iteration is then constructed to

$$\Delta\mathbf{q} = \mathbf{K}_{\mathrm{T}}^{-1}(\mathbf{q})\mathbf{r}_n^*(\mathbf{q})$$
$$\mathbf{q}_{n+1} = \mathbf{q}_n + \Delta\mathbf{q} \tag{144}$$

In general Newton-Raphson algorithm is used to solve equation systems in iterative manner and it is suitable for linear and nonlinear problems. In case of linear systems the stiffness matrix is constant and solution is achieved with one step. In nonlinear equation systems algorithm gives quadratic convergence near the solution. Although this algorithm is a general algorithm in mathematics, in mechanics it is exploited when the deformed state of the loaded system is computed.

2.9 Newmark integration algorithm

To obtain the solution for the equation set (140) we need a numerical algorithm for the time integration of the equations of motion. One basic method used widely in mechanics is to use implicit Newmark time integration. Presentation in this master's thesis is based on Geradin & Cardona (2001) and Marjamäki & Mäkinen (2007). Newmark method is effective in mechanics while it can be applied to second order differential equations directly whereas many algorithms solve only first order differential equations. In this case the equation needs to be transformed into first order differential equation systems.

First step in time integration is to define predictors for acceleration, velocity and displacements. When choosing these predictors there are several alternatives but in this case the zero acceleration prediction is chosen. In following formulas subindices represent the time step and superscripts note the iterations. Now the zero acceleration predictors can be written

$$\begin{aligned}
&\ddot{\mathbf{q}}_{n+1}^{0} = \mathbf{0} \\
&\dot{\mathbf{q}}_{n+1}^{0} = \dot{\mathbf{q}}_{n+1} + (1-\gamma)h\ddot{\mathbf{q}}_n \\
&\mathbf{q}_{n+1}^{0} = \mathbf{q}_n + h\dot{\mathbf{q}}_{n+1} + \left(\frac{1}{2} - \beta\right)h^2\ddot{\mathbf{q}}_n \\
&\left(\dot{\mathbf{x}}_{\mathrm{cyl}}\right)_{n+1}^{0} = \left(\dot{\mathbf{x}}_{\mathrm{cyl}}\right)_n \\
&\left(\mathbf{x}_{\mathrm{cyl}}\right)_{n+1}^{0} = \left(\mathbf{x}_{\mathrm{cyl}}\right)_n + h\left(\dot{\mathbf{x}}_{\mathrm{cyl}}\right)_n \\
&\left(\dot{\mathbf{x}}_{\mathrm{hyd}}\right)_{n+1}^{0} = \left(\dot{\mathbf{x}}_{\mathrm{hyd}}\right)_n \\
&\left(\mathbf{x}_{\mathrm{hyd}}\right)_{n+1}^{0} = \left(\mathbf{x}_{\mathrm{hyd}}\right)_n + h\left(\dot{\mathbf{x}}_{\mathrm{hyd}}\right)_n
\end{aligned} \tag{145}$$

where h is the time step and β and γ are integrator parameters. These parameters can be written using third parameter α as follows

$$\gamma = \frac{1}{2} + \alpha \qquad \beta = \frac{1}{4}\left(\gamma + \frac{1}{2}\right)^2 \tag{146}$$

Parameter α defines numerical damping to the integrator. Usually it is assumed as zero but in cases where spurious vibrations occur the behavior of the system can be smoothen.(Géradin, et al., 2001 p. 31)

The predictors in equations (145) are initial guess for the iteration at time step *n+1* and therefore these values need to be corrected. For this purpose we introduce Newmark's formulas which state that changes in accelerations and velocities can be written using only displacements changes and integrator parameters.

$$\begin{aligned} \Delta\ddot{\mathbf{q}} &= \frac{1}{\beta h^2}\Delta\mathbf{q} \\ \Delta\dot{\mathbf{q}} &= \frac{\gamma}{\beta h}\Delta\mathbf{q} \end{aligned} \tag{147}$$

These same equations are valid also for the hydraulic and cylinder variables. Using these connections it is now possible to write system equation (140) by using only the state variables and not their time derivatives

$$\begin{pmatrix} \mathbf{S}_\mathrm{T} & \mathbf{U}_\mathrm{c} & \mathbf{0} \\ \mathbf{L}_\mathrm{c} & \mathbf{H}_\mathrm{c} & \mathbf{U}_\mathrm{h} \\ \mathbf{0} & \mathbf{L}_\mathrm{h} & \mathbf{H}_\mathrm{h} \end{pmatrix} \begin{pmatrix} \Delta\mathbf{q} \\ \Delta\mathbf{x}_\mathrm{cyl} \\ \Delta\mathbf{x}_\mathrm{hyd} \end{pmatrix} = \begin{pmatrix} \mathbf{r}^* \\ \mathbf{s}^* \\ \mathbf{t}^* \end{pmatrix} \tag{148}$$

where the right hand side can be calculated from (141) and the components of the multiplier matrix are defined as

$$\begin{aligned} \mathbf{S}_\mathrm{T} &= \mathbf{K}_\mathrm{T} + \frac{\gamma}{\beta h}\mathbf{C}_\mathrm{T} + \frac{1}{\beta h^2}\mathbf{M} \\ \mathbf{U}_\mathrm{c} &= -\frac{\partial \mathbf{g}}{\partial \mathbf{x}_\mathrm{cyl}} & \mathbf{L}_\mathrm{c} &= -\frac{\partial \mathbf{f}_\mathrm{cyl}}{\partial \mathbf{q}} - \frac{\gamma}{\beta h}\frac{\partial \mathbf{f}_\mathrm{cyl}}{\partial \dot{\mathbf{q}}} \\ \mathbf{H}_\mathrm{c} &= -\frac{\partial \mathbf{f}_\mathrm{cyl}}{\partial \mathbf{x}_\mathrm{cyl}} + \frac{\gamma}{\beta h}\mathbf{I} & \mathbf{U}_\mathrm{h} &= -\frac{\partial \mathbf{f}_\mathrm{cyl}}{\partial \mathbf{x}_\mathrm{hyd}} \\ \mathbf{L}_\mathrm{h} &= -\frac{\partial \mathbf{f}_\mathrm{hyd}}{\partial \mathbf{x}_\mathrm{cyl}} & \mathbf{H}_\mathrm{h} &= -\frac{\partial \mathbf{f}_\mathrm{hyd}}{\partial \mathbf{x}_\mathrm{hyd}} + \frac{\gamma}{\beta h}\mathbf{I} \end{aligned} \tag{149}$$

These matrices are considered only as system matrices.

From equation (148) it is now possible to calculate the change vectors of mechanics, cylinder and hydraulics. The new point where the linearization is made can be achieved by using equation (147) and the change vectors

$$
\begin{aligned}
\ddot{\mathbf{q}}_{n+1}^{k+1} &= \ddot{\mathbf{q}}_{n+1}^{k} + \frac{1}{\beta h^2}\Delta\mathbf{q} \\
\dot{\mathbf{q}}_{n+1}^{k+1} &= \dot{\mathbf{q}}_{n+1}^{k} + \frac{\gamma}{\beta h}\Delta\mathbf{q} \\
\mathbf{q}_{n+1}^{k+1} &= \mathbf{q}_{n+1}^{k} + \Delta\mathbf{q} \\
\left(\dot{\mathbf{x}}_{\mathrm{cyl}}\right)_{n+1}^{k+1} &= \left(\dot{\mathbf{x}}_{\mathrm{cyl}}\right)_{n+1}^{k} + \frac{\gamma}{\beta h}\Delta\mathbf{x}_{\mathrm{cyl}} \\
\left(\mathbf{x}_{\mathrm{cyl}}\right)_{n+1}^{k+1} &= \left(\mathbf{x}_{\mathrm{cyl}}\right)_{n+1}^{k} + \Delta\mathbf{x}_{\mathrm{cyl}} \\
\left(\dot{\mathbf{x}}_{\mathrm{hyd}}\right)_{n+1}^{k+1} &= \left(\dot{\mathbf{x}}_{\mathrm{hyd}}\right)_{n+1}^{k} + \frac{\gamma}{\beta h}\Delta\mathbf{x}_{\mathrm{hyd}} \\
\left(\mathbf{x}_{\mathrm{hyd}}\right)_{n+1}^{k+1} &= \left(\mathbf{x}_{\mathrm{hyd}}\right)_{n+1}^{k} + \Delta\mathbf{x}_{\mathrm{hyd}}
\end{aligned}
\tag{150}
$$

Time integration process proceeds as shown in Figure 14.

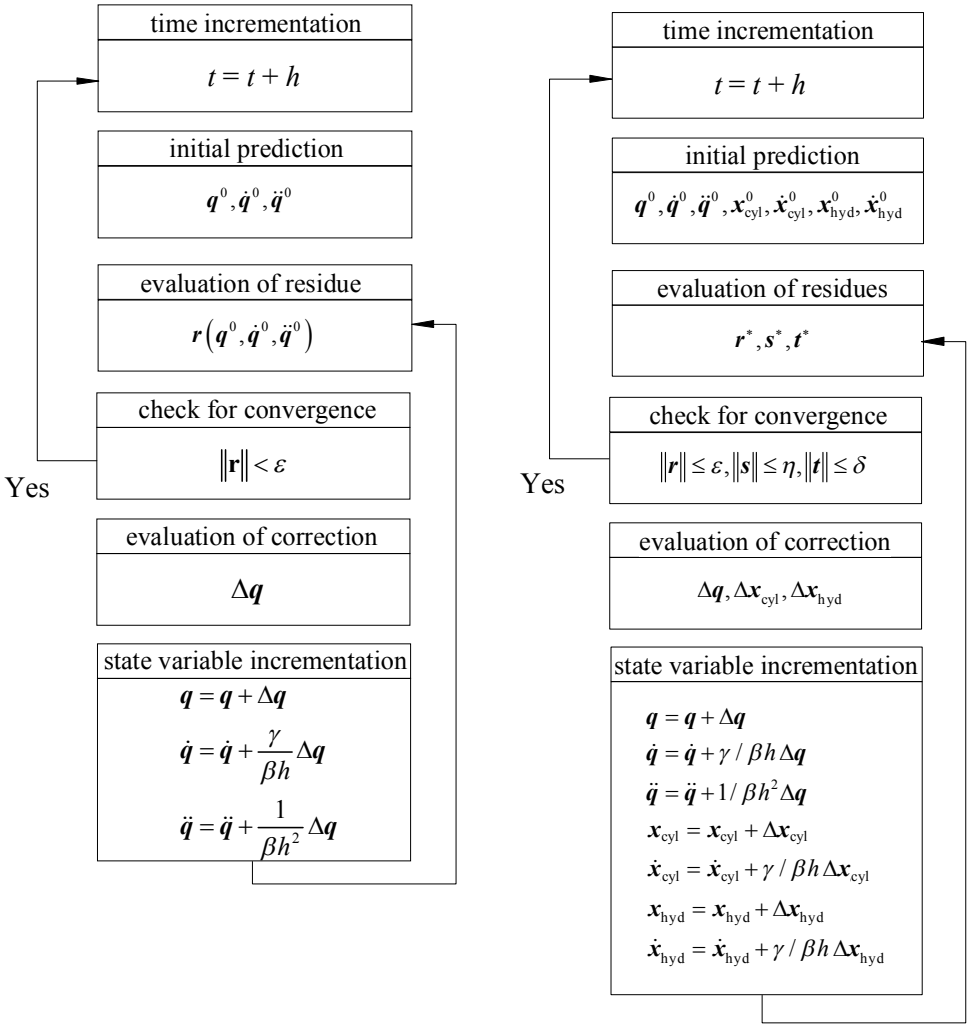

Figure 14 *The Newmark integration procedure for two cases: On the left mechanical system and on the right coupled hydro-mechanical system*

Time integration of the coupled hydro-mechanical system is more complicated than the time integration of the plain mechanical system because there are more tangent matrices and three different convergence criteria. In system matrices in (149) it can also be noted that hydraulic system and hydraulic cylinder both are only first order differential equations whereas mechanical system is second order differential equation.

3 CASE STUDY

In this chapter all presented theories are applied to a numerical example. Purpose was to find a structure that is mechanically complex enough to show that beam elements are effective tool when total stiffness of the structure is considered. Besides, the system has to be hydraulically driven so that the hydraulic elements can also be exploited. Traditional lifting boom is fairly simple hydro-mechanical system but these examples have been presented in literature widely. Therefore Cassette Multifunctional Mover (CMM) of the ITER fusion reactor was chosen as the case study. It offers complex mechanical system and also hydraulic system. This is also very suitable case because all information considering the ITER project has been declared open.

3.1 Computational model

In this chapter the calculation model is introduced. The CMM is a hydraulic driven multibody system and the introduction is therefore divided into two segments. First we take a look at the mechanical system. Modeling techniques are presented and discussed mainly concerning the beam element modeling. In the second part the hydraulic system is introduced and the modeling technique for hydraulic system is discussed.

In this thesis two different models are used and compared. In the first model, the lift cylinder is modeled as length controlled rod element and in the other model the cylinder is modeled as cylinder element and it is controlled by a hydraulic system. In next chapters the mechanical system and the hydraulic system are presented.

At this point it has to be noted that the model parameters used in this master's thesis does not correspond exactly to the real parameter values of the CMM. Main idea is to show that the theory presented in Chapter 2 can be applied to real structures and to point out differences with different modeling techniques. In this comparison it is not relevant whether the results match exactly to real values of the CMM. Instead it is important that the compared models are consistent with each other.

All simulations have been made using Matlab as programming environment. However, some other programming languages would perform better in this kind of programming.

3.1.1 Mechanical structure

The CMM has been modeled for this master's thesis with nonlinear geometrically exact Reissner's beam element. The structure itself is not beam-like but it is possible to model it with beams. When this kind of modeling is used total flexibility of the structure can

be taken into account but accurate stress results in pinpointed locations as in bearings or lugs cannot be calculated.

In Figure 15 the CMM model shown as 3D CAD image. The robot consists of four different parts two of which are not replaceable. These two are the lift arm which is shown as light blue in Figure 15 and tilt arm as green part. The three parts are changeable depending on the operation that is performed. These three parts together form the Second Cassette End Efector (SCEE) of the maintenance robot. The brown part in Figure 15 is called the CRO and the final part is the HRO and it is presented in light blue at the right hand side of the figure.

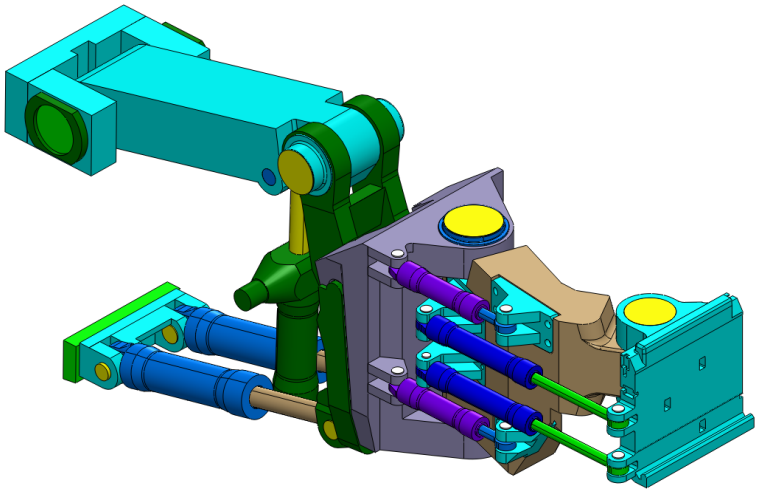

Figure 15 *3D CAD presentation of the Cassette Multifunctional Mover*

The SCEE is attached to the CMM body using special suspended structure where the end-efector is not in rigid connection with the tilt arm. Instead it merely hangs in front of the tilt arm. This construction offers easy end-efector changeability but it also introduces some problems when deformations of the system are studied. Because the connection between tilt arm and end-efector exists at the upper part and the lower part is not supported at all deformations exists at the suspended structure. This deformation then inflicts loss of friction between the end-efector and tilt arm.

For the hydro-mechanical simulations a beam model of the CMM was introduced to represent the actual solid construction. Reason for this simplification is, that when beam elements are exploited the size of the calculation model becomes smaller compared to solid element modeling. If real-time simulation is wanted small computational models are more effective but at the same time they cannot represent all details in the actual structure. The beam element model of the CMM is presented in Figure 16.

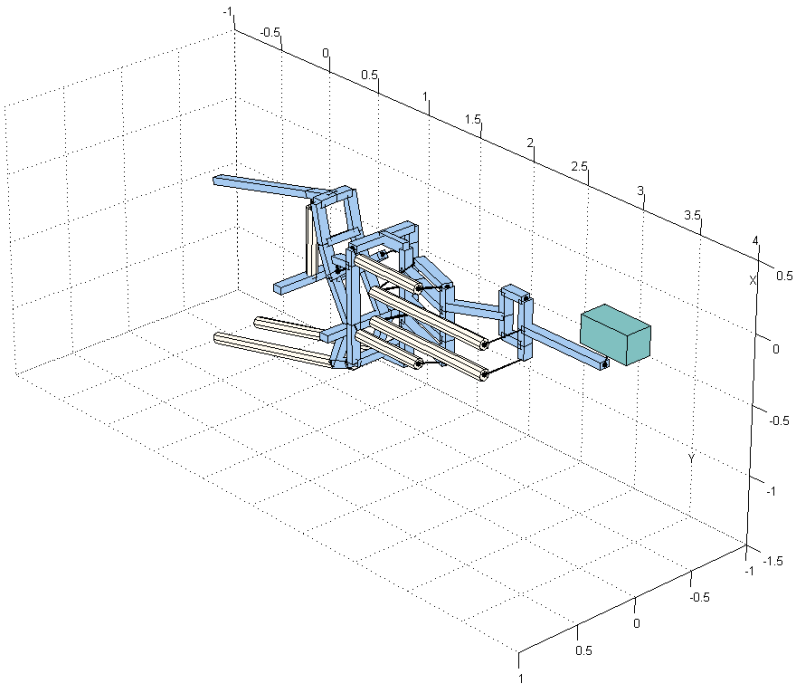

Figure 16 *Cassette Multifunctional Mover model with beam and rod elements*

In the FEM model of the structure 4 types of elements are used. The solid parts are modeled using the geometrically exact beams as stated earlier. These beam elements are presented as blue in Figure 16 and the offset are marked as black lines. The topology of the structure is based on the 3D cad drawings of the CMM. From these drawings it is possible to calculate coordinates for the nodes of the beam elements. The model is parameterized using the joint angles of the CMM and therefore the computational model can be set to different positions easily. Parameterized joint angles are the lift arm angle, tilt arm angle, the CRO angle and finally the HRO angle. It should be noted that while the axis of the lift arm angle and tilt arm angle remain constant the CRO and the HRO joint axis depend on the lift arm and tilt arm rotations. This important observation allows the computational model to undergo large rotations.

The black lines represent the kinematic connection of the offset. Offset beams are used mainly where hydraulic cylinders are connected to the structure. Usage of offset beam elements allows the topology of the structure to remain constant and cylinder connections can be dealt with the offsets only.

In Figure 16 hydraulic cylinders are presented as yellow tubes and these cylinders are modeled as length controlled bar elements presented in 2.3.3 except for the lift cylinder which is also modeled as cylinder element. Stiffness of the bar element is calculated as two springs connected in series: hydraulic stiffness and mechanical stiffness. Because hydraulic fluid is more flexible than the steel used in the cylinder, the flexibility of the fluid is dominant. The stiffness of the rod element is calculated to be same as is the stiffness of the hydraulic cylinder element.

Flexibility of the rotational joints is taken into account with spring elements. Joint pin and the beam connected to the joint pin are not in rigid connection that allows only

rotation about the rotation axis. Instead a spring element is introduced in between these two elements to represent the bearing flexibility. The pin flexibility is taken into account by modeling the pin as a beam element.

External load of the system consist of gravitational loads. The beams themselves have mass which produces force facing downwards. In Figure 16 the green box at the right hand side of the picture represents the movable cassette which weighs 9000 kg. In dynamic simulation these masses also produce inertial loads.

Boundary conditions for the model are applied on the joint of the lift arm where all other degrees of freedom are constrained but the rotation which allows the lift arm to rotate. This constraint is not absolutely correct because the CMM lies on a linear rails and this connection is not rigid. Same type of boundary condition is set for the tilt cylinders. All but the rotational freedom are constrained. One final boundary condition is set for the lift cylinder. It lies between two beam elements and the beam elements are considered to have rigid connections.

3.1.2 Hydraulic system

The hydraulic system in the CMM is a water hydraulic servo system. Servo system is needed because the CMM is designed to lift bundles of 9000 kg and velocities of the system need to be low. The CMM also operates in narrow spaces and positioning accuracy has to be precise. Therefore it is justified to use servo system to operate the CMM. Water is used as hydraulic fluid because a single drop of mineral oil would contaminate the fusion reactor and by using demineralized water this risk is avoided.

In this master's thesis the servo system is simplified to traditional hydraulic system where the servo valve is replaced with on/off 4/3 -hydraulic valve whose model is presented in Chapter 2.5.4. Computational model of the complete hydraulic system model is presented in Figure 17.

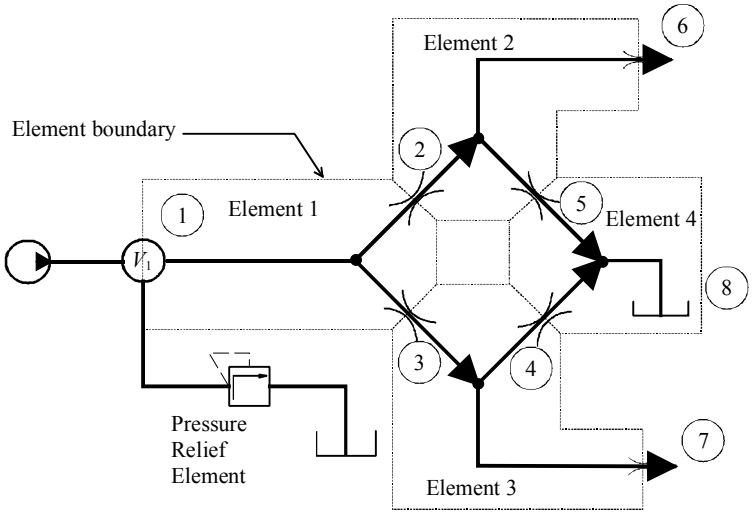

Figure 17 *Computational model of the hydraulic system. Arrows point out the positive flow direction. Boxed numbers present elements and circulated numbers are flow rates*

This model consist of two major parts: transmission line elements and pressure relief element. The transmission line elements are marked with boxed numbers in Figure 17 and they are connected together using technique presented in 2.5.3 to form the hydraulic system. Flow rates between these elements are presented as circulated numbers. The pressure relief element is connected to the system via volume V_1 in Figure 17. Transmission line element 1 is P-QQ-element, elements 2 and 3 are QQ-Q elements and element 4 is QQ-P element because tank is assumed as a volume. The hydraulic pump produces constant flof rate to the system and when the directional valve is closed flow rate is forced to go through the pressure relief element. When the directional valve is opened part of the flow rate goes through the orifice 3. Transmission line element 3 connects directional valve to the A-chamber of the hydraulic cylinder and orifice 7 presents this throttling. On the return line there is orifice 6 and orifice 5 in the way to the tank 8 where constant pressure is assumed. The cylinder element is the lift cylinder of the lift arm. The other hydraulic cylinders are modeled as rod elements.

Although the hydraulic fluid used in the CMM is demineralized water, in this master's thesis the system is considered as more traditional oil hydraulic system. Water is more aggressive pressure medium than oil because it has higher bulk modulus and also viscosity is lower. Due to these differences the response of the hydraulic system is faster and in time integration time step needs to be smaller. Usage of water as pressure medium would not however, introduce more information to the comparison and therefore hydraulic fluid is oil

3.2 Initial deformation

When dynamic simulations are concerned an initial state of the system has to be defined. The deformed state of the CMM is computed by using the Newton-Raphson algorithm that is presented in section 2.8. The only loads that need to be taken into account in this analysis are gravitational loads. This initial state is then used in equation (145) at the first step of the time integration.

In this master's there are two different systems that are simulated. In first model the lift cylinder is modeled as length controlled rod element and in the other model we have special hydraulic cylinder element and hydraulic system that produces flow rate to the cylinder. This flow rate then moves the cylinder. Statics is solved first in both of these models but in the hydraulic model the cylinder is replaced with a rod element in statics computation. This means that the hydraulic system is not included in the computation of initial state. The compressibility of the hydraulic fluid is taken into account in the flexibility of the rod element and therefore this method is justified. The cylinder element is then introduced to the model at the first time step of the Newmark time integration. Pressure for the cylinder can determined using the definition of pressure: $p = F/A$. The force is the norm of the internal force vector of the rod element in (51) and area is the area of the piston of the cylinder. In the B-chamber pressure is assumed to be 1 bar.

3.3 Dynamic simulation

Main concentration on this master's thesis is on the dynamic simulation of the CMM. Initial deformation is calculated only for the first step of the Newmark time integration. In this chapter we introduce the simulation cases and explain why these simulations have been chosen for this thesis. In addition the matter of stable initial solution is discussed because it is plays a significant role in the results of the simulation. Finally we discuss the calculation parameters and their affect on the response of the system.

3.3.1 Computation case

In this thesis two different simulation models are used. In first simulation model all hydraulics is replaced with length controlled rod elements and in the second model the lift cylinder of the CMM is modeled as hydraulic cylinder and the hydraulic system is also included. Main focus is on comparing responses of the mechanical system when the lift cylinder is modeled in two different ways. To do this comparison two different simulation cases are presented in both of which we have both length controlled rod element and hydraulic cylinder in them. Difference in the simulation cases is the length change for the rod element. Hydraulics is simulated only once and these results are used in both simulation cases.

In both simulation cases we track the vertical displacement of the cylinder rod and the cassette. This is a natural choice because the gravitational field is in the direction of the y-axel and this displacement is the most representational displacement. Due to the asymmetric nature of the CMM there are also displacements in the other directions but they are not as natural to present.

In first simulation case we compare hydraulic system and the length controlled rod element in case where the length change of the rod element is calculated from the stationary condition of the hydraulic system. Stationary condition design is usually used in hydraulics when systems are designed and therefore it is also used here. The length chance of the hydraulic cylinder on the other hand is defined by the hydraulic system and the only way to affect on the cylinder is to change the parameters of the hydraulic system or the hydraulic cylinder.

Time when the rod element changes length is defined from the time that the directional valve is open. The length change starts at the moment when the directional valve starts to open and length change stops when the valve starts to close.

In the simulation case 2, the only difference to the simulation case one is the length change of the rod element. When in first simulation case the length change was defined from the stationary condition of the hydraulic system, in second simulation case the length change is defined from the simulation results of the hydraulic system. Length chance is defined from the time period when the directional valve starts to open and when it starts to close.

The length change of the length controlled bar element can be given as function of time as Chapter 2.3.3 states. Therefore different functions are also given in this thesis.

In hte simulation case 1 where the length change is calculated from the stationary state of the hydraulic system we use two different functions. First is linear function where we know the time period and the length of the rod at the end of the simulation and the change in length is linear. The other model introduces the Hermite polynomial which is also used in the pressure relief element model. The change of length as function of time is very similar to equation (107).

In the simulation case 2, we introduce third length function for the rod element. In this function we combine the linear model and the Hermite polynomial model. Length change starts with Hermite polynomial and with zero derivative but it ends up changing length in linear fashion.

Main focus on comparing these computational cases is to find out how well the length controlled rod element can model actual hydraulic cylinder and to find out new methods for representing behavior of the cylinder. When the hydraulic system is introduced to the system the differential equation system (139) becomes stiff which forces the time step to be very short. Short time steps then leads to long computation times. Therefore it would be more effective to use non-stiff equation and computation could be in real time.

3.3.2 Simulation parameters

Calculation parameters are the most influential things in simulation results when the modeling technique has been chosen. Of course the mathematical modeling plays the most important thing when the results are concerned. If wrong modeling techniques are applied on the problem the results can be anything. In this problem the modeling techniques are presented in the theory chapter. In short, the mechanical system is modeled using non-linear element method and the hydraulic system is also modeled using variational method which leads to element method formulation.

It has been noted earlier that the calculation parameters in this thesis are not taken from the real system because it would not bring any additive information to the objective in this thesis. In addition the real CMM is a water hydraulic servo system and in this thesis the hydraulic system is considered to be traditional on/off oil hydraulics. If the parameters are coherent in each simulation case the results are comparable and it leads to solid conclusions about the modeling techniques presented.

The most interesting parameters are connected to the hydraulic system and to the hydraulic cylinder and on the other hand on the length controlled rod element. The most crucial parameters are tabulated in Table 1. We pay no attention on the mechanical system because it remains constant between the two simulation models and thus it brings no wanted information.

Table 1 *The most essential simulation parameters*

	Value	Unit
Density of the fluid, ρ_0	780	kg/m^3
Bulk modulus of the fluid, B_0	1.1	GPa
Kinematic viscosity of the fluid, ν_0	1.60E-04	m^2/s
Orifice radius 3	1	mm
Orifice radius 7	3.5	mm
Orifice radius 6	3.5	mm
Orifice radius 5	1	mm
Length of transmission line 1	2	m
Length of transmission line 2	2	m
Length of transmission line 3	2	m
Length of transmission line 4	2	m
Inner diameter of transmission line 1	4	mm
Inner diameter of transmission line 2	4	mm
Inner diameter of transmission line 3	4	mm
Inner diameter of transmission line 4	4	mm
Valve closing time	0.1	s
Valve opening time	0.1	s
Valve starts to open	0.05	s
Valve starts to close	2	s
Setup pressure for the PRV	150	bar
Flow rate from the pump	14.1	l/min
Cylinder piston diameter	125	mm
Cylinder rod diameter	80	mm
Cylinder stroke	454	mm
Stationary flow to the cylinder	8.8	l/min
Static friction, F_{st}	1000	N
Coulomb friction, F_{Cou}	100	N
Viscose friction, F_{v}	1000	N
Stribeck velocity, v_{Str}	0.002	m/s
Friction stiffness coefficient, k_0	8000000	N/m
Friction damping coefficient, k_1	2828	kg/s

The valve opening and closing time is adjusted to be excessive when compared to the real values for on/off –valves. Times are usually 40 ms but in this simulation 100 ms is used. This choice has been made to point out the differences between the length controlled rod element and the cylinder element.

3.3.3 Stable initial solution

The deformed state for the system is computed with Newton-Raphson algorithm and as explained, the algorithm computes only mechanical system. Therefore in simulations where hydraulic system is present the hydraulic cylinder is changed to rod element when the initial state is computed and in time integration it is changed back to cylinder element. This method makes the computation of initial deformation effective but it also introduces problems.

In initial state the residual vector of mechanics is near zero vector but because hydraulics and cylinder residuals are not calculated in initial state calculations there is no information on these vectors, see (141). If the residual vectors are far from zero vector the time integration fails at first time steps because the hydraulic system starts to oscillate and at some point it does not converge.

The method for finding a stable value for the state variables is needed and in this thesis it is done manually. The process happens by keeping the directional valve openings closed and thereby transmission line elements have no connection with each other, see Figure 17. However, the cylinder element in connection with transmission line elements 2 and 3. The state vector for the cylinder is easily computed because it contains only chamber pressures and the bristle deflection, see (121). The chamber pressures are calculated from the initial state and the bristle deflection is assumed to be zero.

Using the information of the cylinder state vector the state vector for the transmission line element 3 is calculated. The pressure in the element is the same as in the A-chamber of the cylinder and no flow rates exist. Same strategy is applied on the transmission line element 2. Transmission line element 1 is balanced in same manner. Because the directional valve is closed all flow rate from the pump goes through the pressure relief element and the pressure in element 1 and in volume 1 is same as the setup pressure of the pressure relief element. When the initial values for the state vectors are correct enough, the time integration converges and produces accurate state vectors that can be given as initial values for the integration.

This procedure for finding a stable initial state vector for hydraulics and cylinder is very slow and it does not allow easy parameter changing. For instance when the diameters of the transmission line elements are changed, the initial value for the hydraulic state variables has to be updated because the hydraulic volume changes and it changes the pressure in element 1. Therefore a new initial state vector has to be found by computing short time period where the oscillation dampens and then the state vector is saved and used as initial value.

3.4 Results

In this chapter the simulation results are presented for the two simulation cases described in section 3.3.1. First we present the results for simulation case 1 and discuss the results. In following section results for the simulation case 2 are presented and discussed. Finally the results for the hydraulic system and for the friction are shown.

3.4.1 Simulation case 1

In this simulation case the hydraulic system is simulated using parameters in Table 1 and the corresponding mechanical system with lift cylinder as length controlled rod element where the length change of the rod is calculated from the stationary flow rate to the lift cylinder. Traditionally hydraulic systems are designed for the stationary state of the system and in this case we have no better understanding of the hydraulic system so it is justified to use this stationary condition. We also use two different functions for the length change of the rod: linear model and Hermite polynomial model.

In Figure 18 are the displacement results of the hydraulic cylinder. Curves show how the rod of the cylinder moves upwards during the simulation period. There is huge difference in the displacements between the mechanical models and the cylinder model. This implies that the hydraulic system has not reached the stationary state and therefore the cylinder velocity does not reach the maximum velocity. From the mechanical models it can be noted that the stationary value for the cylinder is not correct way to calculate the length change for the rod element.

There are also differences in the behavior between the linear length function and Hermite polynomial function if only the rod element is concerned. Hermite polynomials are widely used in the field of mechanics because it introduces additional damping to the system because the function has zero derivatives in the beginning and at the end of the domain where the function is defined. However, from the velocity curves in Figure 18 we can see that the Hermite polynomial does not represent the behavior of the cylinder in any way. The linear model introduces intense vibration to the velocity curve while the Hermite polynomial is smooth curve. Therefore the linear model is the better to use of these mechanical models. However, when the hydraulic system curves are compared with the mechanical system curves, no conclusions can be made due to the huge difference in the length changes of the systems.

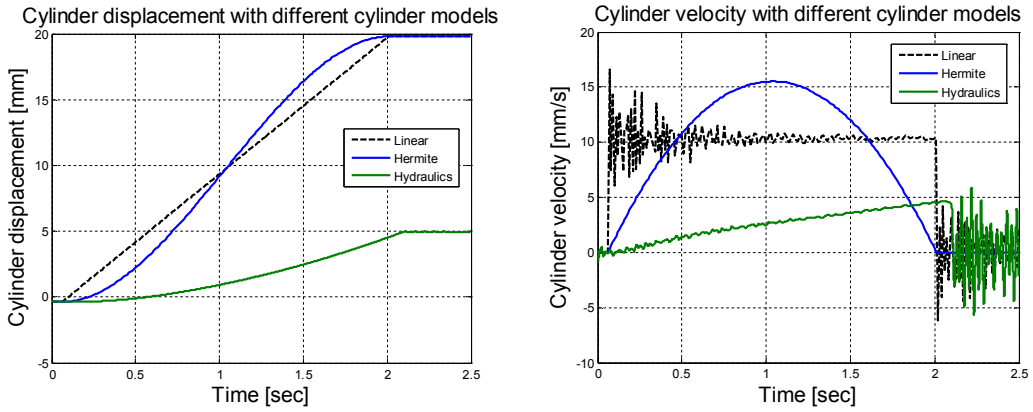

Figure 18 *Lift cylinder displacement and velocities as function of time*

In stopping phase the velocity of the mechanical models is defined by the length change function. In case of the Hermite polynomial the velocity is zero as it is defined in the derivation of this function. Linear length change function then has constant derivative and the velocity is constant.

Figure 19 shows the response of the cassette y-displacements in this simulation case. Due to the difference in cylinder model displacements there is also difference in the response of the cassette. With the length controlled rod element the cassette raises more than with the cylinder element. Also the y-velocities of the cassette are greatly different. When the fluctuation of the velocity is great the inertial forces are also significant. That's why the displacement of the cassette using the linear length function for the rod element is so wavy. The Hermite polynomial on the other hand produces much more smoother curve but it is not physically realistic.

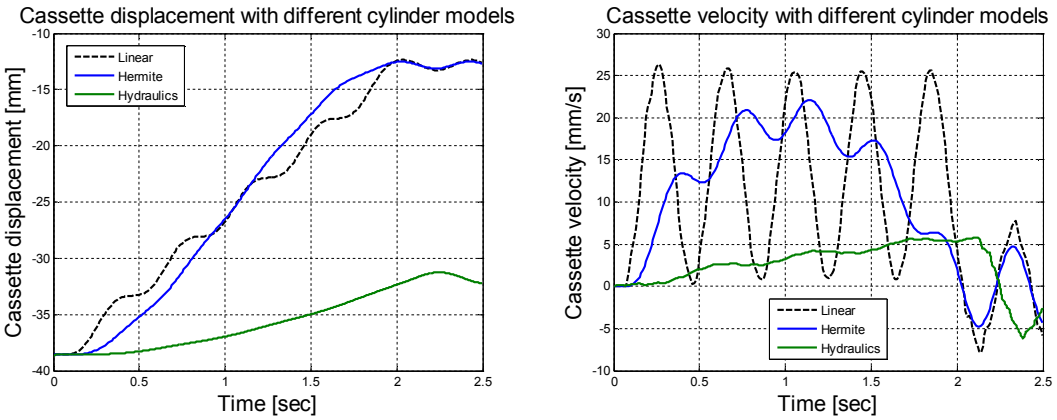

Figure 19 *Cassette displacement and velocity with different cylinder modeling methods*

When the system is stopped the actual hydraulic system does not oscillate as much as the length controlled rod elements and this is explained by taking notice of the cassette velocity. When the system is stopped at time 2 seconds the rod element is reducing velocity whereas the cylinder model is gaining velocity. When the velocities are greater

the momentum of the 9000 kg mass is greater and this explains why the time period of the vibrations is different.

3.4.2 Simulation case 2

The previous simulation case presented response of the system when the length change of the rod elements was calculated using the stationary condition of the hydraulic system. The computation clearly showed that the stationary condition is not relevant method for calculating the length change for the rod element in this case. The valve opening is small and the load is 9000 kg and together these factors cause low accelerations for the hydraulic system and the time when the system reaches stationary values is relatively long. Therefore a better way of calculating the length change of the rod element is needed.

The improvement on this matter is achieved by assuming the hydraulic simulation results as known information and using values from this simulation as input values for the length controlled rod element. This action constraints the maximum velocity of the cylinder but it needs response from the hydraulic system. In this case it is computed but it could be obtained from measurements.

As Table 1 shows the valve starts to close at $t = 2\,\mathrm{s}$ and the valve closes in 0.1 seconds. In this simulation case, the length change for the rod element is taken from the time when valve starts to open to the time when the valve closes. Using this value as input the cylinder displacement and velocity is as Figure 20 shows. The curve with actual hydraulic cylinder is exactly the same as in Figure 18. In this simulation case also a new length function is introduced where the linear model has been combined with the Hermite polynomial model. The length change first follows the Hermite polynomial and it ends up as linear function. This model is two parameter model where the time and length change of the Hermite polynomial can be adjusted. Where the Hermite polynomial changes to linear function the derivatives are the same.

From Figure 20 we see that the correction to input of the length controlled rod element gives better results than in simulation case 1 although there is still difference in the cylinder displacement when the cylinder is stopped. The main reason for this is that the valve closing time is exceptionally long. Length change for the rod element is defined to stop at the moment when the valve starts to close. At this time there is still opening in the directional valve and flow rate goes to the A-chamber of the cylinder thus keeping it in motion. During this time period the cylinder element can achieve few millimeters more in displacement. However, now the difference is much smaller and thereby we can compare the models more precisely.

If the actual hydraulic cylinder is assumed to have the most correct results we can see, that none of the rod elements models can represent the behavior of the cylinder correctly. The Hermite polynomial is again the worst in modeling the cylinder although it offers some wanted properties like the zero derivatives at the ends of the domain. In

various situations this continuous nature of the Hermite polynomial is very useful but in this situation it is unsuitable.

The linear model is better than the Hermite polynomial but when the linear curve is compared to the hydraulic curve we see that although the displacement at time $t = 2\,\mathrm{s}$ is nearly correct the velocity profile is completely different. The hydraulic cylinder is in accelerated motion the whole time period when the directional valve is open while the linear length variation produces constant velocity for the rod element. The oscillation in the velocity curve of Figure 20 occurs from the vibration of the whole system and this vibration dampens during the 2 second time period.

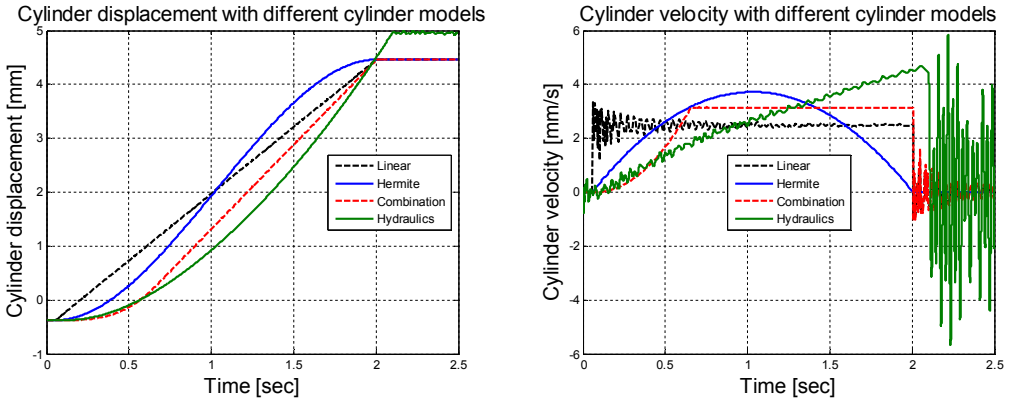

Figure 20 *Cylinder displacement and velocity with different cylinder modeling techniques*

A new length variation function was also introduced in this simulation case where the linear model is combined with the Hermite polynomial model. The red curve in Figure 20 represents this combination. It can be seen that this curve is the best of these three length functions for the rod element because it follows the hydraulic cylinder the most accurately. However, this curve has been fitted to follow the hydraulic cylinder curve in position wise but the velocity is still incorrect because the combined model also ends up changing length in linear fashion. This combination line then merely shows that it is possible to fit the length change of the rod element to represent the behavior of the hydraulic cylinder precisely.

In the first simulation case the positions and velocities of the hydraulic cylinder and the rod elements were too far from each other and therefore it is hard to draw conclusions from those simulation results. In case two the difference is narrower and it is possible to discuss the stopping of the system as well. Hermite polynomial introduces no oscillation because the derivative of the displacement is zero and thus the velocity is zero, see Figure 20. This behavior would be ideal but it is not physically relevant. The linear model and combination model come to stop from constant velocity and therefore the oscillation is far greater than the Hermite polynomial introduces. Naturally the combination model introduces more oscillation than the linear model because the velocity of the combination model is greater.

The actual hydraulic cylinder then behaves in different manner. First of all it is still in accelerated motion when the valve starts to close and the velocity is greater than the rod element has. Naturally greater velocity introduces greater oscillation. There is also difference in the stiffness of the cylinder element and rod element. The unstressed length of the rod element can be defined but of course the external load produces strains to the rod element. Therefore the oscillation of the rod element is only oscillation of the strains. In case of the hydraulic cylinder there are two different oscillating phenomena: the pressure fluctuation in the A-chamber of the cylinder and the deflection of the piston sealing. Together these two inflict the oscillation of the cylinder.

In Figure 21 are the cassette displacements and velocities. As stated earlier, the Hermite polynomial produces smooth response but it is not physically meaningful and thus it can be ignored. The linear model oscillates the most due to the fact that the length change of the unstressed element is changed by force. It does not notice the state of the system as the hydraulic system does. If the external load would be added the rod element would still reach almost the same position, although the strain of the element would be greater. The hydraulic system however, would respond slower.

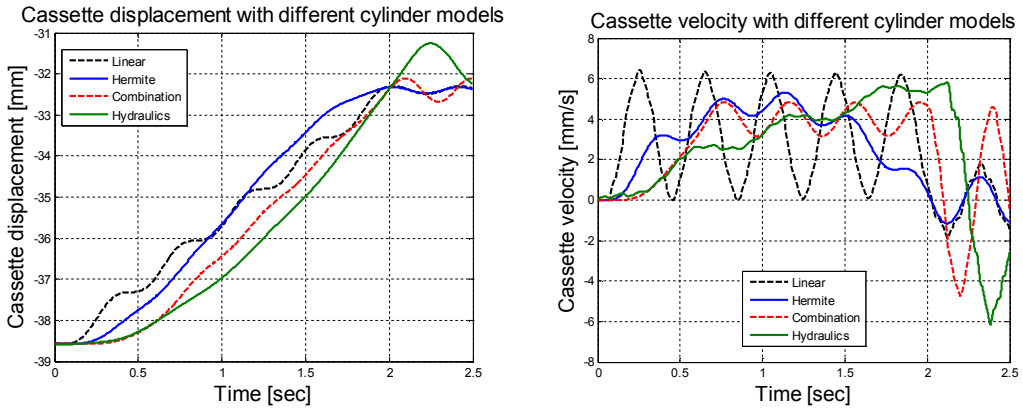

Figure 21 *Cassette displacement and velocity with different cylinder modeling methods*

The combination model follows the curve of the hydraulic system quite well for the first 0.6 seconds but then the linear nature of this length function starts and therefore the curves are not overlapping. The same behavior is noticed in the velocity curves in Figure 21. Of course it is possible to make the length function to overlap the hydraulic curve but it needs accurate information of the hydraulic system.

3.4.3 Hydraulic system results

In this Chapter the results for the hydraulic system are presented. In Chapters 3.4.1 and 3.4.2 are simulation results for two different simulation cases but in both of these cases the hydraulic system is the same and therefore also the results are the same. In those two chapters the focus is on the mechanical system and on the cylinder displacement. In this chapter the hydraulic system is studied.

In Figure 22 are the pressures of the pressure line elements and the A-chamber pressure of the hydraulic cylinder. The element numbering corresponds to the numbering shown in Figure 17. The element 1 is the first element in the hydraulic system and in Figure 22 the black dotted line presents the pressure in the volume 1 which is the system pressure or the pump pressure. This pressure has been set with the pressure relief element. The blue line then is the pressure in the end of this first element. There occurs a pressure drop in the transmission line and the pressure drop increases when the flow rate increases, see Figure 23.

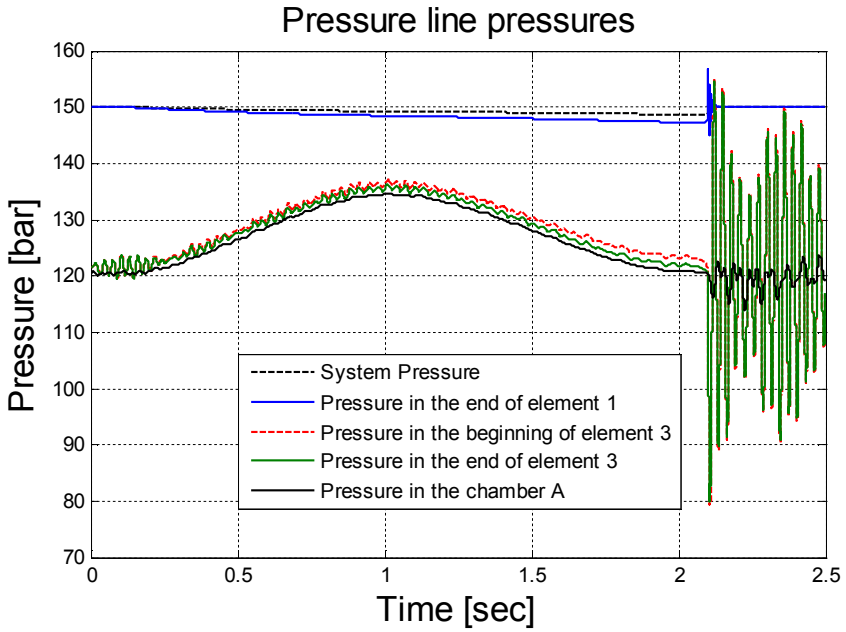

Figure 22 *Pressure line pressures in the hydraulic system*

It should also be noted that the pressure relief element has been set so that when the whole flow rate from the pump goes through this element the system pressure is 150 bars. When the directional valve is opened the flow rate goes also to the cylinder and therefore the system pressure also lowers. When the directional valve is closed the system pressure raises back to the 150 bars because all flow rate goes through the pressure relief valve, see Figure 23.

Pressure drop also occurs in the orifice 4 and in the transmission line element 3. The pressure drop in element 3 also increases as the flow rate increases as it is supposed. The pressure in the transmission line element 3 starts to oscillate because the orifice area in orifice 4 is relatively small whereas the orifice area 8 is large in area wise. Also the volume of the element 3 $(\approx 0.9\,\text{liters})$ is small compared to the volume of the hydraulic cylinder $(\approx 2.4\,\text{liters})$ and therefore small changes in the displacement of the cylinder induce large pressure fluctuation into the transmission line element 3. In addition, the flow rate through the orifice 8 oscillates because of the pressure fluctuation, see Figure 23.

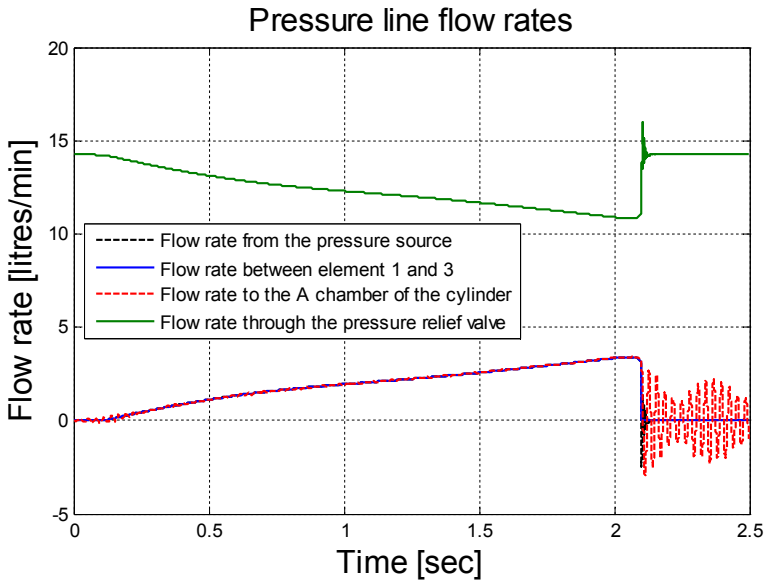

Figure 23 *Pressure line flow rates in the hydraulic system*

When the directional valve closes the flow rate to the cylinder goes to zero and the flow rate travels through the pressure relief element. This raises the pressures of the first element to 150 bars and because no flow rates exits there is no pressure difference between the beginning and end of the first element. However, the pressure oscillates intensely in the transmission line element 3. This occurs from the small movement of the hydraulic cylinder. Because the volume of the cylinder is far greater than the volume of the element 3 small change in cylinder A-chamber pressure induces intense fluctuation to the element 3. Same behavior is seen in the flow rate through orifice 8. It takes more time for the mechanical system to stop vibrating and after this period the hydraulic system also dampens to stationary values.

3.4.4 Friction model

In previous chapters differences between the length controlled bar element and hydraulic cylinder element have been pointed out but one key difference is the friction. The rod element is considered to be frictionless while the hydraulic cylinder is embedded with the Olsson's friction model presented in Section 2.6 .

The friction model introduces a new variable to the system: the piston sealing deflection. The main difference in friction is that it allows the cylinder to carry load not only with the hydraulic fluid but also with the friction force. Friction force plays important role when flow rate starts to flow to the cylinder and movement begins and on the other hand when the movement is stopped. In these situations the friction force affects on the response of the system. The movement begins smoothly which can be seen for instance in Figure 20 and when the system is stopped the friction dissipates energy. The bristle deflection also allows movement for the cylinder without actual sliding of the piston sealing.

Friction force and the bristle deflection are both presented in Figure 24. When the maximum value of the friction is compared to the Table 1 we can see that the friction

reaches the static friction value as well as the bristle deflection reaches stationary state. This implies that the piston sealing is sliding instead of just deflecting and giving movement through this deflection. The friction force builds smoothly and this explains partly the smooth starting of the cylinder movement.

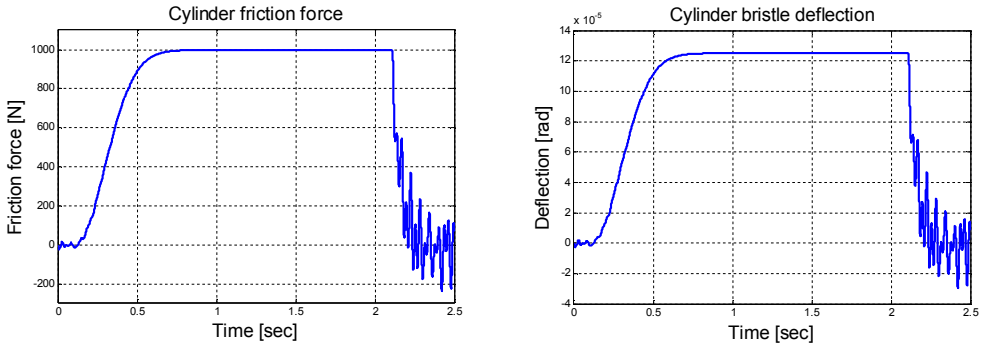

Figure 24 *Cylinder friction force on the left and sealing deflection on the right*

Figure 25 shows a close up on the friction force curve because from Figure 24 it is impossible to identify the behavior of the friction. The bristle deflection in Figure 24 remains absolutely constant but the friction force undergoes minor changes and this is portrayed in Figure 25.

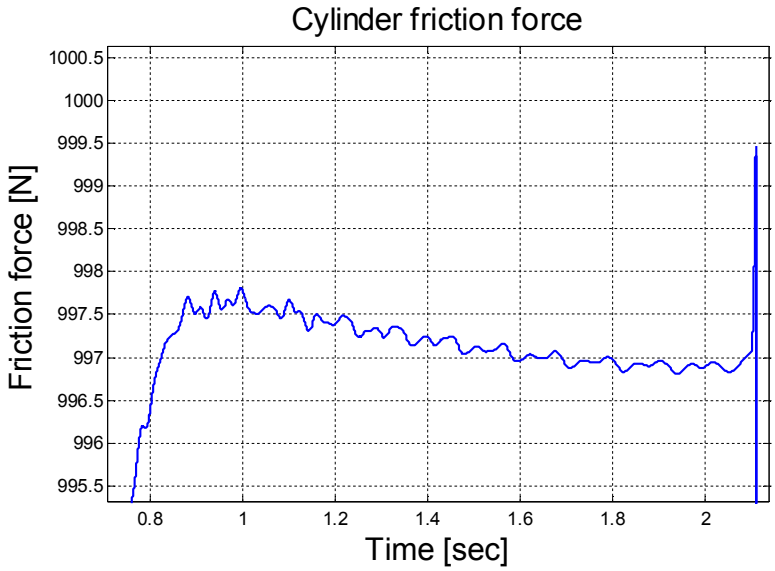

Figure 25 *Close up on the cylinder friction force*

Friction force lowers as the velocity of the cylinder increases, see for instance Figure 20. This lowering of the friction at low velocities is called the Stribeck's effect. If the velocity would increase even more the viscous friction would start to increase the friction force but in this simulation case the cylinder velocity remains fairly low and therefore the effect of the viscous friction is not visible in this simulation. However, when the cylinder is stopped the friction reaches the static friction level and this is clearly visible in Figure 25.

Olsson's friction model can describe all phenomena of the friction but it is fairly sensitive for the friction parameters. In this thesis the friction parameters are chosen so that the friction phenomenon can be identified but they are not from any physical appliance. If simulation results are wanted to be correct the friction parameters need to be accurate.

4 DISCUSSION

In this master's thesis new method for simulating coupled hydraulically driven flexible multibody systems is presented and applied on a simulation case. Hydraulically driven mechanical systems can be treated as three-field problems because hydraulic system, hydraulic cylinder and mechanical system can be identified as separate systems which are in connection with each other. Traditionally hydraulic driven mechanical systems have been computed as separate systems and the coupling has been made in the actuator. However, the formulation is inconsistent because it does not deal the coupling accurately. In addition when the systems are solved separately the convergence degrades and is usually very ineffective. Using the new accurate formulation these connections are also taken into account. The hydraulic cylinder is then in connection with the hydraulic system via orifices and this connection is also modeled accurately within the limits of the orifice model. Finally the mechanical system is modeled using non-linear beam elements which allow large displacements and large rotations. This modeling technique in general can be exploited in any hydraulic driven flexible mechanism.

Adopting the hydraulic system to the simulation model is a sophisticated method for computing the response of the mechanical structure but usually more robust methods are used. These methods are to use the length controlled rod element which is also presented in this thesis. In some cases this modeling provides sufficient accuracy to the response of the system but in many cases the enforcing nature of the rod element is too intense. However, the rod element provides one advantage which is the simulation time. Systems with hydraulics adopted are slow to compute due to the stiffness of the equation of motion. Stiff systems require short time steps in time integration whereas non-stiff equations can be integrated with long time steps. Adopting the hydraulic system Jacobian matrix to the equation of motion itself does not add the simulation time. Instead the computation time increases while the time step is short and the mechanical system becomes the millstone. The internal force vector for non-linear Reissner's beam element is slow to compute and the offset beam element is even slower. When the cylinder is modeled as length controlled rod element the equation of motion is non-stiff and long time steps can be used and the simulation can achieve real time speed.

The downside of the rod element is that it cannot model the hydraulic cylinder accurately as stated earlier when the computational model results were presented. In these simulation cases the length change was incorrect and the linear model introduced oscillation to the system. This vibration then would produce false results for instance if fatigue analysis is to be conducted. In addition the length function for the rod element cannot be defined without simulating the actual hydraulic system with cylinder element and

then using this length change as input for the rod element. Same results would be achieved by measuring the system and then using these results as input for the rod element. However, this procedure can be exploited mainly in systems where the cycle of the system remains constant. For instance if the cycle is changed or the external load increases the input for the rod element has to be computed over. In case of excavators, for example, the cycle is different and the external load is not in any means constant whereas the CMM has constant cycles and external load. Therefore the rod element would be suitable for this kind of applications. If the rod element is to be used in the simulations it has to be developed further.

In order to use the rod element in the simulation the input for the length change has to be relevant. It has been seen that using the stationary state of the hydraulic system does not lead to truthful results. In simulation models where the throttling of the directional valve is not as drastic as it is in this case the stationary value can be good assumption. In this simulation case the problem is that the cycle simulated is so short that the hydraulic system cannot reach the stationary state. If the orifice area in directional valve was greater the response of the hydraulic system would be faster and it would reach the stationary state in shorter period of time. Due to this matter it is not sufficient to control the length of the rod element but also the velocity of the length change. It would be also good idea to add a feedback from certain joints of the system thus creating a servo system for the rod element. Using this technique input of the system could be given to rotations of these joints and then the rod element could calculate its length according to the position error. This then leads to servo modeling.

One feature that the rod element lacks is the friction model. If only mechanical system is wanted in the simulation Olsson's friction model should be added to the rod element. The friction model plays an important role when the length of the element starts to change because in first stages the length does not change because the friction force builds up. This then leads to smoother response of the system and at the same time it adds damping for the mechanism. The rod element can present the hydraulic cylinder correctly when the cylinder reaches stationary velocity but the problem lies in phases when the length chance is started or stopped.

Instead of developing a new length controlled rod element, the hydraulic cylinder element can be used without adopting the whole hydraulic system. If only the differential equations for chamber pressures and sealing ring deflections are taken into account the system would not become stiff and long time steps can be used. In this case the cylinder needs flow rates to the chambers as input but these flow rates can be defined using only models of the hydraulic system. In case of the CMM this is also justified because the system is a servo system and thus the flow rate to the cylinder is always known. Using appropriate ramps for the flow rate the simulations can be made effectively. This modeling works only when the mechanical system is in the point of interest and merely when servo systems are concerned. If traditional on/off hydraulics is exploited it is hard to define the flow rate to the cylinder and the problem is the same as it is with the rod element, what is the correct input?

Input is not needed when the whole hydraulic system is adapted to the simulation model because it defines the flow rates to the cylinder using the differential equations presented in the theory section. If the whole system is to be simulated the integration algorithm could be modified. It is also possible to change the algorithm completely. Newmark integration algorithm is a Runge-Kutta algorithm which iterates the system to equilibrium at every time step. If Rosenbrock algorithm is implemented no iteration is needed because this method takes sample points and using these point it advances and takes a new time step. When the system reaches the stationary state oscillation dampens and also longer time steps could be used and therefore variable time step would also be effective.

Stiffness of the equation of motion can also be reduced so that the integration algorithms would work more effective. One key matter in the stiff problem is the orifice model used to combine the transmission line elements together. In denominator of equation (90) is the volume of the orifice and if this volume is relatively small the differential equation stiffens. Replacing these orifice models with algebraic orifice models the system could be more easily solved using Newmark integration or Rosenbrock methods. This algebraic orifice models has been used in the development of the pressure relief element and it works fine. First order model for the orifice is however, easier to implement to the system.

Using this algebraic orifice model the directional valve could be developed in different manner and the mass of the spool could be adapted to the model as it is in the pressure relief element. For instance if a servo valve is modeled it is crucial to have the inertia of the valve in the model. This same behavior can be modeled using time delay circuit but if the valve is studied from the mechanical point of view the equation of motion can be written for the spool and the external loads from the centralizing springs can be taken into account as well as the force induced by the magnets in solenoid valves. In servo valves the deflecting force is from torque motor and from fluid pressure. If servo system is to be modeled also the control system has to be modeled as it has to be modeled if servo system is to be used with length controlled rod element.

In general more components for the hydraulic system can be developed and existing components can be improved as is the case with the directional valve element. For instance the pump model used in this thesis is a fixed displacement pump which produces constant flow to the system. The flow is also even although in real pumps the flow rate fluctuates due to the structure of the pump. This behavior could be modeled in the pump. Efficiency of the pump could also be taken into account. For instance the volumetric efficiency is strongly depended on the system pressure, the higher the pressure the lower the volumetric efficiency. This is explained with the internal leakage of the pump. Leakage flow is greater when pressure is higher. On the other hand the mechanical efficiency of the pump is the other way around, higher pressures lubricates pump better thus the efficiency raises. Mechanical efficiency is important if also the external power supply, like diesel engine, is wanted on the system.

When pump model is concerned also variable displacement pumps are a point of interest. Energy-saving hydraulic systems are under considerable study at the moment because energy costs are raising all the time. When hydraulic systems are wanted to be energy-saving variable displacement pumps and different pump controlled systems become more general.

Special interest is on modeling the cylinder element because in point of mechanics the cylinder is the component that interacts with the mechanical system. As it is stated the cylinder can be reduced to rod element but the problem with this element is the lack of friction model and how to define the input. However, when the cylinder element is added to the system the computational model changes from one-field problem to two field problem and it can add instability in the sense of convergence and the problem can become stiff. Therefore it would be tempting to remain in purely mechanical model. The rod element however, needs to be derived with friction model and also the hydraulic flexibility needs to be taken into account as function of the length of the element. Now the volume of the hydraulic fluid in the rod element remains constant because the reduced Young's modulus contains both mechanical and hydraulic flexibility and it remains constant in computation. Adding these two fairly simple features to the rod element it would be very useable and it would represent the hydraulic cylinder. Problem of the input is still open but if servo system is used this control system can be adapted to the model removing the input problem. In case of on/off hydraulics there is no technique to estimate the length change velocity but the stationary condition which can, in some cases, be very accurate. In this thesis's simulation model the cylinder velocity is relatively small compared to the maximum flow rate from the pump and the system does not reach the stationary values. At current form the rod element is not suitable to model the hydraulic system as it has been stated.

In the actual hydraulic cylinder lies the same problem of the input as it is for the rod element if the hydraulic system is excluded from the simulation model. In case of a servo system, the flow rate can be defined from the feedback signal but when on/off hydraulics is simulated the stationary condition can be used. When the hydraulic system is included all possible systems can be simulated if corresponding elements are available. Still the hydraulic cylinder can be improved in various ways.

The cylinder element used in this thesis is considered to be rigid in mechanical point of view and these strains of the cylinder rod could be added into the model. However, it is also justified to exclude these strains because the hydraulic fluid is more flexible than the steel used in the cylinder rod. One phenomenon that this current cylinder model cannot represent is buckling. In order to see the buckling beam elements with rotational freedoms needs to be used. The cylinder can be modeled as telescope with sliding beams, see (Marjamäki, et al., 2009), and then adding the fluid field to support the telescope. In derivation of this super element the curvature of the cylinder sleeve has to be taken into account because the pressure of the fluid tends to straighten the cylinder sleeve. These properties can be useful for instance when cylinder malfunctions are studied. End cushioning or lack of it is also a matter of study in accident cases.

Finally the friction model and the parameters for the Olsson's model are an interesting research case. Friction occurs in every sliding contact and the Olsson's model has all phenomena modeled but the research study is to create measurement system and calculation method for finding out the correct friction parameters. Static friction is easily measured but the pressure coefficients and viscous friction are more complicated. This problem could be approached by creating a measurement system where the efficiency of a work cycle is computed and then the parameters are fitted to these results. This though is a long research project and it is not discussed thorough in this master's thesis.

This master's thesis presents a new way of modeling and simulating coupled hydromechanical systems. Results are encouraging and further study of this coupling and hydraulic cylinder is required to model systems accurately. This study however, is not simulation of any real structure but more like an opening to a new simulation technique where the old models can be improved using more advanced simulation models.

REFERENCES

Bonet, Javier and Wood, Richard D. 2009. *Nonlinear Continuum Mechanics for Finite Element Analysis.* Cambridge : Cambridge University Press, 2009. p. 318. ISBN 978-0-521-83870-2.

Cardona, Alberto and Géradin, Michel. 1988. A beam finite element non-linear theory with finite rotations. *International journal for numerical methods in engineering.* 1988, Vol. 26.

Ellman, Asko and Piché, Robert. 1996. A Modified Orifice Flow Formula for Numerical simulation. Atlanta : ASME International Mechanical Engineering Congress and Exposition, November 17-22, 1996.

Fonselius, Jaakko, Rinkinen, Jari and Vilenius, Matti. 2006. *Hydrauliikka II.* Tampere : Tampereen Yliopistopaino Oy - Juvenes Print, 2006. p. 226. Vol. 3. ISBN 952-92-0114-1.

Géradin, Michel and Cardona, Alberto. 2001. *Flexible Multibody Dynamics; A Finite Element Approach.* West Sussex : John Wiley & Sons Ltd., 2001. p. 327. Vol. 1. ISBN 0 471 48990 5.

Gottlieb, Davie and Orszag, Steven A. 1977. *Numerical Analysis of Spectral Methods: Theory and Applications.* Bristol : Society for Industrial and Applied Mathematics, 1977.

Hairer, Ernst and Wanner, Gerhard. 1991. *Solving Ordinary Differential Equations II - Stiff and Differential-Algebraic Problems.* Berlin : Springer-Verlag, 1991. Vol. 1. ISBN 3-540-53775-9.

Marjamäki, Heikki and Mäkinen, Jari. 2006. Modelling a telescopic boom - the 3D case: Part II. *Computers & Structures.* 2006, 84.

Marjamäki, Heikki and Mäkinen, Jari. 2009. Total Lagrangian beam element with C1-continuous slide-spring. *Computers & Structures.* 2009, 87.

Mäkinen, Jari and Marjamäki, Heikki. 2006. Total and Updated Lagrangian Geometrically Exact Beam Elements. *III European Conference on Computational Mechanics, Solids, Structures and Coupled Problems in Engineering.* Lisbon; Portugal : s.n., 2006.

Mäkinen, Jari. 2001. Critical study of Newmark-schema on manifold of finite rotations. *Computer methods in applied mechanics and engineering.* 2001, 191.

Mäkinen, Jari. 2008. Rotation manifold SO(3) and its tangential vectors. *Computational Mechanics.* 2008, Vol. 42, 6.

Mäkinen, Jari. 2007. Total Lagrangian Reissner's geometrically exact beam element without singularities. *International Journal for Numerical Methods in Engineering.* 2007, Vol. 7, 9.

Mäkinen, Jari, Piché, Robert and Ellman, Asko. 2000. Fluid Transmission Line Modeling Using a Variational Method. *Journal of Dynamic Systems, Measurement, and Control.* 2000, Vol. 122.

Olsson, Henrik. 1996. *Control Systems with Friction.* Lund : Department of Automation Control Lund Institute of Technology, 1996. Doctoral Thesis. ISSN 0280-5316.

Reddy, J. N. 1986. *Applied Functional Analysis and Variational Methods in Engineering.* Singapore : McGraw-Hill, 1986. p. 546. Vol. 1. ISBN 0-07-100274-X.

Viersma, Taco J. 1980. *Analysis, synthesis, and design of hydraulic servosystems and pipelines.* Amsterdam : Elsevier Scientific Publishing Company, 1980. p. 279.

Wolfram. MathWorld. *Circular Segment.* [Online] [Cited: 11 11, 2010.] http://mathworld.wolfram.com/CircularSegment.html.

APPENDIX A

In this appendix derivatives of the transformation operator **T** are presented. These derivatives are exploited in formulation of the Reissner's geometrically exact beam element. Matrix $\mathbf{C}_1$ is defined with the aid of directional derivative of the vector $\mathbf{T}\cdot\mathbf{V}$ in direction $\Delta\boldsymbol{\Psi}$. Vector **V** can be considered as arbitrary vector that is only used to aid the derivation. (Mäkinen, et al., 2006)

$$\begin{aligned}&\mathbf{C}_1(\mathbf{V},\boldsymbol{\Psi})\cdot\Delta\boldsymbol{\Psi}=\mathrm{D}_{\boldsymbol{\Psi}}\left(\mathbf{T}\cdot\mathbf{V}\right)\cdot\Delta\boldsymbol{\Psi},\quad \forall\mathbf{V}\in\mathrm{E}^3\ ,\\&\mathbf{C}_1(\mathbf{V},\boldsymbol{\Psi})=c_1\mathbf{V}\otimes\boldsymbol{\Psi}-c_2(\tilde{\boldsymbol{\Psi}}\mathbf{V})\otimes\boldsymbol{\Psi}+c_3(\boldsymbol{\Psi}\cdot\mathbf{V})\boldsymbol{\Psi}\otimes\boldsymbol{\Psi}-c_4\tilde{\mathbf{V}}+c_5\left((\boldsymbol{\Psi}\cdot\mathbf{V})\mathbf{I}+\boldsymbol{\Psi}\otimes\mathbf{V}\right),\end{aligned}\tag{A.1}$$

where coefficients c_i are given by

$$\begin{aligned}&c_1=\frac{\psi\cos\psi-\sin\psi}{\psi^3}\qquad c_2=\frac{\psi\sin\psi+2\cos\psi-2}{\psi^4}\\&c_3=\frac{3\sin\psi-2\psi-\psi\cos\psi}{\psi^5}\quad c_4=\frac{\cos\psi-1}{\psi^2}\qquad c_5=\frac{\psi-\sin\psi}{\psi^3}\end{aligned}\tag{A.2}$$

A very similar expression (in the spatial description) comes from the directional derivative of the vector $\mathbf{T}^{\mathrm{T}}\cdot\mathbf{V}$ in the direction $\Delta\boldsymbol{\Psi}$ where the matrix $\mathbf{C}_2$ is defined via relation

$$\begin{aligned}&\mathbf{C}_2(\mathbf{V},\boldsymbol{\Psi})\cdot\Delta\boldsymbol{\Psi}:=\mathrm{D}_{\boldsymbol{\Psi}}\left(\mathbf{T}^{\mathrm{T}}\cdot\mathbf{V}\right)\cdot\Delta\boldsymbol{\Psi},\quad \forall\mathbf{V}\in\mathrm{E}^3,\\&\mathbf{C}_2(\mathbf{V},\boldsymbol{\Psi})=c_1\mathbf{V}\otimes\boldsymbol{\Psi}+c_2(\tilde{\boldsymbol{\Psi}}\mathbf{V})\otimes\boldsymbol{\Psi}+c_3\left(\boldsymbol{\Psi}\cdot\mathbf{V}\right)\boldsymbol{\Psi}\otimes\boldsymbol{\Psi}+c_4\tilde{\mathbf{V}}+c_5\left((\boldsymbol{\Psi}\cdot\mathbf{V})\mathbf{I}+\boldsymbol{\Psi}\otimes\mathbf{V}\right),\end{aligned}\tag{A.3}$$

where coefficients are given in (A.2).

We also need the time derivative of the transformation matrix **T**, giving

$$\dot{\mathbf{T}}(\dot{\boldsymbol{\Psi}},\boldsymbol{\Psi})=c_1\left(\boldsymbol{\Psi}\cdot\dot{\boldsymbol{\Psi}}\right)\mathbf{I}-c_2\left(\boldsymbol{\Psi}\cdot\dot{\boldsymbol{\Psi}}\right)\tilde{\boldsymbol{\Psi}}+c_3\left(\boldsymbol{\Psi}\cdot\dot{\boldsymbol{\Psi}}\right)\boldsymbol{\Psi}\otimes\boldsymbol{\Psi}+c_4\dot{\tilde{\boldsymbol{\Psi}}}+c_5\left(\dot{\boldsymbol{\Psi}}\otimes\boldsymbol{\Psi}+\boldsymbol{\Psi}\otimes\dot{\boldsymbol{\Psi}}\right),\tag{A.4}$$

where the coefficients are given in (A.2).

The directional derivative of the term $\mathbf{C}_1^{\mathrm{T}}(\boldsymbol{\Psi}',\boldsymbol{\Psi})\cdot\mathbf{V}$ can be written as

$$
\begin{aligned}
&\mathbf{C}_3(\mathbf{V},\boldsymbol{\Psi}',\boldsymbol{\Psi})\cdot\Delta\boldsymbol{\Psi} := \mathrm{D}_{\boldsymbol{\Psi}}\left(\mathbf{C}_1^{\mathrm{T}}(\boldsymbol{\Psi}',\boldsymbol{\Psi})\cdot\mathbf{V}\right)\cdot\Delta\boldsymbol{\Psi}, \quad \forall\mathbf{V}\in\mathrm{E}^3,\\
&\mathbf{C}_3(\mathbf{V},\boldsymbol{\Psi}',\boldsymbol{\Psi}) = \left(c_1(\boldsymbol{\Psi}'\cdot\mathbf{V}) + c_2(\boldsymbol{\Psi}\cdot\tilde{\mathbf{V}}\boldsymbol{\Psi}') + c_3(\boldsymbol{\Psi}\cdot\boldsymbol{\Psi}')(\mathbf{V}\cdot\boldsymbol{\Psi})\right)\mathbf{I} + c_2(\boldsymbol{\Psi}\underset{\mathrm{S}}{\otimes}\tilde{\mathbf{V}}\boldsymbol{\Psi}') +\\
&\quad + c_3(\boldsymbol{\Psi}\cdot\boldsymbol{\Psi}')(\boldsymbol{\Psi}\underset{\mathrm{S}}{\otimes}\mathbf{V}) + \frac{1}{\psi}\left(c_1'(\boldsymbol{\Psi}'\cdot\mathbf{V}) + c_2'(\boldsymbol{\Psi}\cdot\tilde{\mathbf{V}}\boldsymbol{\Psi}') + c_3'(\boldsymbol{\Psi}\cdot\boldsymbol{\Psi}')(\mathbf{V}\cdot\boldsymbol{\Psi})\right)(\boldsymbol{\Psi}\otimes\boldsymbol{\Psi}) +\\
&\quad + c_3(\mathbf{V}\cdot\boldsymbol{\Psi})(\boldsymbol{\Psi}\underset{\mathrm{S}}{\otimes}\boldsymbol{\Psi}') + c_5(\boldsymbol{\Psi}'\underset{\mathrm{S}}{\otimes}\mathbf{V}),
\end{aligned}
\tag{A.5}
$$

where $\underset{\mathrm{S}}{\otimes}$ denotes the symmetric matrix outer product, and c_i' represents the derivatives of the coefficients (A.2), given by

$$
\begin{aligned}
&(\mathbf{a}\underset{\mathrm{S}}{\otimes}\mathbf{b}) = (\mathbf{a}\otimes\mathbf{b}) + (\mathbf{b}\otimes\mathbf{a}), \quad \forall\mathbf{a},\mathbf{b}\in\mathrm{E}^3,\\
&\quad c_1' = \frac{3\sin\psi - \psi^2\sin\psi - 3\psi\cos\psi}{\psi^4}, \qquad c_2' = \frac{\psi^2\cos\psi - 5\psi\sin\psi - 8\cos\psi + 8}{\psi^5},\\
&\quad c_3' = \frac{7\psi\cos\psi + 8\psi + \psi^2\sin\psi - 15\sin\psi}{\psi^6}.
\end{aligned}
\tag{A.6}
$$

The variation of the angular rotation vector $\boldsymbol{\Omega}_{\mathbf{R}}$ reads in terms of the total rotation vector

$$
\delta\boldsymbol{\Omega}_{\mathbf{R}} = \mathbf{T}\cdot\delta\dot{\boldsymbol{\Psi}} + \mathbf{C}_1(\dot{\boldsymbol{\Psi}},\boldsymbol{\Psi})\cdot\delta\boldsymbol{\Psi},
\tag{A.7}
$$

The variation of material angular acceleration tensor $\dot{\boldsymbol{\Omega}}_{\mathbf{R}}$

$$
\delta\dot{\boldsymbol{\Omega}}_{\mathbf{R}} = \mathbf{T}\cdot\delta\ddot{\boldsymbol{\Psi}} + \mathbf{C}_4(\dot{\boldsymbol{\Psi}},\boldsymbol{\Psi})\cdot\delta\dot{\boldsymbol{\Psi}} + \left(\mathbf{C}_1(\ddot{\boldsymbol{\Psi}},\boldsymbol{\Psi}) + \mathbf{C}_5(\dot{\boldsymbol{\Psi}},\boldsymbol{\Psi})\right)\cdot\delta\boldsymbol{\Psi},
\tag{A.8}
$$

where $\mathbf{C}_1$ is given in A.1 and the matrices $\mathbf{C}_4$ and $\mathbf{C}_5$ are defined by the following derivative formulas

$$
\begin{aligned}
&\mathbf{C}_4(\dot{\boldsymbol{\Psi}},\boldsymbol{\Psi})\cdot\Delta\dot{\boldsymbol{\Psi}} := \mathrm{D}_{\dot{\boldsymbol{\Psi}}}\left(\dot{\mathbf{T}}\dot{\boldsymbol{\Psi}}\right)\cdot\Delta\dot{\boldsymbol{\Psi}} \quad \text{and} \quad \mathbf{C}_5(\dot{\boldsymbol{\Psi}},\boldsymbol{\Psi})\cdot\Delta\boldsymbol{\Psi} := \mathrm{D}_{\boldsymbol{\Psi}}\left(\dot{\mathbf{T}}\dot{\boldsymbol{\Psi}}\right)\cdot\Delta\boldsymbol{\Psi},\\
&\mathbf{C}_4(\dot{\boldsymbol{\Psi}},\boldsymbol{\Psi}) = (c_1+c_5)(\boldsymbol{\Psi}\cdot\dot{\boldsymbol{\Psi}})\mathbf{I} + 2c_3(\boldsymbol{\Psi}\cdot\dot{\boldsymbol{\Psi}})(\boldsymbol{\Psi}\otimes\boldsymbol{\Psi}) + 2c_5(\boldsymbol{\Psi}\otimes\dot{\boldsymbol{\Psi}}) +\\
&\qquad + (c_1+c_5)(\dot{\boldsymbol{\Psi}}\otimes\boldsymbol{\Psi}) - c_2(\tilde{\boldsymbol{\Psi}}\dot{\boldsymbol{\Psi}})\otimes\boldsymbol{\Psi} - c_2(\boldsymbol{\Psi}\cdot\dot{\boldsymbol{\Psi}})\tilde{\boldsymbol{\Psi}},\\
&\mathbf{C}_5(\dot{\boldsymbol{\Psi}},\boldsymbol{\Psi}) = \left(c_3(\boldsymbol{\Psi}\cdot\dot{\boldsymbol{\Psi}})^2 + c_5(\dot{\boldsymbol{\Psi}}\cdot\dot{\boldsymbol{\Psi}})\right)\mathbf{I} + \left(\frac{c_3'}{\psi}(\boldsymbol{\Psi}\cdot\dot{\boldsymbol{\Psi}})^2 + c_3(\dot{\boldsymbol{\Psi}}\cdot\dot{\boldsymbol{\Psi}})\right)(\boldsymbol{\Psi}\otimes\boldsymbol{\Psi}) + 2c_3(\boldsymbol{\Psi}\cdot\dot{\boldsymbol{\Psi}})(\boldsymbol{\Psi}\otimes\dot{\boldsymbol{\Psi}}) +\\
&+\left(\frac{c_1'}{\psi} + c_3\right)(\boldsymbol{\Psi}\cdot\dot{\boldsymbol{\Psi}})(\dot{\boldsymbol{\Psi}}\otimes\boldsymbol{\Psi}) - \frac{c_2'}{\psi}(\boldsymbol{\Psi}\cdot\dot{\boldsymbol{\Psi}})(\tilde{\boldsymbol{\Psi}}\dot{\boldsymbol{\Psi}})\otimes\boldsymbol{\Psi} - c_2(\tilde{\boldsymbol{\Psi}}\dot{\boldsymbol{\Psi}})\otimes\dot{\boldsymbol{\Psi}} + c_2(\boldsymbol{\Psi}\cdot\dot{\boldsymbol{\Psi}})\tilde{\dot{\boldsymbol{\Psi}}} + (c_1+c_5)(\dot{\boldsymbol{\Psi}}\otimes\dot{\boldsymbol{\Psi}}).
\end{aligned}
\tag{A.9}
$$